UNIVERSIDAD DE LA REPÚBLICA URUGUAY

FACULTAD DE CIENCIAS
UDELAR fcien.edu.uy

PEDECIBA
Geociencias

Universidad de la República

Facultad de ciencias (UDELAR)

PEDECIBA Geociencias

Tesis de Doctorado en Geociencias

CHARACTERISTICS, VARIABILITY AND PREDICTABILITY OF LONG-LIVED ROSSBY WAVE PACKETS IN AUSTRAL SUMMER

Student: Iago Pérez Fernández

Supervisor: Marcelo Barreiro (Departamento de Ciencias de la Atmósfera y Física de los Océanos, Facultad de Ciencias, Universidad de la República)

Co Supervisor: Cristina Masoller (Departament de Física in the Universitat Politècnica de Catalunya (UPC)

Montevideo,Uruguay

(30/05/2023)

To my mother, father and sister, who always pushed me to do my best.

ACKNOWLEDGMENTS

First of all I would like to express my heartfelt gratitude towards my PhD director Dr. Marcelo Barreiro, for all the time, effort and most of all, patience shown during these last 4 years, and also for giving me the chance to be part of the department of Science of the atmosphere and physics of the ocean. He was always available for any questions, suggestions and feedback, and also helped me to learn and continue in this project with passion.

Additionally, I would also like to thank Cristina Masoller, the co director of this PhD project, for all her support and assistance during this project.

To all the companions of the Departamento de Ciencias de la Atmósfera y Física de los Océanos (Santiago, Camila, Yilean, Gaston,Mariana, Madeleine, Matilde, Romina, Natalia, Roxana, Rafael and Juan) for the warm welcome into the departament and for all the good vibes during this period. And thanks to Alain for all his assistance for computer issues.

To all my companions of the CAFE project (Nicolas Rieger, Mónica Mijares, Emmanuel Rogues, Ricardo Silini, Xinjia Hu, Pedro Herrera, Noemie Ehstand, Amal John, Shaddha Gupta, Meriem Kouma, Nikos Mastrantonas), thank you for all the (in)formal reunions, experiences and laughs shared during this period. It was a real pleasure to get to know all of you and I hope the best for all of you. Also, I would like to specially thank Noemi for her help and assistance in the last part of the thesis.

I would also like to thank the European Union's Horizon 2020 research and innovation programme and the Programa de Desarrollo de las Ciencias Básicas (PEDECIBA) which financed the development of this project.

And last, but not least, to all my family and friends that always supported and cheered me to start, continue and finish this project. Without you, completing this project would not have been possible.

TABLE OF CONTENTS

Resumen

Características y variabilidad de los paquetes de ondas de Rossby de larga duración en el verano austral

Los paquetes de Ondas de Rossby (RWPs, en inglés) son perturbaciones atmosféricas que aparecen como meandros de la corriente en chorro, y son considerados precursores de eventos extremos como olas de calor. Este trabajo se centra en estudiar RWPs que duran más de 8 días en la atmósfera (RWPs de larga duración ó LLRWPs) porque son importantes para mejorar la predicción de eventos extremos entre 10-30 días de antelación.

Comparado con el hemisferio norte, los LLRWPs en el hemisferio sur se han estudiado muy poco. En este estudio determinamos: (1) cómo los modos de variabilidad climáticos del hemisferio sur influyen en la ocurrencia y características de los LLRWPs, (2) si los modelos de pronóstico predicen correctamente la formación de LLRWPs, y (3) si los LLRWPs están ligados al desarrollo de bloqueos atmosféricos.

Para ello se desarrolló un algoritmo que rastrea RWPs durante el verano austral del hemisferio sur (Diciembre-Marzo), reteniendo los LLRWPs. Después, estudiamos cómo el Modo Anular del Sur (SAM) y El Niño-Oscilación Sur (ENOS) afectan a la actividad de los LLRWPs, y qué condiciones atmosféricas favorecen/desfavorecen su desarrollo. Encontramos que durante años de SAM negativo la guía de ondas donde los RWPs se propagan se extiende hacia el Pacifico, favoreciendo la propagación de LLRWPs, y que estos duran más tiempo en la atmósfera.

Estudiamos la capacidad de los modelos de pronóstico para predecir los LLRWPs en dos modelos de predicción sub-estacional, identificando bajo qué condiciones obtenemos buenas/malas predicciones. Para ello, comparamos la trayectoria de los LLRWPs observados respecto a la trayectoria predicha por los modelos de pronóstico. Obtenemos las mejores predicciones de LLRWPs en años de SAM negativo y cuando la oscilación de Madden-Jullian está inactiva.

Finalmente, examinamos si los LLRWPs están ligados al desarrollo de bloqueos atmosféricos usando dos algoritmos adicionales, uno detecta eventos de rotura de onda de Rossby (RWB) y otro rastrea bloqueos atmosféricos. Observamos que alrededor del 20% de los bloqueos atmosféricos se manifiestan cerca de un RWB, pero apenas hay eventos de RWB ligados a RWPs, consecuentemente, no parece existir vínculo directo entre LLRWPs y el desarrollo de bloqueos atmosféricos

Abstract

Characteristics and variability of long-lived Rossby wave packets in austral summer

Rossby Wave Packets (RWPs) are atmospheric perturbations that manifest as meanders of the jet stream, and which are considered precursors of extreme weather events such as heat waves. Therefore, studying RWPs that last more than 8 days (long-lived RWPs or LLRWPs), is key to improve extreme weather events prediction between 10-30 days in advance. Thus, in this study we focus on the LLRWPs.

Compared to the northern hemisphere, the LLRWPs in the Southern hemisphere have been much less studied. In this study we determine: (1) how the main modes of variability of the southern hemisphere influence the occurrence of LLRWPs, (2) if LLRWPs are correctly represented on weather forecast models, and (3) whether LLRWPs are linked to atmospheric blocking development.

To reach these objectives we developed an algorithm that tracks propagating RWPs during the Southern Hemisphere summer (December-March), retaining the LLRWPs. Afterwards, we measured the impact of the Southern Annular Mode (SAM) and El Niño Southern Oscillation (ENSO) on LLRWPs variability, and identified the atmospheric conditions that favour/disfavour high LLRWPs activity. Results show that during negative SAM years the waveguide where RWPs propagate extends further into the Pacific, thus favouring the development of LLRWPs that last longer in the atmosphere.

We also studied whether weather forecast models can predict the development of LLRWPs in two sub-seasonal forecast models, and under which circumstances we obtain good/bad LLRWPs forecasts. This is done by comparing the trajectory of the LLRWPs observed in the reanalysis against their predicted trajectory in forecast models. We obtain the best LLRWPs forecasts with the manifestation of negative SAM events, and when the Madden-Jullian Oscillation is inactive.

Lastly, we examined whether LLRWPs are associated with wave breaking events (RWB) that develop into atmospheric blockings by applying two additional algorithms, one that detects RWB events, and another one that follows atmospheric blockings. Results show that around 1/5 times a blocking event appears, it is preceded by a RWB. However, we barely find RWB events linked to RWPs, and thus, it seems that there is not a direct link between LLRWPs and atmospheric blocking development.

Key Words

Rossby Wave packets, Rossby wave breaking, atmospheric blocking, El Niño Southern Oscillation, Southern Annular Mode, sub-seasonal forecast model

Figure and tables list

Figure list

Tables list:

1| INTRODUCTION

1.1 Motivation

Extreme weather events such as heatwaves, cold spells or intense rainfall are events with low frequency of occurrence, but due to their intensity, they cause severe destruction and human losses in the areas they cross. In fact, between 1979-2020 it was estimated that extreme weather events caused over 2 million deaths and damages worth 3.64 trillion US$ (WMO Atlas of Mortality and Economic Losses from Weather). Additionally, activities from the primary sector such as agriculture, farming or fishing, which are highly dependent on climate and weather, are especially vulnerable to extreme weather events (Rosenzweig *et al.,* 2001). Therefore, regions whose economical activity heavily relies on the primary sector such as South East South America, are extremely vulnerable to these phenomena (Bidegain *et al.,* 2012). One example is the country of Uruguay, where more of the 70% of the exports come from livestock and agriculture.

Several studies have shown that these extreme weather events will appear more often and with higher intensities in the future, and thus, damages and casualties caused by these events will increase worldwide (Aguilar *et al*., 2005, Marengo *et al.,* 2009, Skansi *et al.,* 2013, Stot *et al.,* 2016). As a result, this will endanger not only the food security of several continents, such as South America (Reyer *et al*., 2017), but also reduce the total land available for agriculture purposes (Zhang and Ximing 2011), and increase the vulnerability of several regions to climatic hazards in the medium-long term (IPCC Sixth Assessment Report 2022). Therefore, it is key the early detection of these extreme events in order to mitigate future damages. Nonetheless, the weather forecast is limited to 7-10 days due to the chaotic nature of the atmosphere. To expand the prediction horizon the international community is currently embarked in understanding the oceanic-atmospheric processes and phenomena that may increase the predictability in the sub-seasonal time scale (10-90 days). One of these phenomena are the Rossby Wave Packets or RWPs.

RWPs are upper-level atmospheric waves represented as high amplitude meanderings of the jet stream, which travel by downstream development (Tu-Cheng Yeh, 1949; Chang & Yu, 1999; Chang, 2000). During their propagation, they transport large quantities of energy, modifying the weather in

the areas they cross. RWPs are related to storm track variability (Souders *et al*., 2014a), and are considered as precursors of extreme weather events such as heatwaves, extreme rainfall (Chang, 2005; O'Brien & Reeder, 2017; Wirth *et al.,* 2018), as well as extratropical cyclone development (Chang *et al.,* 2005; Sagarra & Barreiro, 2020). They also increase the uncertainty of short-middle range forecast (Zheng *et al.,* 2013; Souders *et al.*, 2014b). Most RWPs last less than a week in the atmosphere, but under certain conditions, RWPs can survive up to 2-3 weeks in the atmosphere, thus providing a source of predictability beyond the synoptic time scale. When a RWP lasts more than 8 days in the atmosphere it is considered a long-lived RWP or LLRWP.

Sometimes, at the end of their lifespan, atmospheric packets lose their stability and "break" in the atmosphere, interrupting the local wind and energy flow. This is called a Rossby Wave Breaking event or RWB (Simmons and Hoskins 1978, McIntyre and Palmer 1983, 1984). RWB events are linked to weather systems such as upper level cutoff lows and anticyclones (Pelly and Hoskins 2003, Ndarana and Waugh 2010, Jing and Banerjee 2018). Also, with enough temporal and spatial scale, a RWB event can behave like an atmospheric blocking event (Berrisford *et al., 20*07), which is linked to the development of extreme weather events such as heatwaves and droughts (Masato *et al.*, 2011, Weijenborg *et al.,* 2012, Patterson *et al.,* 2019).

RWPs have been extensively studied in the northern hemisphere, however, there are much less studies in the southern hemisphere, and most of them focus on the climatology of these wave packets. Hence, we need to understand which processes modulate LLRWPs variability, as well as to determine whether weather forecast models can accurately predict the development and trajectory of these wave packets. It is also important to assess whether the RWB events associated with RWPs are able to trigger an atmospheric blocking, causing the development of heatwaves or droughts. Addressing these issues is not only crucial to understand the mechanisms that affect weather and climate in southern hemisphere mid-latitudes, but also to enhance the detection of extreme weather events between 10-30 days before they occur. Throughout this study we focus on the austral summer as it is a season that presents large variability and the extended prediction would strongly help the economy of South American countries.

In order to improve our understanding of the variability and predictability of RWPs and their link to atmospheric blocking, we need to answer 3 questions:

(1) What atmospheric conditions favour the development of long-lived episodes of RWPs?

(2) Are these long-lived episodes of RWPs well represented in the weather forecast models?

(3) Do RWPs cause the development of RWB events with enough spatial and temporal scale to behave like atmospheric blocking?

Regarding the first question, Barreiro (2017) found that there is an increase in transient RWP activity in the Pacific during El Niño years. Also, Sagarra and Barreiro (2020) studied the climatology of RWPs during austral summer and suggested a possible relationship with SAM and RWPs activity. Nonetheless, neither of the mentioned studies assess in a systematic way the interannual variability of RWPs, and how the main global climate modes influence RWPs activity.

With reference to the second question, some studies such as Gray *et al.,* (2014) and Quinting and Vitart (2019) reported about the predictability of RWPs in forecast models focusing only on the northern hemisphere and did not take into special consideration the representation of LLRWPs, which is around 10% of the total RWPs.

As regard to the third question, there is a fair number of studies about RWB events, both in the northern hemisphere (Strong and Magnusdottir 2008, Masato *et al*., 2011, Michel and Riviére 2011, Ryoo *et al.,* 2013) and southern hemisphere (Ndarana and Waugh a,b 2010, Wand and Magnusdottir 2010, Barens *et al.,* 2012). On the other hand, atmospheric blocking is a topic that has been extensively studied in both hemispheres (Renwick 1999, Berrisford *et al.,* 2007, Masato *et al.,* 2011, 2013, Mendes *et al.,* 2011, Nakamura and Huang 2018, Lupo 2020). Some studies try to assess the link between atmospheric blocking and RWB (Berrisford et al., 2007,Weijenborg *et al.,*2012, Masato *et al.,* 2013), but we did not find a study which directly assessed the link between the dissipation of a propagating RWP with the development of a RWB event, or that considered whether RWB events caused by RWPs can be linked to the development of atmospheric blockings.

Thus, the goals of this study are: first, to have a better understanding of the large scale atmospheric conditions that affect LLRWPs activity. Second, identify and assess which atmospheric configurations favour/disfavour an accurate forecast of LLRWPs. And third, study the link between RWB events caused by RWPs and atmospheric blocking development. For these three objectives we focus on LLRWPs because their study may contribute to the improvement of extended range forecasting (between 10 and 30 days) of extreme weather events.

1.2 Objectives

The main goal of this study is to analyse the interannual variability of RWPs during austral summer, and their representation in forecast models, focusing on LLRWPs, as well as to assess whether the dissipation of transient RWPs is linked to atmospheric blocking development. In order to fulfil this goal, the specific objectives are:

1.-Determine how the main climate modes that affect the southern hemisphere circulation, that is the El Niño Southern Oscillation (ENSO) and the Southern Annular Mode (SAM), influence the development of LLRWPs.

2.-Assess how sub-seasonal to seasonal (S2S) forecast models are able to represent the development and trajectories of LLRWPs, as well as to determine the conditions that lead to accurate/inaccurate forecasts of LLRWPs.

3.-Study the link between RWB events and RWPs, and identify whether RWB events are linked to atmosphere blocking development.

This thesis is organised in 9 chapters, chapter 2 describes the large-scale atmospheric circulation in the southern hemisphere during the austral summer, and defines extratropical Rossby Wave Packets, Rossby Wave Breaking and atmospheric blocking events. Chapter 3 describes the main modes of variability that affect weather and climate in the southern hemisphere. Chapter 4 explains the tracking algorithms used to detect and follow Rossby Wave Packets, Rossby Wave Breaking and atmospheric blocking events. Chapter 5 consists of a study about the impact of SAM and ENSO on LLRWPs development during austral summer. Chapter 6 includes the assessment of the representation of the long-lived RWPs in two S2S models. Chapter 7 presents the study of Rossby Wave breaking episodes linked to the dissipation of RWPs. Chapter 8 is a summary of the results. Finally, chapter 9 includes the scientific articles published with the results obtained during the PhD and the appendix describes basic Rossby Wave theory.

2| LARGE-SCALE ATMOSPHERIC CIRCULATION DURING AUSTRAL SUMMER

Large scale atmospheric circulation shapes weather and climate on a global scale. Therefore, without the knowledge of the mean atmospheric flow, it is not possible to understand the climate and weather of a region. Thus, the goal of this chapter is to describe the main atmospheric global circulation patterns of the southern hemisphere, as well as to define the large-scale synoptic structures considered in this study, such as the RWPs.

The southern hemisphere is strongly dominated by the ocean (only about 20% of this hemisphere is covered by land) and lacks high altitude orography compared to the northern hemisphere. Consequently, the mean wind flow of the southern hemisphere is different compared to its northern counterpart. For example, in the northern hemisphere, low pressure systems manifest over the ocean and high pressure systems over the continents in boreal winter, and the opposite occurs in boreal summer. Oppositely, in the southern hemisphere there are less seasonal changes and the circulation is more zonally symmetric, as a result, stationary eddies are much less prominent and stable compared to the northern hemisphere due to a more zonal and narrow wind flow (Randall 2004 chapter 3).

As mentioned before, in this work, we focus on austral summer, here considered as the time period between December-March months (DJFM). Thus, in this chapter we focus exclusively on this season. The next sections describe the mean flow, and define extratropical RWPs, Rossby Wave Breaking events or RWB, and atmospheric blocking events.

2.1 Large-scale circulation in the Southern Hemisphere

The atmospheric global circulation is triggered due to the uneven distribution of solar radiation received across the Earth, with the largest amount reaching at the equator and the minimum at the poles. Ideally, the resultant temperature gradient would cause the rise of warm air masses at the equator from the surface towards the upper levels. Then, these warm air masses would travel to the pole, descend to the surface and lastly, return to the equator, restarting the cycle. Nonetheless, due to the Earth's rotation and orography, the wind and energy flow in the atmosphere is altered, causing the development of three main wind cells (Hadley, Ferrel and polar) in both hemispheres which redistribute heat

and energy in the atmosphere. Moreover, the upper levels are characterised by jet streams in the subtropics and polar latitudes that appear due to conservation of angular momentum and the convergence of eddy momentum fluxes, respectively (Fig 1). During summer both jets merge into one located inside the Ferrel cell, that is in midlatitudes, with the core close to the level of 300 hPa (Lachmy and Harnik 2014).

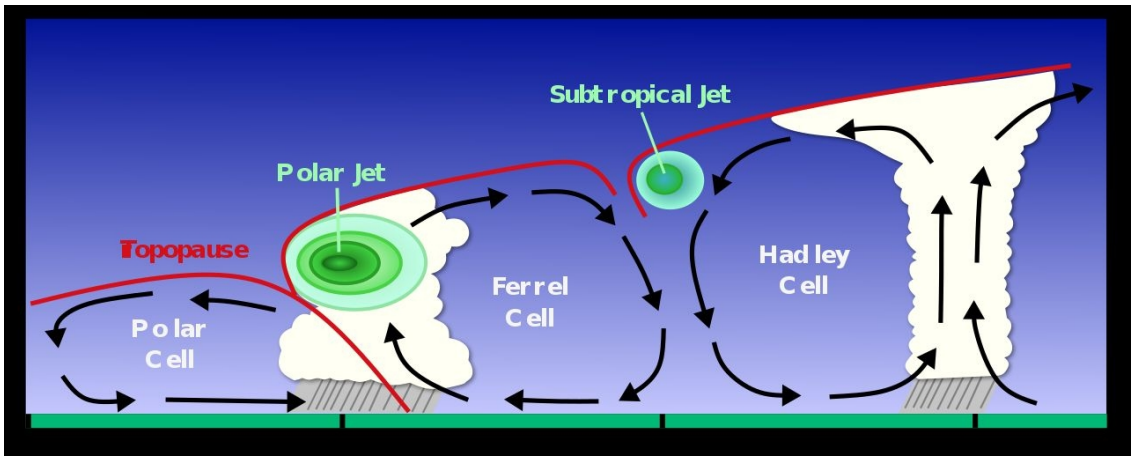

Fig 1. Position of the global jet streams in relation to atmospheric circulation cells. (Source: NOAA).

The location and intensity of the jet streams greatly affects the weather and climate conditions in the lowest layers in the atmosphere. For example, in the southern hemisphere, a strengthening of the polar jet reinforces the polar vortex, limiting the interaction between warm air masses from the subtropics and cold air from the poles. As a result, it favours pleasant and dry weather at mid-latitudes (Thompson and Wallace 2002). On the other hand, if the polar jet stream weakens, the polar vortex is debilitated, enabling the interaction between polar and warm air in mid latitudes (Shulmesiter *et al.,* 2004,, Mayewski *et al.,* 2017), consequently, it enables the development of cold fronts that bring humid and cold air as well as precipitation in mid-latitudes. As we stated earlier in this section, in this hemisphere there is a lack of high altitude orography and it is mainly dominated by the ocean, consequently, the mid-latitudes jet stream has a more intense and zonal wind flow and less eddy structures compared to its northern counterpart. As a result, the climate and weather of the southern hemisphere shows more precipitation and wind extremes compared to the northern hemisphere (Pfahl and Wernli 2012, Messmer and Simmons 2021, Shaw *et al.,* 2022).

Fig 2 shows the climatological monthly mean of the zonal wind at 300 hPa, U_{300}, during DJFM season. It is seen that the polar jet stream is centred at around 50ºS, showing the highest values of zonal wind speed within the South Atlantic-Indian basin, and its lowest at the Pacific basin (also Chang 1999).

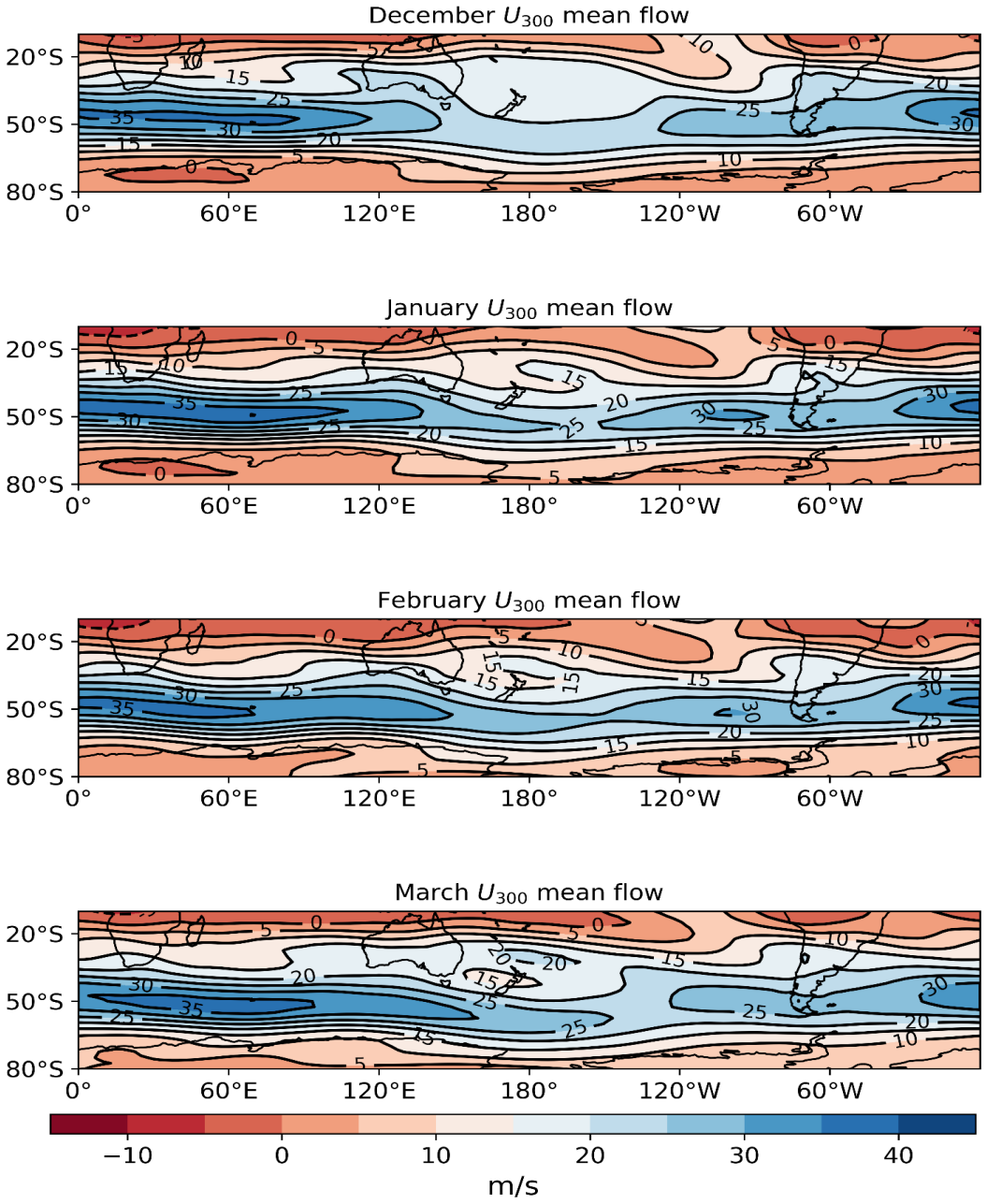

Fig 2. Climatological U_{300} from December to March between 1979-2020 in the southern hemisphere (ERA5 reanalysis).

The more zonal and narrow the wind flow is, the better it acts as a waveguide where atmospheric waves propagate (Chang and Yu 1999, Souders *et al.,* 2014b, Manola *et al.,* 2013, Wirth *et al.,* 2020). One way to estimate the narrowness of the wind flow is to measure the isentropic gradients of the potential vorticity (PV) field, which has been used as a measure of the strength and position of the waveguide where RWPs propagate (Hoskins & Ambrizzi, 1993). Another, and simpler, approach is to calculate the meridional gradient of absolute vorticity or mAvg (defined in equation 1), which is a good approximation of the potential vorticity field for a given altitude (Wirth *et al.,* 2018).

$$mAvg = \partial \frac{(\partial v/\partial x - \partial u/\partial y) + f}{\partial y} \quad (1)$$

With *f* as the planetary vorticity and u (v) the zonal (meridional) wind speed at a given altitude. Positive (negative) values of mAvg indicate that RWPs propagation is favoured (damped) in the area (Hendon 2018).

Fig 3 displays the mean zonal wind speed and mAvg gradient at 300 hPa during DJFM season. As expected, the climatological zonal wind flow in the southern hemisphere is close to the observed in Fig 2. Furthermore, the areas of maximum mAVg are located where the jet stream reaches its peak intensity, that is in the Atlantic-Indian basin. Oppositely, in the Pacific basin, where the jet stream weakens, the positive mAvg field is the weakest of the mid-latitude region, and it is shifted towards polar latitudes. On the other hand, in subtropical and polar latitudes the mAVg field is less intense or even negative compared to mid-latitudes, suggesting that the propagation of atmospheric waves is restricted.

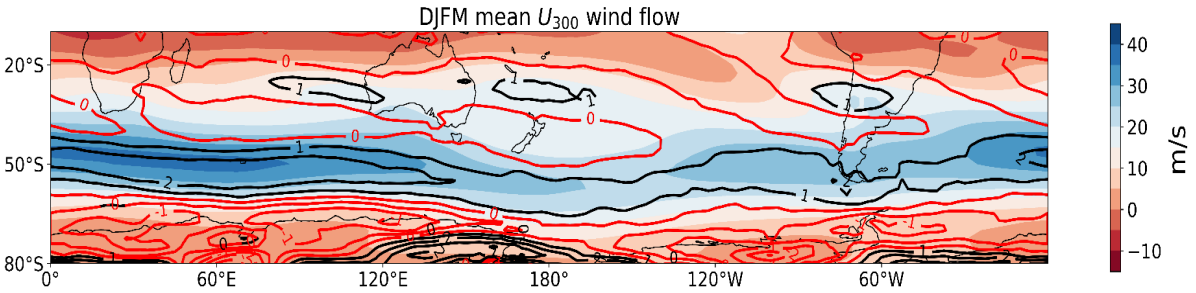

Fig 3. Climatological U_{300} wind and mAvg flow from December to March between 1979-2020. Black (red) contours show positive (negative) areas of mAVg (ERA5 data).

2.2 Characteristics of Rossby Wave Packets

Appendix A describes the theory behind the propagation of Rossby waves with a sinusoidal shape. However, in the real atmosphere it is very rare to find a Rossby Wave with such a pattern. Instead, the amplitude of the wave packet changes with time and longitude [A(λ,t)], and consequently, Rossby waves appear as a series of troughs and ridges that travel in a confined longitudinal section. Consequently, Rossby Waves propagate in coherent wave packets or wave trains (Chang *et al.,* 1999, Chang 2005, Wirth *et al.,* 2018), and hence they are called Rossby Wave Packets or RWPs.

Fig 4 shows the lagged anomalies of meridional wind speed at 300 hPa during the manifestation of a RWP. In that figure, we observe alternating positive and negative centres of meridional wind speed propagating between the eastern Pacific-South Atlantic western basin at mid-latitudes. This pattern represents the troughs and ridges that appear in the upper levels westerlies while the RWPs are propagating; the observed packet has a wavenumber close to 6.

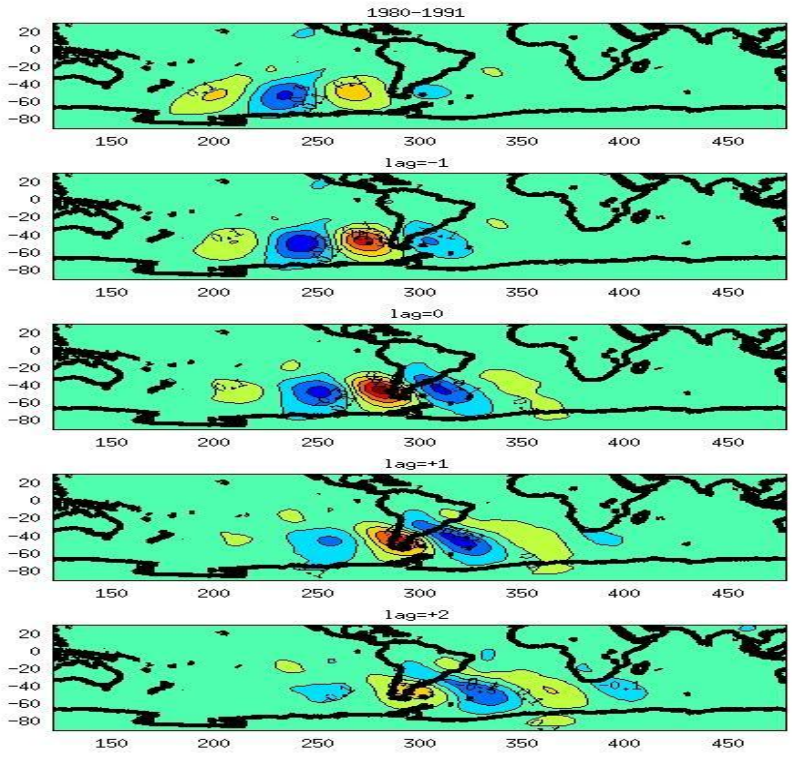

Fig 4. Linear regression of meridional wind speed at 300 hPa with respect to a point located at 80ºW 40ºS using different lags (-2 to +2) days in order to show the RWPs propagation during southern hemisphere summer. Positive values (yellow-red colours) highlight anomalies to the north and negative values (blue-dark blue colours) to the south.

The characterization of wave packet propagation is usually done in terms of the envelope, which travels at the group velocity. Moreover, the group velocity for Rossby waves is larger than the phase speed of individual troughs and ridges. This can be shown using the dispersion relation of Rossby waves on the beta-plane (expression 2) assuming a purely zonal basic flow u_0 (e.g. Wirth *et al.,* 2020)

$$w = u_0 k - k\beta/(k^2 + l^2) \quad (2)$$

where k and l are the zonal and meridional wavenumbers of the packet and β the northward gradient of planetary vorticity.

From the dispersion relation we can calculate the zonal phase speed of the packet (the speed at which individual troughs and ridges propagate) as c= w/k, and the zonal group velocity (the entire RWP propagation speed) as $c_g = \partial w/\partial k$. Since β >0, we find that $c_g > c$, and therefore, the envelope of the Rossby waves travel eastwards faster than the individual troughs and ridges.

The eastward propagation of energy can be described by computing the eddy kinetic energy equation, which shows that it is the result of the divergence of the ageostrophic geopotential flux (Lackmann 2012 Chapter 2). In particular, there will be convergence of energy flux ahead (or downstream) of the wave packet making it grow, and divergence behind (or upstream) that result in a weakening. Consequently, new troughs will appear at the east of the original packet, which is downstream of the original packet. This phenomena is called “downstream development” because the mid-latitude winds flow eastward, and the new troughs appear to the east, which is downstream of the original packet (Tu-Cheng Yeh, 1949; Chang & Yu, 1999, Chang, 2000, Wirth *et al.,* 2018). Downstream development processes enable the extension of the storm tracks from very unstable baroclinically regions towards areas with low baroclinicity (Orlanski and Sheldon 1995). Consequently, downstream development favours the transport of large quantities of energy, moisture and momentum across large distances (Tu-Cheng Yeh 1949, Chang and Yu 1999; Chang 2000).

2.3 State of the art of the study of extratropical Rossby Wave Packets

This study focuses on extratropical RWPs, that is, synoptic scale RWPs that propagate within mid-latitudes, here considered as the band (40-65ºS). As mentioned above these packets are related to storm track variability (Souders *et al.,* 2014a), and are considered precursors of extreme weather events, such as extratropical cyclone development, extreme rainfall among other events (Grazzini and Vitart 2015, Wirth *et al.,* 2018). RWPs can appear for several

reasons that involve diabatic heating in the atmosphere. For example, they can be created due to the extratropical transition of a tropical cyclone, by a burst of tropical convective systems associated to the Madden-Jullian Oscillation, by flow distortion caused by the orography, or even as a result of the downstream propagation of a pre-existing packet (Chang and Yu 1999, Grazzini and Vitart 2015). Baroclinic conversion from the mean flow available potential energy is an important mechanism for the amplification of an initially small perturbation, consistent with studies reporting that RWPs form preferentially in regions of enhanced baroclinicity (e.g., Chang *et al.,* 2002, Wirth *et al.,* 2018). Usually, RWPs survive less than a week in the atmosphere, although under certain circumstances these packets can last up to 2-3 weeks before disappearing (Grazzini and Vitart 2015, Sagarra and Barreiro 2020).

The lifespan, extension and propagation of RWPs are highly dependent on the PV gradient and the distribution of diabatic heating sources (Grazzini & Vitart, 2015). A very intense and narrow gradient of PV, associated with the jet stream, favours the development of coherent RWPs that will last longer while, on the other hand, weaker gradients tend to stop or attenuate wave propagation (Chang & Yu, 1999; Manola *et al.*, 2013, Souders *et al.,* 2014b, Grazzini and Vitart 2015, Wirth 2020).

RWPs have been extensively researched in the northern hemisphere, whereas in the southern hemisphere there are less studies, and most of them focused on the climatology of the packets. Chang (1999) concluded that during the summer season of both hemispheres the RWPs propagate following mid-latitude waveguides. Oppositely, during the winter season, RWPs tracking is more difficult in both hemispheres due to the split of the jet stream which causes the manifestation of more waveguides (Chang 1999b). Souders *et al.,* (2014b) studied the climatology of RWPs and found that in the northern hemisphere RWPs activity reaches its peak in January and the minimum during boreal summer. However, in the southern hemisphere RWPs activity did not show a marked seasonal cycle. Additionally, Grazzini and Vitart 2015 observed that the presence of RWPs with long lifespan in the northern hemisphere forecast increases the skill of the forecast of 2-3 weeks in advance.

Some studies showed that RWPs detected in the southern hemisphere are more coherent and easier to track compared to their northern hemisphere counterparts (Chang 2001, Grazzini and Vitart 2015). Also, in the southern hemisphere RWPs are more easily detected due to the absence of baroclinically unfavourable continental areas, and have a higher lifespan compared to packets found in the northern hemisphere (Souders *et al.,* 2014b, Grazzini & Vitart, 2015). As shown in Figs 2 and 3, during austral summertime,

the storm track is almost zonally symmetric at 50ºS, and the jet stream presents a wind speed maximum in the Atlantic-Indian sector that acts as a waveguide (Hoskins & Ambrizzi, 1993; Chang, 1999). Chang, (1999) found that the RWPs zonal group velocity in the southern hemisphere summer is about 20–25 m/s, and that RWPs travel mainly zonally. In addition, Chang (2000) showed that most wave packets propagate when dominated by downstream development, and that during the propagation of a RWPs, a surface cyclone manifested in nearly all cases to the east of the upper-level troughs. Chang (2000) also found a positive trend in the annual mean activity of RWPs that they hypothesise may be related to an improvement of the quality of the reanalysis (consistent with Barreiro *et al.*, 2014) or to the observed trend in the Southern Annular Mode (SAM) during summer.

Barreiro (2017) studied the interannual variability of wave activity during austral summertime in the southeast Pacific-Atlantic sector, and found that the leading pattern of variability in this region is correlated with El Niño-Southern Oscillation (ENSO), such that there is an increase in transient wave energy in the Pacific during El Niño years. However, this study did not address the characteristics of RWPs. Sagarra and Barreiro, (2020) performed a climatological study of RWPs during the austral summer in the Southern Hemisphere and found a mean of 32 packets per season. Moreover, they report that 90% of the trajectories have a lifespan of 3–8 days and 80% of the waves propagate between 30 and 170 degrees of longitude. No main area of dissipation/formation on seasonal or monthly timescales was detected and the study did not find a relation between the interannual count of RWPs and ENSO, but suggested a possible relationship with SAM.

2.4 Rossby Wave Breaking

Rossby wave breaking or RWB is a phenomenon that occurs when Rossby waves attain very large amplitudes, and reach a critical point at which the crest or trough of the wave packet overturns (Jing and Banerjee 2018). This causes the deformation of the PV field on the potential temperature surface (McIntyre and Palmer 1983). As a result, the usual meridional PV gradients become zero or even reverse, enabling the exchange of air masses between the upper troposphere and the stratosphere (Simmons and Hoskins 1978, McIntyre and Palmer 1983, 1984, Berrisford *et al.*, 2007, Michel *et al.,* 2011).

RWB events modify the local wind and energy flow in the area they occur, and are considered precursors of weather regime transitions (Michel and Riviére 2011) Hence, they are key to understand atmospheric processes like atmosphere blockings, (Pelly and Hoskins 2003; Berrisford 2007, Ndarana and

Waugh 2010b) cutoff lows (Ndarana and Waugh 2010 a,b). Also, RWB events can also increase the prediction skill of precipitation (Ryo *et al.,* 2013). When RWB events reach a certain spatial and temporal extent, they are synoptically recognized as an atmospheric blocking (Berrisford *et al.,* 2007). Nonetheless, even if we find some RWB events prior to the onset of some atmospheric blockings (Altenhoff *et al.,* 2008), not all RWB events will be associated with blocking (Hitchman and Huesmann 2007, Masato *et al.*, 2013).

RWB events can be classified according to their shear (Thorncroft *et al*., 1993):

(1) cyclonic RWB events, where air from the dynamical tropopause with low potential temperature ("cold" air), goes eastward from high to mid-latitudes, at the same time, at the east of this "cold" air, there is an air mass from the high troposphere with high potential temperature (warm air) that goes poleward and westward from mid-latitudes towards the high latitudes.

(2) anticyclonic RWB events, where "cold" air from the tropopause goes westwards from middle to high-latitudes. Simultaneously, at the west of this "cold" air, a "warm" air mass from the upper troposphere goes eastward and towards equatorial latitudes.

Fig 5 shows an example of an anticyclonic (Fig 5a) and cyclonic (Fig 5b) RWB event.

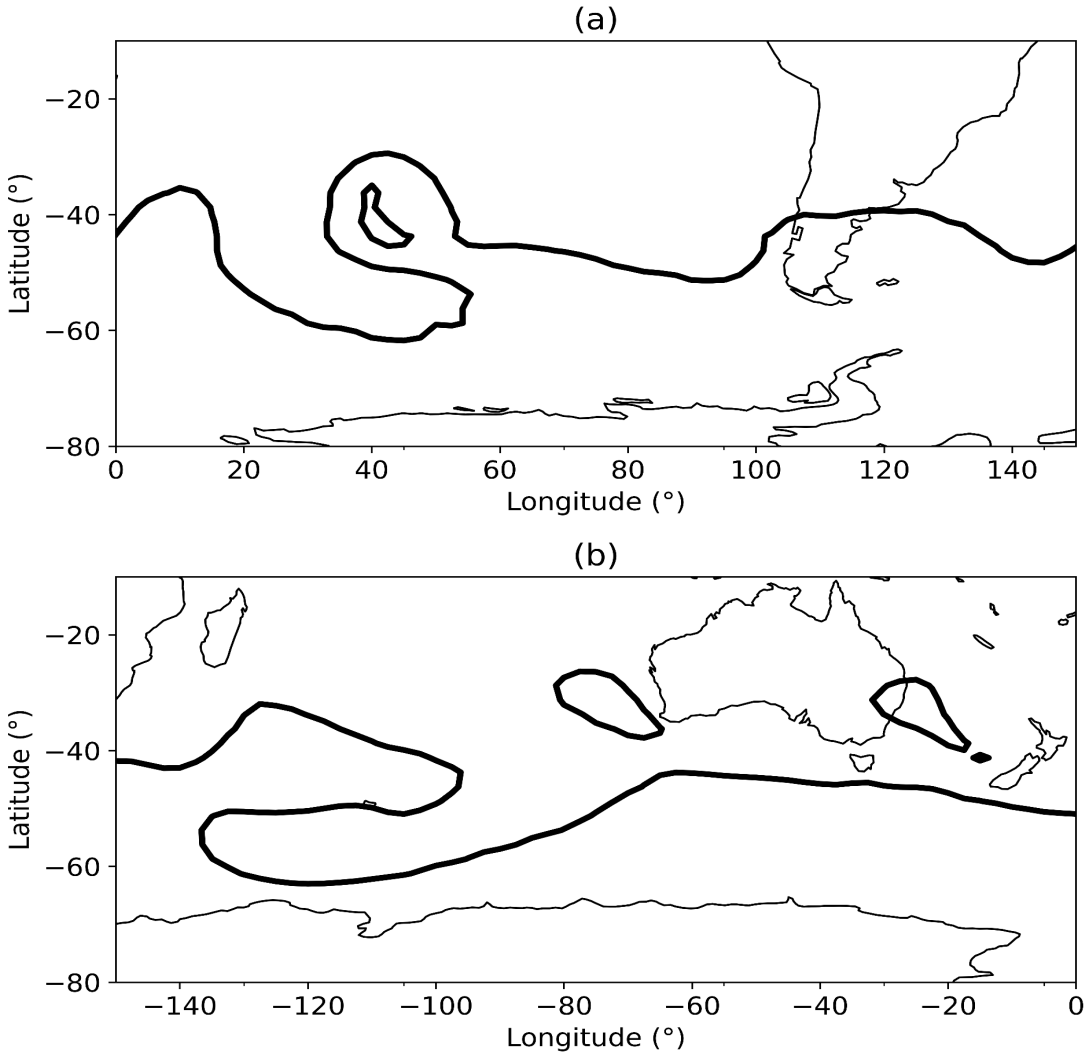

Fig 5. Potential vorticity contour of -2PVU units (1PVU= m^{-2} K kg^{-1} s^{-1}) following the 330º K isentropic isosurface during a RWB event with anticyclonic (a) and cyclonic (b) shear.

RWB events have been studied both in the northern hemisphere (e.g. Strong and Magnusdottir 2008, Masato *et al*., 2011, Michel and Riviére 2011, Ryoo *et al.,* 2013) and in the southern hemisphere (Ndarana and Waugh 2010 a,b, Barnes and Hartmann 2012). Thorncroft *et al.,* 1993 showed that in the northern hemisphere, anticyclonic RWB events are much more common than cyclonic RWB, and the same pattern was observed in the southern hemisphere (Ndarana and Waugh (2010b), Peters and Waugh 2003). This tendency was associated with the fact that the dynamical tropopause tends to be within regions of anticyclonic shear, and consequently Rossby Waves that travel in the tropopause tend to break in an anticyclonic fashion. Also, they found that during austral summer (December to February) RWB activity is mostly focused on the western Indian ocean-Pacific basin, and that the seasonal displacement of the

jet stream affects the frequency and main areas of RWB activity. Finally, they report that RWB activity is the weakest during the austral summer.

Thorncroft *et al.,* (1993) highlighted that RWB frequency is affected by phenomena that are able to alter the usual wind flow. In that regard, Strong and Magnusdottir (2008) observed that the positive (negative) Northern Annular mode favours anticyclonic (cyclonic) RWB activity in the northern hemisphere. For the southern hemisphere, Berrisford *et al.,* (2007) discovered that during wintertime, mid-latitude RWB is centred in the east Pacific whereas during summertime it is more scarce and occurs mostly in the west Pacific, which is in qualitative agreement with the main blocking detection areas in the Southern hemisphere. Gong *et al.,* (2010) studied how SAM and ENSO influence RWB activity in the southern hemisphere during austral summer, and concluded that years with positive SAM phases showed higher RWB activity compared to years with negative SAM phase. Also, Wang and Magnusdottir (2010) concluded that changes in the background flow induced by ENSO affect RWB frequency of occurrence.

2.5 Atmospheric blocking

An atmospheric blocking is defined as a nearly-stationary large scale pattern in the pressure field that arises from the reversal of the westerly wind flow, which can last from several days to weeks in the atmosphere (Rex, 1950). There are three main types of blockings: the inverted omega, the inverted high-over-low, and the stationary ridge. During their lifetime, this phenomenon blocks the displacement of low pressure systems due to the development of a quasi-stationary anticyclone of great magnitude. As a result, blocking events drastically changes the atmospheric flow, impeding the propagation of synoptic systems (Sinclair, 1996, Wiedenmann *et al.,* 2002). Consequently, atmospheric blocking development is linked to the manifestation of extreme weather events such as heat waves or droughts (Woollings, *et al.*, 2018).

Atmospheric blocking is one of the most studied atmospheric phenomena by meteorologists in the last century (e.g. Garriott 1904, Lupo 2020). In the northern hemisphere, atmospheric blocking events occur at the end of climatological storm tracks (Lupo and Smith 1995, Wiedeman 2002, Davini *et al.,* 2012). Also, Narinesingh *et al.,* (2020) showed that blocking maxima are located near stationary or standing high pressure anomalies as well as at the end of the storm tracks, whereas the minima appeared near jet maxima as well as the entrance of the storm track. The areas of maximum blocking activity are located in the eastern Atlantic-Asian continent, and the western region of the North-America continent. Furthermore, previous studies found around 30-35

annual blocking events in the northern hemisphere with a mean lifespan of 9 days (Lupo 2019, 2020). Lastly, blocking events occurred most frequently in winter and early spring, whereas during summer and early fall these events occurred less often (White 1975, Lupo 1995). In addition, studies have shown that atmospheric blocking is linked to intraseasonal variability, such as the Pacific North pattern (Renvwick *et al.,* 1996) or the MJO (Henderson *et al.,* 2016, Gollan and Greatbatch 2017, Lupo 2020).

In the southern hemisphere results showed that most blocking activity occurs at the Pacific basin, mostly near Australia and New Zealand, followed by the Southeastern Pacific. On the other hand, the number of blocking events in the Southern Atlantic and Indian Ocean are much lower in comparison (Lejenas 1984, Wiedenmann 2002 Mendes *et al.,* 2011, Lupo 2019, Giacosa *et al.,* 2020). Southern hemisphere blocking displays large variability, especially over the western Pacific and the Australian region (Lejenas 1984), where the highest blocking activity is found in winter and early spring (Damião 2007, 2008, Mendes *et al.,* 2011, Lupo 2020). Additionally, the mean blocking lifespan is around 7-8 days, and they are not as intense as in the northern hemisphere (Damião 2012, Lupo 2020).

The occurrence of atmospheric blocking events in the southern hemisphere decreased during the previous century to a relative minimum during the 1990s, and then increased again during the early 21st century (Lupo 2019, 2020). Also, in this hemisphere, the interannual variability in relation to ENSO did not change over the 50-year time series and blocking was found more frequent and stronger during El Niño years when compared with La Niña years (Lupo 2020).

Fig 6 shows the geopotential height anomaly at 500 hPa (Z_{a500}) flow during the manifestation of an atmospheric blocking that was found at the western Pacific basin, near the South America continent during different seasons.

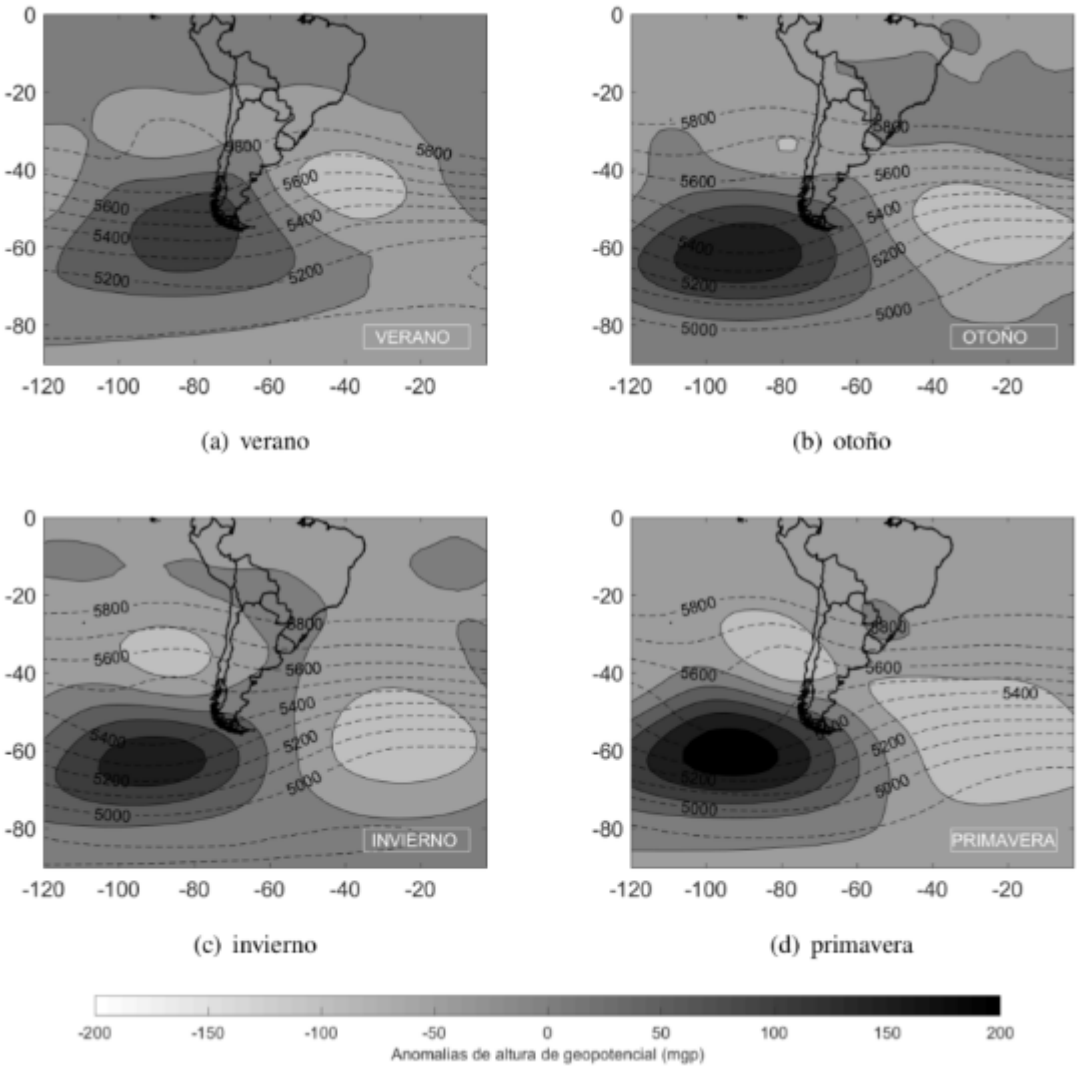

Fig 6. Composite of Z_{a500} (dashed lines) and their anomaly (coloured region) for atmospheric blockings centred in South America in (a) summer, (b) autumn, (c) winter and (d) Spring. Source: Giacosa *et al.,* 2020.

3| CLIMATE MODES OF VARIABILITY THAT INFLUENCE THE SOUTHERN HEMISPHERE CIRCULATION

Weather and climate of the southern hemisphere are strongly affected by remotely forced climate teleconnections. Because these teleconnections can influence the structure and intensity of the mean wind flow, they might play a key role in the formation and development of RWPs. Thus, in this section we will describe the three main climate modes that influence climate and weather in the southern hemisphere from intraseasonal to interannual time scales, which are the Southern Annular Mode (SAM), the El Niño-Southern Oscillation (ENSO) and the Madden-Jullian Oscillation or MJO, and their influence in mid-latitudes.

We describe these climate modes during austral summer (December-March) from 1979 to 2020. We used the ONI (Oceanic Niño index) and SAM indices to characterise ENSO and SAM, respectively, and the RMM index (Wheeler and Hendon 2004) to identify the phase and amplitude of the MJO. The SAM and ENSO indices can be downloaded from the NOAA website (https://www.noaa.gov/), whereas the RMM index is available at the web of the Bureau of Meteorology (http://www.bom.gov.au). The fields considered to represent the associated anomalies in the atmospheric and surface oceanic circulation are sea surface temperature (SST), and zonal wind speed and geopotential height at 300 hPa (U_{300} and Z_{300}) from ERA 5 reanalysis (REF).

3.1 Southern Annular Mode

The SAM is the main mode of tropospheric circulation variability of the Southern hemisphere, and it modulates the large-scale atmospheric circulation in the extratropics (Gong and Wang 1999, Thompson and Wallace, 2000, Li and Wang 2003 Zheng *et al*., 2017). This climatological pattern is characterised by the development of a pressure anomaly centred in the Antarctic, and anomalies of the opposite sign in a circumglobal band around 40-50ºS (Thompson and Wallace 2000). This pattern is mainly zonally symmetric and is believed to be the result of the interaction between eddies and the zonal mean flow (Codron 2005).

SAM can manifest in two possible phases, positive and negative. During SAM positive phases, positive pressure anomalies appear in mid-latitudes, whereas negative pressure anomalies develop in the centre of Antarctica. As a result, the

jet stream is southwardly displaced from its mean position and the westerly winds are intensified in high latitudes (50-70ºS) and weakened in the mid latitudes (30-50ºS) (Gong and Wang 1999). As a result, the polar vortex is intensified, limiting the mixing of cold polar air with warm air that comes from the extratropics. Consequently, positive SAM enables the development of warm and dry weather conditions over South America, increases the chance of winter/summer rainfall in the east of Australia, and also diminishes the mean temperature in the Antarctic continent. On the other hand, during a negative SAM phase, low pressure anomalies are located at mid-latitudes and positive anomalies in Antarctica and, as a result, the jet stream is northerly displaced and the polar vortex is weakened. This enables the interaction and mixing of air masses from high and mid latitudes, favouring the propagation of cold fronts in mid latitudes. As a result, negative SAM events cause humid and cold weather in the South America region (Thompson and Wallace 2000) and at the south-south east of Australia, as well as increase the mean temperature in the Antarctic. Fig 7 shows a graphical representation of the atmospheric circulation associated with the two phases of the SAM.

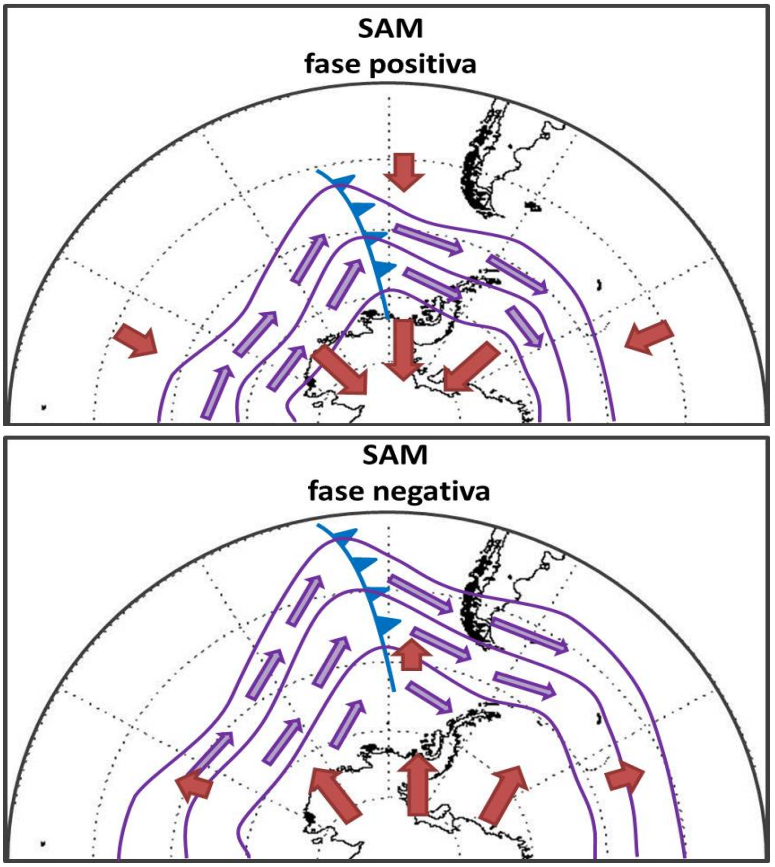

Fig 7. Graphical representations of atmospheric circulation anomalies during the different phases of SAM. Red arrows signal the meridional displacement of the westerlies, purple arrows show the westerlies mean position and blue lines highlight the propagation of a cold front.

In order to identify the phase and intensity of the SAM, we used the Antarctic Oscillation index or SAM index. This index is constructed by projecting the daily 700 hPa height anomalies between 20-90ºS onto the main pattern of the AAO, which consists in the zonal pressure differences between 40-65ºS. A SAM index above 0 signals that the SAM is in its positive phase, and the opposite for the negative SAM.

It is also important to highlight that the SAM has a near 10-day intrinsic time scale, (Feldstein and Lee 1998; Feldstein 2000; Lorenz and Hartmann, 2001, 2003) and, as a result, this phenomenon has large variance in intermonthly and interannual timescales. Moreover, it shows a significant trend towards its positive phase in the last part of the twentieth century (Thompson and Solomon, 2002).

Some studies (Gong *et al.*, 2010) have shown that the SAM is modulated by ENSO, that is, ENSO strongly projects into the symmetrical component of the extratropical wind flow. In particular, during El Niño (La Niña) the subtropical jet stream strengthens (weakens), and favours the manifestation of the negative (positive) phase of SAM (Gong *et al.,* 2010).

Fig 8 displays maps of linear regressions of different fields against the standardised SAM index, as well as the temporal evolution of the SAM index during austral summer between 1979-2020. The index and fields are averaged over the 4 months of the summer season. As expected, Fig 8a shows that with the increase of the SAM index the mean U_{300} flow in mid (high) latitudes weakens (strengthens), consistent with the changes in Z_{300} shown in Fig 8c. On the other hand, Fig 8b displays a decrease in SST in high latitudes with the increase of the SAM index and there is a hint of indication of La Niña in the Pacific, suggesting that the connection between ENSO and SAM is weak. Lasty, in Fig 8d we can observe that during austral summer there is a positive linear trend in the SAM index, consistent with the literature (e.g. Thompson and Solomon, 2002).

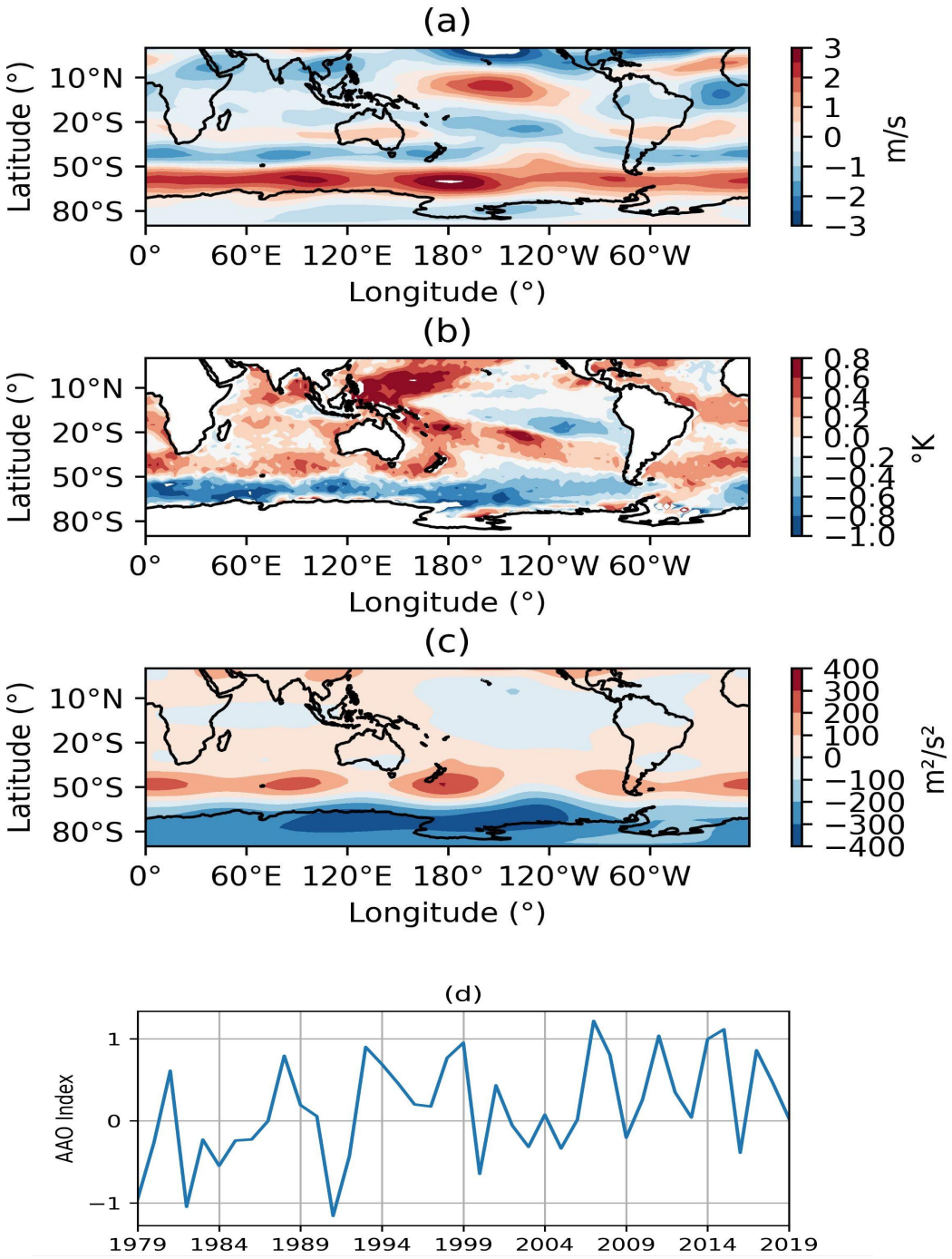

Fig 8. Regression maps different fields against the standardised seasonal mean SAM index, (a) U300, (b) SSTa (c) Z300 (d) Temporal evolution of SAM index during the DJFM season.

Given that SAM directly affects the mean wind flow in mid latitudes, and because the jet stream acts as a waveguide where RWPs propagate, it is plausible to think that SAM could somehow impact on RWPs activity. Sagarra and Barreiro (2000) suggested that SAM events seem to favour the

development of RWPs, but to our knowledge there is no study that assessed the impact of SAM in the interannual variability of RWPs.

3.2 El Niño-Southern Oscillation

El Niño-Southern Oscillation, or ENSO, is the most important climatic mode of variability. It consists of an ocean-atmosphere coupled system associated with a warming/cooling pattern of sea-surface temperature water across the tropical Pacific and changes in the tropical circulation. ENSO affects weather and climate on a global scale, and it is the major source of interannual variability (Aceituno 1988, Marengo 1992, Garreaud *et al.,* 2009, Grimm *et al.,* 2000, Grimm 2011). In particular, in spring about 50% of rainfall variability in the South eastern South America region is explained by the ENSO (Barreiro 2010), and it also plays a key role in rainfall distribution in the eastern and southern regions of Africa (Sazib *et al.,* 2020). Additionally it also affects the areas of baroclinic instability, which are linked with cyclogenesis development (Machado *et al.,* 2020). It is also worth noting that ENSO is able to influence the RWPs activity, such as that years with El Niño stimulates RWP activity in the Pacific basin (Barreiro 2017), but no study has assessed its impact on RWPs characteristics.

The positive phase of ENSO is called El Niño, and it is characterised by warmer than average ocean conditions and weakened trade winds in the equatorial Pacific. Examples of El Niño influence are lasting dry periods over the southern South America region (Ambrizzi 2004), decrease rainfall in Australia during Spring, and increase mean rainfall and the probability of observing extreme rainfall events in the north of Uruguay during the same period (e.g. Barreiro 2010, Ungerovich *et al.,* 2020). On the other hand, the negative phase of ENSO is referred to as La Niña, characterised by cold surface ocean conditions and strengthened trades in the equatorial Pacific. La Niña events tend to have opposite effects to those of El Niño on remote regions: for example they tend to reduce mean rainfall in southeastern South America (e.g. Barreiro 2010). These influences are transmitted to remote regions through the forcing of extratropical wave trains that alter the mean flow and are called atmospheric teleconnections.

The teleconnections during the summer season can be seen by regressing upper level fields onto Fig 9, Fig 9 show the ONI index averaged over the austral summer season (Fig 9d) for several atmospheric and oceanic variables. Figs 9a,c clearly show the upper level anticyclonic anomalies at both sides of the equator consequence of the latent heat release associated with increased precipitation, as well as extratropical anomalies in the south Pacific that resemble the Pacific South American pattern (PSA, Karly 1989). The SST

anomalies include not only the equatorial warming characteristic of El Niño, but also a strong warming in the southern Pacific caused by the atmospheric circulation anomalies forced by El Niño described above.

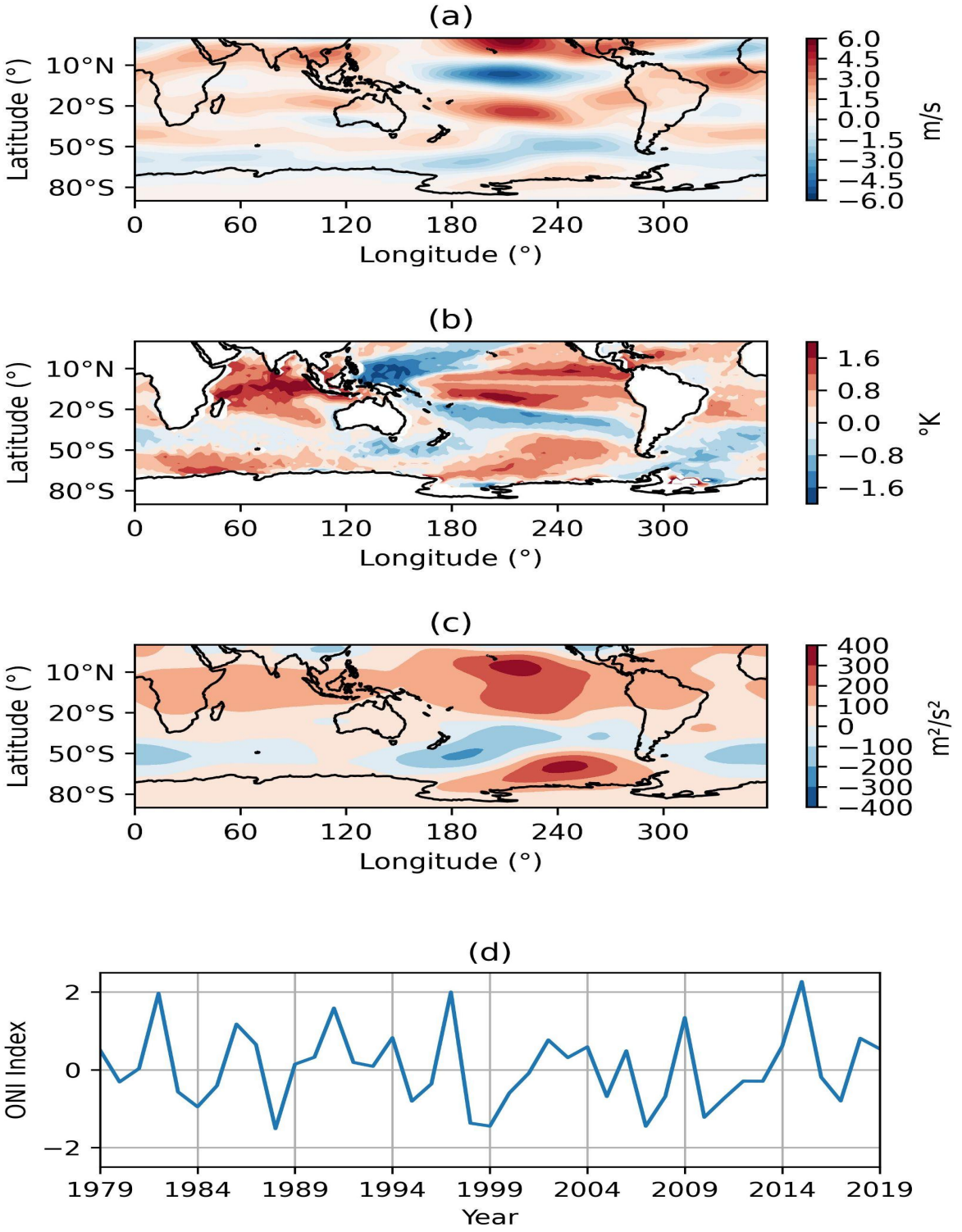

Fig 9. Analogous to Fig 8, but for the ONI index.

3.3 The Madden-Jullian Oscillation

The MJO consists of a series of disturbances of clouds, rainfall, winds and changes of pressure that travel eastward in equatorial latitudes, and then returns to its initial position after 30-60 days on average. The MJO is responsible for the major fluctuation in tropical weather on weekly to monthly timescales and it is composed of two phases, the convective phase, which enhances rainfall, and the suppressed rainfall stage. The propagation of the MJO produces changes in clouds and rainfall in the areas it crosses, and also modifies the weather conditions in regions far away from the equator (Barlow *et al.*, 2006). For example, the MJO increases the frequency of occurrence of extreme dry and wet weather events in South America during austral summer (Alvarez *et al.*, 2016, Muza *et al*., 2009). It also influences El Niño events and tropical cyclones development in the Pacific ocean (Zhang 2005). In addition, the diabatic heating anomalies caused by the MJO excite the formation of Rossby wave trains that can propagate to the Southern Hemisphere (Matthews *et al.,* 2004).

In order to quantify the strength and location of the MJO, Wheeler and Hendon (2004) developed the Real-time Multivariate MJO index, (RMM), which is formed by two indexes: RMM1 and RMM2. These indices are obtained from the two leading Principal Components of the Outgoing Longwave Radiation, and the zonal wind flow at 800 and 250 hPa levels averaged between 15ºS and 15ºN. The state of the MJO is represented as a point in a two dimensional phase space defined by RMM1 and RMM2. The root mean square of RMM1 and RMM2 gives the amplitude of the MJO, quantifying its intensity. When the amplitude of the MJO is below 1, the MJO is considered to be inactive or in its neutral stage. The RMM1, RMM2 space is divided into 8 sectors or phases, each sector marking the geographical location of the MJO, such that phases 1-3 indicate that convection is over Africa or in the Indian Ocean, phases 4-5 within the Maritime continent, and phases in 6-8 in the western Pacific and dateline region (Kiladis *et al.,* 2014). Fig 10 shows the trajectory described by the MJO in RMM1, RMM2 space from 10/12/2022 to 18/01/2023. It shows that between 12-20 of December the MJO was inactive. Next, from the 21 of December up to the 4th of January an active MJO propagated eastward from the Maritime Continent (phase 4) until the centre of the Western Pacific (phase 7). Lastly, on the 5th of January it returned to neutral conditions, and remained inactive until the end of the time period considered.

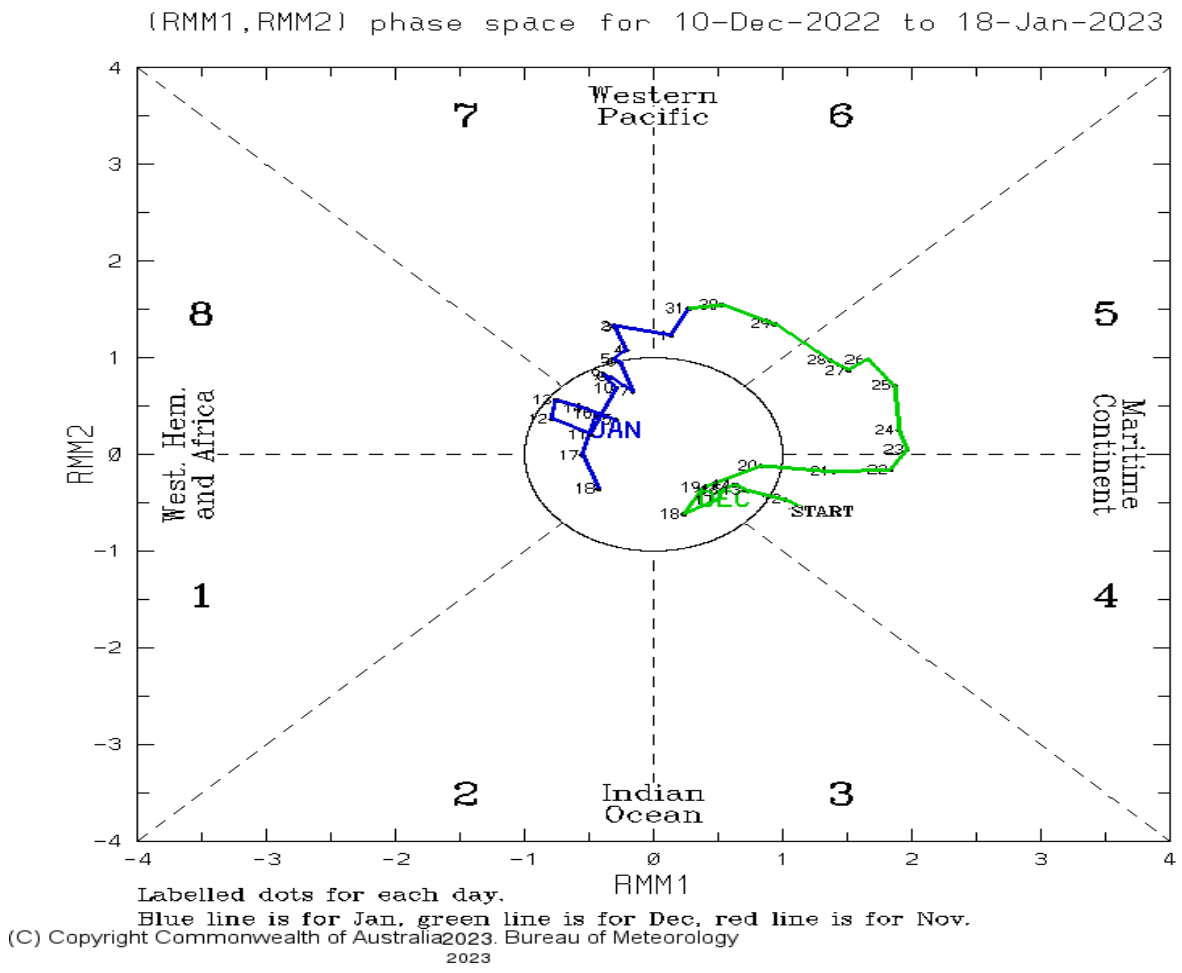

Fig 10. Propagation of the MJO between middle December 2022 to middle January 2023. Green (blue) line signals the propagation of the MJO in the month of December (January). When the MJO is within the centre circle of the Fig, the MJO is inactive or in its neutral phase (source: http://www.bom.gov.au/climate/mjo/).

4| DESCRIPTION OF TRACKING ALGORITHMS

The goal of this chapter is to give a detailed explanation of the tracking algorithms used to detect and follow the evolution of RWPs (section 4.1), RWB events (section 4.2) and atmospheric blockings (section 4.3).

4.1 Rossby Wave Packet tracking algorithm

To track RWPs we use daily mean meridional winds (m/s) at 300 hPa as done previously by several authors (e.g. Chang & Yu, 1999; Sagarra & Barreiro, 2020). RWPs are generally composed of a series of through and ridges confined to a certain zonal band, and thus, it is possible to characterise the RWPs if we compute the envelope that encloses the wave packet. As a result, each RWP is characterised by an envelope whose amplitude has highest values at the centre and decreases to the east and west.

Thus, the first step is to transform meridional wind speed at 300 hPa into wind envelope amplitude at 300 hPa or $V_{300env,}$. This is done by: (1) removing the influence of daily climatology, (2) subtracting the seasonal mean to remove the interannual variability (this is, the variability observed in the DJFM season), and (3) applying the methodology of Zimin *et al.,* (2003), retaining wave numbers between 4 and 11, in order to focus on the transients (Trenberth 1981). The methodology of Zimin *et al., (*2003) requires that RWPs propagation has to be predominantly in the zonal direction (e.g Zimin *et al*. 2006), which is what happens during the Southern Hemisphere summer (Chang 1999). The latter study also showed that the maximum intensity and variance of the jet stream is in a band centred at 50ºS. Thus, in order to track RWPs in mid latitudes we considered the latitudinal band between 40-65ºS.

The second step is to filter low frequency values of V_{300env} so we avoid tracking noise. Thus, we need to set a minimum V_{300env} threshold. Nevertheless, the value of this threshold is not obvious because there are no physical properties that separate one packet from another (Souders *et al*., 2014b). Thus, a low threshold will cause the tracking of noisy fluctuations, and a high threshold will miss some RWPs. Therefore, the selection of the threshold will change depending on the meandering and intensity of the jet stream in the dataset considered.

Lastly, we apply the tracking algorithm, which is based on the maximum envelope method (Grazzini and Vitart 2015, Sagarra and Barreiro 2020, Perez *et al.,* 2021). This technique locates areas with the maximum daily value of the V_{300env}, (which is the centre of activity of the RWPs), and follows their propagation to the east assuming that wave packets travel with speeds between 15-45º/day (Chang 1999). It consists of the following steps:

1.- Search for the highest daily value of the amplitude in the longitudinal axis (X_n) on the first day of the data matrix.

2.-Detection of the position of the maximum envelope amplitude the next day (X_{n+1}).

3.- If $15º \leq (X_{n+1} - X_n) \leq 45º$, X_{n+1} and X_n are considered part of the same trajectory (Sagarra and Barreiro 2020), and we repeat steps 2 and 3 for the next day.

4.- When we find a maximum X_{m+1} such as that $X_{m+1} - X_m$ is outside the range established in step 3 or when we reach the end of the datamatrix, we finish the tracking and save the trajectory. Afterwards we resume the tracking process since the last day we detected the beginning of a trajectory.

5.- After all longitudes for one day were analysed, we proceed to the next day and repeat steps 1-4 until the whole data matrix is empty.

6.- Linking of trajectories that might have been truncated in the tracking stage by applying proximity criteria as follows. If two trajectories are separated by a distance of 1000 km or less and their difference in slope is below 20º/day, they are considered part of the same trajectory and joined. In addition, for those slow trajectories that are 1-2 days apart, but the mean speed between the end of a trajectory and the beginning of the next one is below 15º/day, they are considered as a single trajectory if:

1.- Between the points L_{f-1} or L_f, (being L_f the ending point of the first trajectory) to I_i or I_{i+1}, (being I_i the first point of the second trajectory) is above 15º/day.

2.- Mean V_{300env} located at the points located between L_{f-1} or L_f, I_i or I_{i+1}, is above the minimum threshold.

7.- Lastly, trajectories that last less than 3 days are filtered out because they are not relevant for the study.

Fig 11 shows a graphical representation of the performance of the algorithm during the propagation of a RWPs.

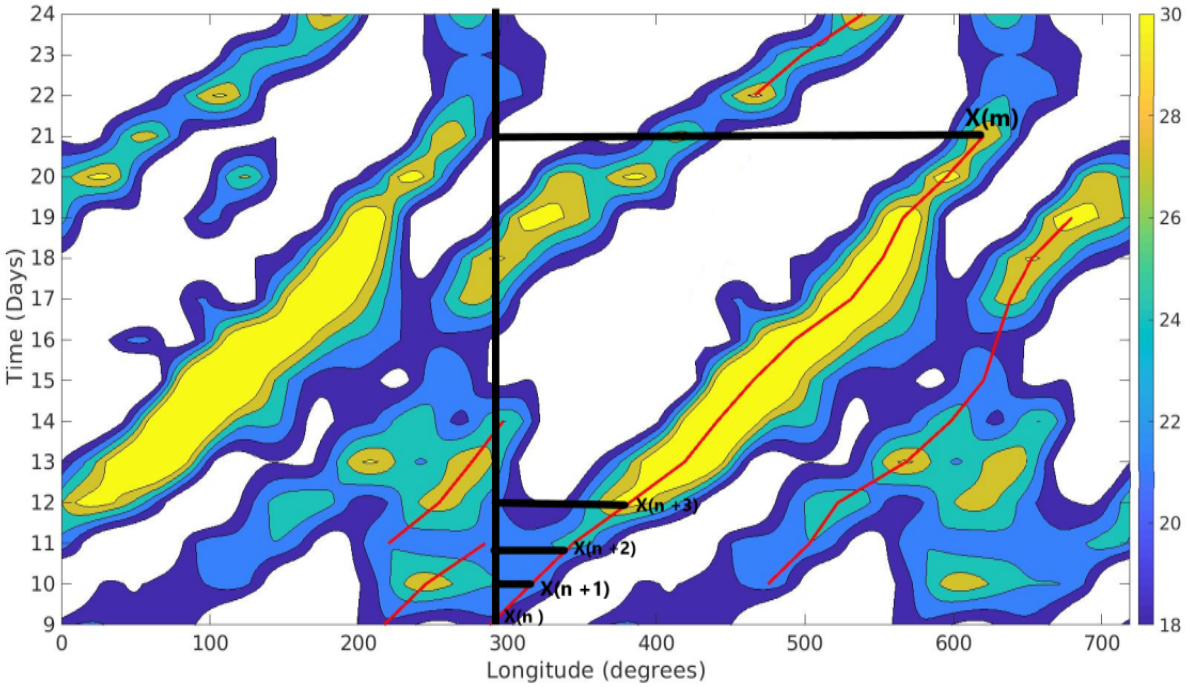

Fig 11. Hovmoller diagram of the evolution of V_{300env} (m/s) during the propagation of a LLRWPs. Red lines show the trajectories of the RWPs detected by the tracking algorithm. X_n signals the centre of the RWPs at time n, and X_m the last point of the trajectory found by the algorithm. The Hovmoller diagram is repeated twice in the zonal direction in order to enable a better graphical representation of the algorithm' performance.

After the end of the tracking stage, we measure different characteristics of the RWPs such as: mean propagation speed (m/s) taking into consideration that a speed of 1º/day ~ 0.82 m/s in the region considered (40-65ºS), lifespan (number of days that a RWP was tracked in the atmosphere until it disappears), extension of the packet (degrees), area of formation/disappearance, activity areas and V_{300env} values at the centre of activity of the RWPs.

4.2 Rossby Wave Breaking seeking algorithm

As we mention in chapter 2, RWB events are the irreversible deformation of the PV contours in the upper troposphere. Thus, it is possible to detect RWB events by observing the areas where the PV contour lines overturn in a longitudinal section following isentropic coordinates (McIntyre and Palmer 1983).

Having this in mind, we developed an objective algorithm able to detect the overturning of PV contours based on the methodology of Barnes and Hartmann (2012), and it follows the following steps:

1.-Selection of the longest contour for a certain PV value for a given day t.

2.-Identification of areas where the PV contour line crosses, at least, 3 times the same longitudinal sector; these locations will be referred to as wave breaking points.

3.-All wave breaking points that are located 500 km from each other are assumed to belong to the same wave breaking event, and thus they will be grouped together (Barnes and Hartmann 2012).

4.- Retention of RWB events with a longitudinal extension above 5º. This criteria avoids registering meridional extended PV tongues that do not show overturning.

5.-Classification of the RWB event regarding their shear. This is done by measuring the latitudinal mean of the 4 most eastward and westward overturning points of the RWB episode. In the Southern Hemisphere, cyclonic RWB events have their western-most overturning point located equatorward, while their east-most overturning point is poleward. By contrast, in anticyclonic RWB events their eastern-most overturning point is equatorward whereas their western-most overturning point is poleward. Thus, if the latitudinal mean of their most westward points of the RWB event is closer to poleward latitudes than the latitudinal mean measured in the most eastward points, we assume that the wave packet shows an anticyclonic shear, whereas if the latitudinal mean of the most westward points is closer to the equator than the mean found on the most eastward points, the breaking event is classified as cyclonic RWB.

6.- Measurement of the longitudinal and latitudinal extension of the RWB event, and day of formation of the RWB event.

7.- Save all characteristics of the RWB found at day t, (area and date of detection, longitudinal and latitudinal extension, shear), and repeat steps 1-6 until all the data is analysed.

An example of the RWB tracking algorithm performance is shown in Fig 12.

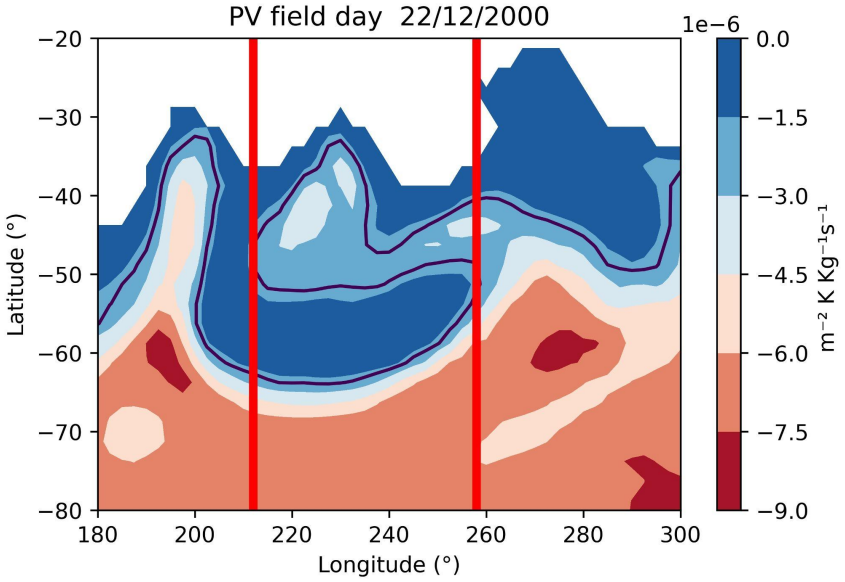

Fig 12. PV field following the iso-coordinates of 330ºK during the manifestation of a RWB event. The black line represents the contour where the potential vorticity field is -2PVU (1 PVU = 10^{-6} m^2 s^{-1} K kg^{-1}), whereas the red line indicates the longitudinal extension of the RWB event detected by the tracking algorithm.

4.3 Atmospheric blocking detection algorithm

In order to detect the development of atmospheric blocking in the atmosphere, we use the methodology of Tibaldi *et al.* (1990), but modified to consider a range of latitudes in the Southern Hemisphere following Mendes *et al*. (2011). This methodology focuses on the identification of areas where the meridional gradients of Z_{500} is reversed to indicate that a certain longitudinal section is blocked.

The first step of this methodology starts by measuring two geopotential height meridional gradients from a central latitude, one to the north (Z_{500N}) and another one to the south (Z_{500S}) by using expressions 1 and 2.

(1) $Z_{500N} = (Z(\lambda,q_1) - Z(\lambda,q_N)) / (|q_1 - q_N|)$
(2) $Z_{500S}=(Z(\lambda,q_S)- Z(\lambda,q_2)) / (|q_S - q_2|)$

Where:

q_N= 40ºS + Δ

q_2 =50ºS + Δ

q_1 =55ºS + Δ

q_S=65ºS + Δ

$Z(\lambda,q)$ is the Z_{500} in a latitude q and longitude λ, and Δ belongs to the set {-10,-7.5, -5, -2.5, 0, 2.5, 5, 7.5, 10}. If on a specific day, at a given longitude λ, $Z_{500N} > 0$ and $Z_{500S} < -10$ m/degree of latitude for, at least, one value of Δ, the longitude is considered to be "blocked". Note that, we measure Z_{500N} and Z_{500S} using slightly different expressions from Mendes *et al*., (2011). The definition chosen here implies a stronger requirement on the blocked longitudes than the one considered in the latter study.

When instantaneous, local, blocked conditions have been identified, we retain only those blocking situations that showed enough lifespan and extension to be considered as atmospheric blockings. As we mentioned in section 2.4, atmospheric blocking events appear more often in the northern hemisphere and display higher amplitudes and lifespan compared to the southern hemisphere. This is due to the fact that the mean flow in the southern hemisphere favours the development of transient over stationary structures. Consequently, the minimum spatial and temporal scale for a blocking situation to be considered as an atmospheric blocking is slightly less strict in the Southern hemisphere. Patterson *et al.,* (2019) defined an atmospheric blocking event when a blocked longitudinal sector covers, at least, 11º and when this condition persists for a minimum of 4 days in the atmosphere. On the other hand, Mendes *et al.*, (2011), used a minimum spatial extent of 7.5º in longitude and persistence of 5 days. In our study, we registered the events that show a minimum longitudinal extension of 7.5, 10, 12.5 and 15º, and that last between 4-5 days. The reason to choose this range of thresholds is to assess if RWPs that are linked to RWB are sensitive to the intensity and strength of the block.

5| ENSO AND SAM INFLUENCE IN THE VARIABILITY OF LONG-LIVED ROSSBY WAVE PACKETS DURING SOUTHERN HEMISPHERE SUMMER

The goal of this chapter is to analyse how the main global climate modes influence the interannual variability of the RWPs during southern hemisphere austral summer, as well as to understand the large scale atmospheric configuration that favour or disfavour LLRWPs propagation. To do so, we applied the tracking algorithm described in chapter 4 to detect and follow RWPs and associate the interannual variability in LLRWPs occurrence to ENSO and SAM phases[1].

The chapter is organised as follows, Section 5.1 describes the data considered in this study as well as the methodologies followed to identify atmospheric/oceanic circulation anomalies that favours LLRWPs propagation. Section 5.2 describes the climatology and interannual variability of RWPs. Section 5.3 analyses the impact of SAM and ENSO on LLRWPs variability. Lastly, section 5.4 addresses which large-scale conditions and processes favour LLRWPs propagation and section 5.5 summarises the results.

5.1 Datasets and methodology

In this study we used daily mean meridional winds (m/s) at 300 hPa as done in previous studies (ex Chang and Yu 1999, Sagarra and Barreiro 2020), from ERA5 reanalysis (Hans *et al.,* 2020), with an horizontal resolution of 0.25x0.25º and from the NCEP-DOE Reanalysis 2 (NOOA/OAR/ESRL), with a spatial resolution of 2.5ºx2.5º (Kanamitsu *et al.,* 2002). The period of study is the austral summer, from December to March (DJFM) from 1979 to 2020, thus retaining data from 41 seasons. The reason to include March in our analysis is to increase the sample size due to the fact that LLRWPs represent barely 10 % of the total packets. In addition, Barreiro (2017) and Sagarra and Barreiro (2020) showed that RWPs found in March are very similar to those found during DJF.

In order to identify and follow RWPs in the atmosphere, we used the methodology described in chapter 4.1. This is, transforming meridional wind

[1] Results presented in this chapter have been published in: Pérez, I., Barreiro, M. & Masoller, C. (2021) ENSO and SAM influence on the generation of long episodes of Rossby wave packets during southern hemisphere summer. *Journal of Geophysical Research: Atmospheres*, 126, e2021JD035467. Available from: https://doi.org/10.1029/2021JD035467.

speed into V_{300env}[2], and applying the tracking algorithm to detect and follow RWPs propagation. Nonetheless, as we stated in the mentioned section, we first need to filter low intensity V_{300env}, but there is not an optimal threshold because RWPs do not have physical properties that separate one packet from the other (Souders *et al*., 2014b). In previous studies, Grazzini and Vitart (2015) applied a threshold of 16 m/s to the NCEP DOE dataset, Sagarra and Barreiro (2020) 15 m/s, and Souders *et al*., (2014b) 14 m/s; thus for this analysis we applied a threshold of 15 m/s for NCEP-DOE2 data. On the other hand, in the case of ERA 5 we used a minimum threshold of 19 m/s because this reanalysis showed higher mean values of the envelope amplitude, indicating that this reanalysis shows a jet stream with stronger meandering compared to the NCEP-DOE2 dataset, most likely due to the higher resolution of the ERA 5 dataset. Nonetheless, in order to test the sensitivity of the results, we also considered a 2 m/s higher and lower threshold for each reanalysis.

After applying the tracking algorithm, we classified RWPs regarding their lifespan: they are considered as short-lived RWPs if they last between 3-6 days, medium-lived RWPs when their lifetime ranges between 7-8 days, and as long-lived RWPs or LLRWPs when they last more than 8 days. Even though this study is mainly focused on the study of LLRWPs, we registered RWPs of different lifespans so we can assess whether their frequency of occurrence is correlated with the occurrence of LLRWPs.

Next, to study the interannual variability of the main global climatic modes, we used the SAM and ONI indices for the ENSO and the Southern Annular Mode, which were described in chapter 3.1. Of the 41 years of data, 14 years correspond to an event of El Niño, 13 to La Niña and 14 to Neutral years. In the case of SAM, we classified years in SAM positive (SAM negative) phase if the absolute value of the detrended SAM index in a year t surpasses the threshold of 0.75σ (σ is the standard deviation of the detrended SAM index), and it shows a positive (negative) value. Oppositely, if the index does not surpass the previous threshold, it is classified as a Neutral SAM year. We chose this threshold in order to retain a similar number of positive and negative SAM years. Consequently, we have 9 years classified as negative SAM, 11 years as positive SAM, and 21 to Neutral SAM.

Additionally, we used geopotential height and zonal wind fields at 300 hPa (Z_{300} and U_{300} respectively) as well as sea surface temperature (SST) from ERA 5 in order to study changes in atmospheric and oceanic circulations associated with

[2]The V_{300env} of the RWPs used in chapter 5 is publicly available at https://doi.org/10.5281/zenodo.5714192, as well as a script to obtain wind envelope data from meridional wind speed at https://doi.org/10.5281/zenodo.5724656. Also, a detailed description of the datasets and methodology used to measure V_{300env} is available in: Pérez I and Barreiro M. Wind envelope amplitude data at 300 hPa for the study of atmospheric waves in the Southern Hemisphere during austral summer [version 1; peer review: awaiting peer review]. Open Res Europe 2023, **3**:68 (https://doi.org/10.12688/openreseurope.15844.1)

the interannual variability of RWPs. In addition, to determine changes in the position and intensity of the extratropical waveguide, we measured the mAVg at 300 hPa, which is an accurate approximation of the isentropic gradients of potential vorticity (Wirth *et al.*, 2018).To identify anomalies that favour LLRWPs development we regressed U_{300}, mAVg, Z_{300} and SST anomalies onto the time series of interannual occurrence of LLRWPs, as well as constructed composite maps. The statistical significance was evaluated using the Student's t-test at 10% of significance.

Results shown are mainly based on ERA 5, and only include NCEP-DOE2 when relevant information is added.

Finally, we calculated the wave coherence index or WCI (Chang & Yu 1999, Chang 1999). Maximum values of WCI indicate regions where the upper level jet acts as a waveguide. Based on previous studies, we expect that years with maximum WCI values and that display a zonally symmetric structure around the hemisphere are those that favour LLRWPs propagation (e.g Seager et al 2010).

5.2 Results and discussion

5.2.1 Mean and interannual variability of RWPs

Fig 13 shows the climatological amplitude of the envelope in the Southern Hemisphere in ERA 5. The maximum values of the amplitude appear in the latitudinal band between 40-60ºS and from 25-150ºE. In addition, we also observe that there is a minimum near the southern tip of South America as noted by Souders *et al.,* 2014a. This spatial pattern is similar to those found on the individual months (not shown). Therefore, RWPs tracked might be interrupted in the section between 280-330ºE when we apply a highly restrictive threshold.

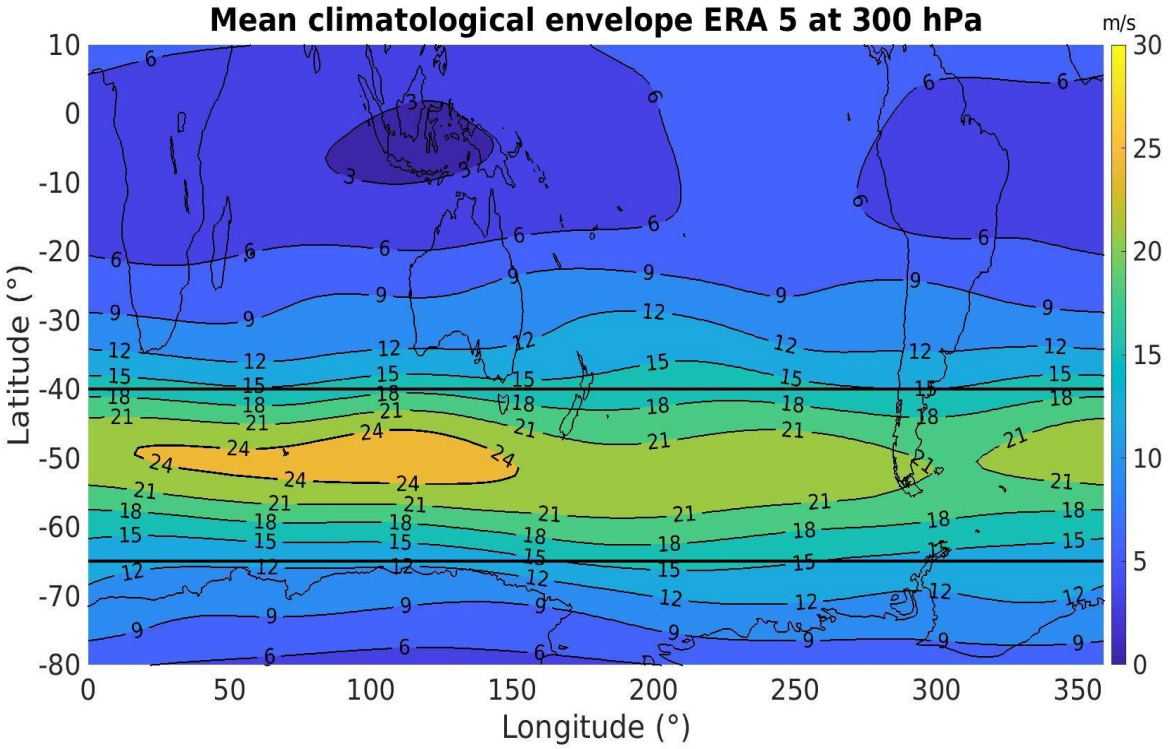

Fig 13. Mean climatological amplitude (m/s) From December to March. The black lines signal the area of study.

During the 41 seasons, a total of 1256 packets were found in the ERA 5 reanalysis, and 141 of the total lasted more than 8 days, therefore, corresponding to about a total of 30 (3) RWPs (LLRWPs) per season. Fig 14 displays a summary of RWPs properties. In Fig 14a we observe an exponential decrease of the RWPs lifespan, 77% of the packets do not last more than 6 days and around 1.1% of the packets have a lifespan above 14 days. The mean lifespan of a RWPs is 5.3 days, with a median of 4 days and an interquartile range of around 6 days. Next, Fig 14b shows that nearly 78 % of the RWPs travel a distance between 30-170º in the longitudinal axis before disappearing, and only around 2.4 % are capable of completing a full latitudinal circle. The mean distance travelled by the packets is 126º, with a median is 96º and an interquartile range of 101º. Lastly, Fig 14c shows the RWPs speed distribution, and shows a mean speed of 20.7 m/s and a standard deviation of 5 m/s.

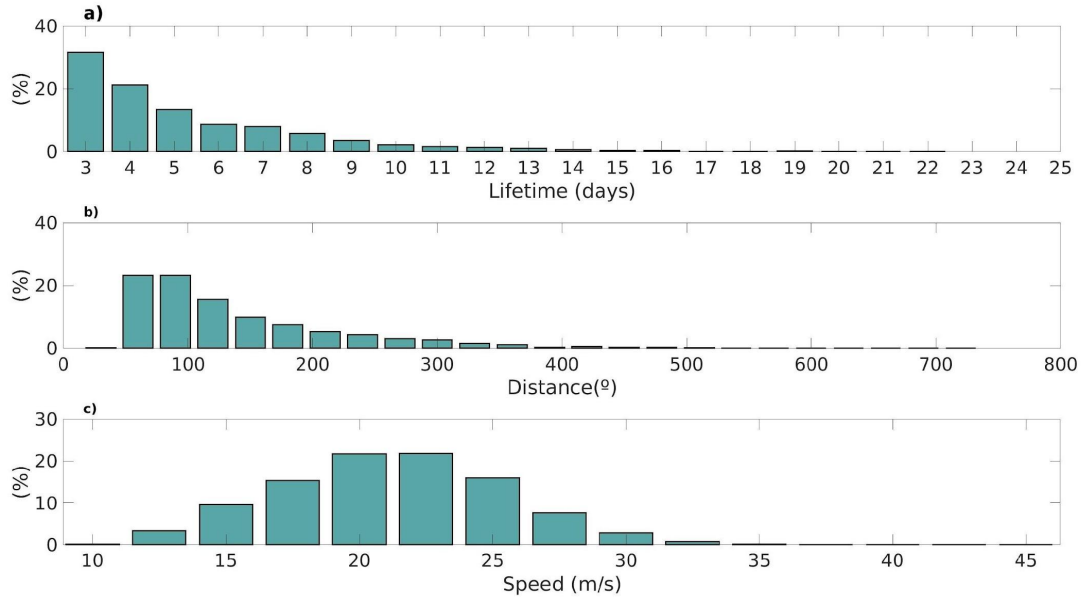

Fig 14. Characteristics of the RWPs detected between 1979-2020 between December-March, using a minimum threshold of 19 m/s for the tracking stage: (a) lifespan, (b) distance travelled and (c) mean speed per packet.

For the NCEP-DOE2 dataset, a total of 1225 RWPs were found, and 101 are LLRWPs. Barely 70% of the trajectories surpass the 6 days, and around 2% of the trajectories found have a lifespan above 14 days. The mean distance travelled by RWPs is 128º with a median of 84º, and an interquartile range of 85º. Mean RWPs lifespan reaches 5 days, with a median of 4 days, and an interquartile range of 3 days. Also, the mean speed is 20.5 m/s, with a standard deviation of 4.3 m/s. Results obtained in NCEP-DOE2 are similar to those observed in ERA 5.

In comparison, in the study of Sagarra and Barreiro (2020) they found that the mean speed of the packets is 20 m/s and showed a standard deviation of 6.6 m/s. Also that the packets have a mean lifespan of 6 days, and 80% of the packets lasted between 3-7 days, and only 1% was able to last more than 14 days. In addition, the mean distance travelled by the packets is around 99º of longitude. By contrast, Souders *et al.,* (2014b) concluded that in the Southern Hemisphere 70% of the RWPs have a lifespan below 8 days and a mean lifetime of 7.9 days, also they displayed a mean of 151º of distance travelled. Hence, RWPs tracked in our study have lower lifespan and travel shorter distances compared to Souders *et al.,* (2014b). In the case of the NCEP-DOE2 dataset this could be partially attributed to the use of a less restrictive threshold in that study (14 m/s).

Fig 15 displays the interannual variability of all the RWPs found in the study, as well as the activity of RWPs with a certain lifespan. In Fig 15a, the frequency of

occurrence of the total number of RWPs in ERA5 shows large interannual variability, with values ranging between 20 and 40 packets per year. Also, the number of total RWPs does not seem to be too sensitive to the minimum threshold, although we observe a considerable reduction in the quantity of the total packets when we choose a threshold of 21 m/s. This might be associated with the fact that near South America, the isoline of 21 m/s breaks, thus RWPs propagation is abruptly interrupted near this region (see Fig 13).

When we observe the subsets of RWPs with different lifespan, it is obvious that the total number of RWPs is mainly determined by the frequency of occurrence of short-lived packets (Fig 15b). Medium lived and long-lived packets (Figs 15c, 15d) show a similar amount of events, and the number of episodes increases the less restrictive the minimum threshold is. In the case of long-lived packets, they display high interannual variability, suggesting that large-scale circulation conditions established by low-frequency climate modes can modulate their occurrence.

Furthermore, it is worth pointing out that between the occurrence of short-lived and long lived packets exists a negative correlation with r=-0.32 for a threshold of 19 m/s, consequently, years with several long-lived wave packets result in less short lived wave packets during that year and vice versa. Also this correlation is statistically significant at 5 % according to the Student's T test.

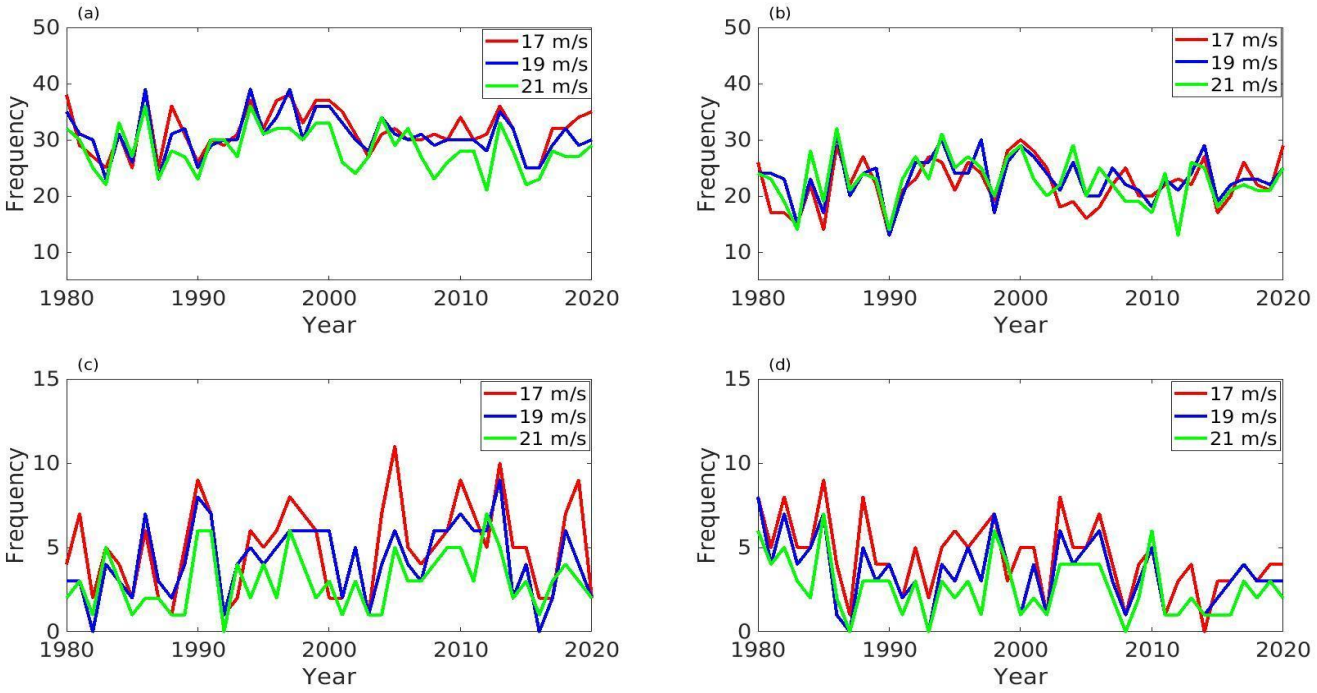

Fig 15. interannual variability of the total amount of RWPs tracked (a), short-lived RWPs (b), medium-lived RWPs (c) and long-lived RWPs (d). Red,blue and green lines indicate the results obtained using thresholds of 17,19 and 21 m/s respectively.

Most of the wave activity of all RWPs (Fig 16a) is centred around 61-121ºE (Indian ocean basin), and a minimum between 181-240º (eastern Pacific basin). These results are close to the observed in Souders *et al., (*2014a). Nonetheless, the median of wave activity for LLRWPs is mostly uniform in all latitudes, although the longitudes located at the east of 120º E seem to have years with less packets (Fig 16b). Findings suggest that neither SAM or ENSO meaningfully affect the areas of activity of LLRWPs. Although there is a strong increase in variance in the eastern Pacific (241-300ºE) during positive SAM events compared to results observed in other longitudinal bands and to its opposite phase.

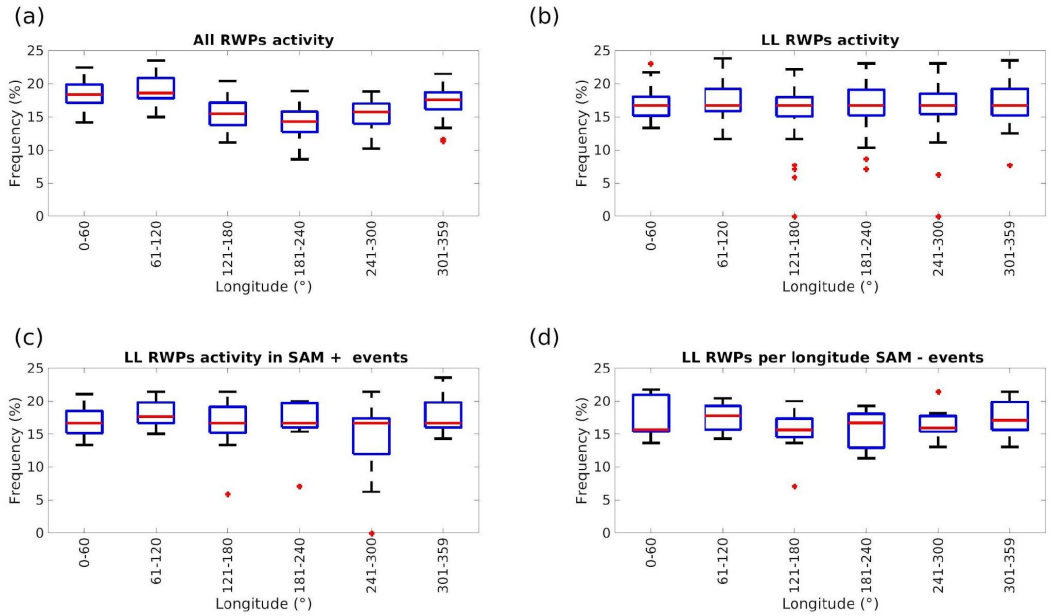

Fig 16. Boxplot of RWPs activity in ERA 5 for all the RWPs (a) and for LLRWPs (b). The bottom panel shows the influence of SAM on wave activity of LLRWPs for positive SAM phase (c) and for negative SAM (d). Red crosses signal the position of outliers.

5.2.2 Impact of SAM and ENSO on the occurrence and duration of LLRWPs

The time series of detected LLRWPs for a threshold of 19 m/s in ERA5 and the SAM index are correlated at –0.31, significant at 5% level. On the other hand, the correlation between the same time series of LLRWPs and the ONI index is 0.19, which is not statistically significant at 10% level. Nevertheless, since the relationship between LLRWPs and ENSO may not be linear, in this section, we further explore the influence of SAM and ENSO on the distribution of the frequency of occurrence and duration of LLRWPs.

Fig 17 shows the frequency of occurrence of LLRWPs during years with different ENSO phases using various thresholds in both reanalyses. The tracking algorithm detected a larger number of LLRWPs during El Niño compared to

neutral and La Niña years in NCEP-DOE2 reanalysis. After applying the Kruskal Wallis test, we found that the differences in the occurrence of LLRWPs during El Niño and La Niña are statistically significant: the p-values obtained are 0.02 for low thresholds (13 m/s), 0.10 for medium thresholds (15 m/s), and 0.09 in high thresholds (17 m/s). Nonetheless, in the case of ERA5, these p-values are close but do not reach the minimum level of significance established, showing p-values of 0.12, 0.12, and 0.23 for low, medium, and high threshold. We also compared the duration of the trajectories during different ENSO phases and we did not find any significant differences. Thus, except for the low-threshold case in NCEP-DOE 2, differences between El Niño and La Niña are marginal or not significant, suggesting that ENSO influence on LLRWPs is weak and not robust.

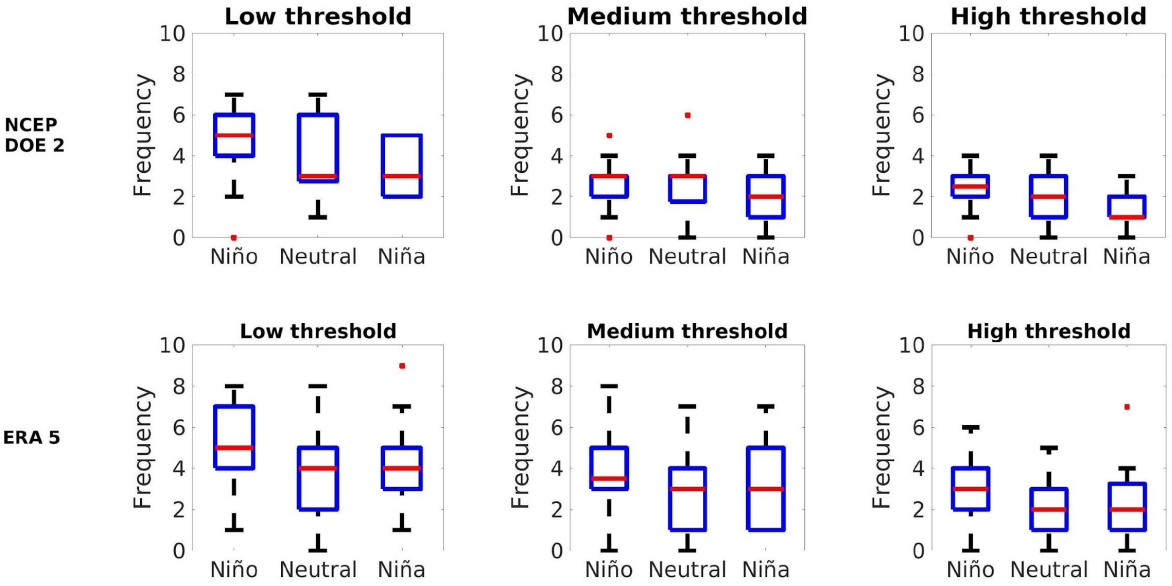

Fig 17. Boxplots of interannual variability of LLRWPs detected during different ENSO phases using NCEP-DOE2 (upper panels) and ERA5 (lower panel) for different thresholds. Red points show outliers and red lines show the median location. The title of each box plot refers to the threshold applied in the tracking stage. Low threshold is 17 (13 m/s), medium threshold is 19 (15) m/s, and high threshold is 21 (17 m/s) for ERA5 (NCEP-DOE 2).

We next turn to the impact of SAM (Fig 18). In contrast to ENSO, independently of the threshold considered in ERA5, positive SAM events display the lowest frequency of occurrence of LLRWPs and in negative SAM the highest, whereas neutral SAM shows intermediate values. Kruskal Wallis test results show that for ERA the occurrence of LLRWPs during positive SAM and negative SAM events are significantly different for all thresholds, showing p-values of 0.03, 0.02, and 0.03 for low, medium, and high thresholds, respectively. For the NCEP-DOE 2 data set, we only found statistically significant differences between positive and

negative SAM for low threshold, (p-values of 0.09, 0.5, and 0.20 for low, medium, and high thresholds). Results are also statistically significant between the interannual variability of positive SAM against neutral SAM for medium threshold (p-values of 0.21, 0.07, and 0.58 for low, medium, and high thresholds, respectively) in NCEP-DOE2 data sets. (See also Table 1)

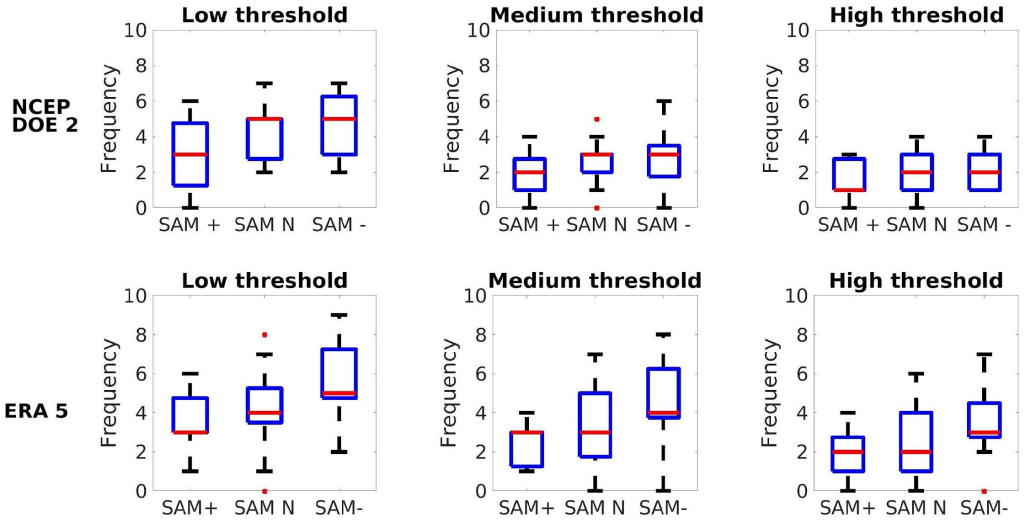

Fig 18. Analogous to Fig 17 but for SAM events.

ERA 5						
		Interannual variability		Duration		
Threshold	Low	Medium	High	Low	Medium	High
SAM + vs SAM -	0.03	0.02	0.03	0.03	0.06	0.22
SAM - vs SAM N	0.16	0.30	0.20	0.39	0.43	0.38
SAM + vs SAM N	0.25	0.20	0.18	0.06	0.21	0.51
NCEP-DOE 2						
		Interannual variability		Duration		
Threshold	Low	Medium	High	Low	Medium	High
SAM + vs SAM -	0.09	0.15	0.2	0.26	0.09	0.44
SAM - vs SAM N	0.36	0.77	0.41	0.80	0.56	0.73
SAM + vs SAM N	0.21	0.07	0.58	0.27	0.09	0.51

Table 1. Overall p values after applying the Kruskall Wallis test for the frequency of occurrence and duration of LLRWPs during SAM events for ERA 5 (up) and NCEP DOE2 (below).

Additionally to having a higher frequency of LLRWPs during negative SAM years, we also registered LLRWPs that last longer compared to the wave

packets found during positive SAM (Fig 19). These differences are statistically significant for low threshold values in ERA 5, and for medium threshold for NCEP-DOE2 dataset (0.06 and 0.09 respectively, see Table 1).

Therefore, results obtained in this section suggest that SAM heavily influences the frequency and duration of LLRWPs. Negative SAM phases favour the development of LLRWPs that last significantly longer compared to years with positive SAM events. On the other hand,the impact of ENSO is not as robust because results change regarding the reanalysis and threshold used.

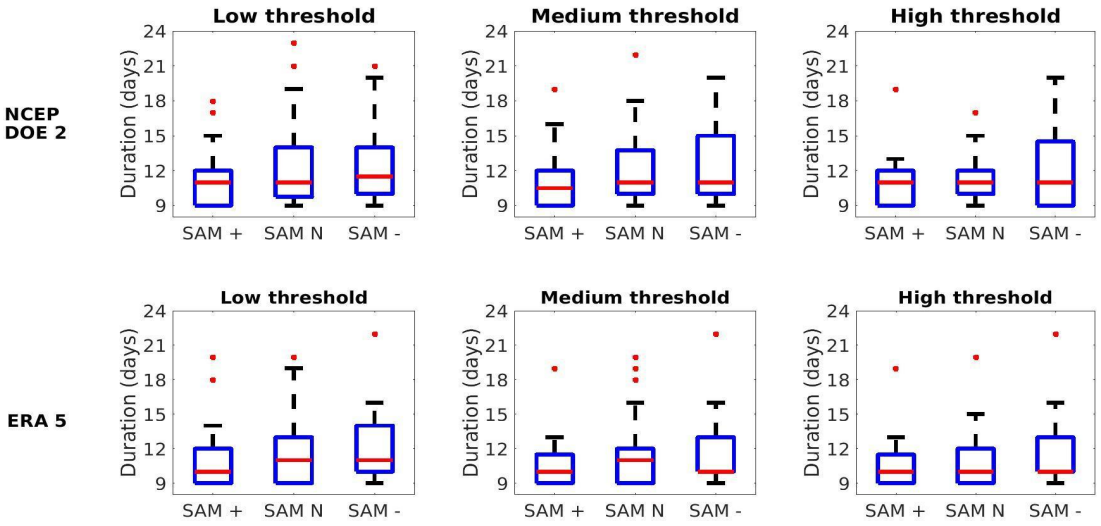

Fig 19. Boxplots of interannual LLRWPs duration for different SAM phases using NCEP-DOE2 (upper panel) and ERA5 (lower panels) for different minimum thresholds. Red point crosses show the outliers and red lines show the median location.

5.2.3 Conditions that favour LLRWPs propagation

Fig 20 displays the composite maps of U_{300} and mAVg during years with the highest (Fig 20a) and lowest (Fig 20b) LLRWPs frequency of occurrence. During the years of maximum frequency of occurrence of LLRWPs, the jet stream is stronger, more zonal, and narrower from the southeastern Atlantic until the southwestern Pacific. Both Figs 20a and 20b show a region with negative values of mAVg to the east of New Zealand. Since the mAVg must be positive to enable RWPs propagation, in that region RWPs propagation is either restricted or blocked (Hendon, 2018). This region of negative mAVg is larger, extending toward higher latitudes during years with the lowest frequency of occurrence of LLRWPs. To further understand the differences in mean wind conditions between years of maximum and minimum frequency of LLRWPs, Fig 20c shows the difference in the 300 hPa wind field. Consistent with the previous maps, circulation changes are characterised by westerly wind anomalies between 40 and 50ºS in the Indian ocean sector and easterlies between 50 and 60ºS over

most of the domain. In addition, superimposed on these zonal anomalies there are weak cyclonic circulation anomalies located in the southwestern Atlantic, southwest of Africa, and southwest of Australia.

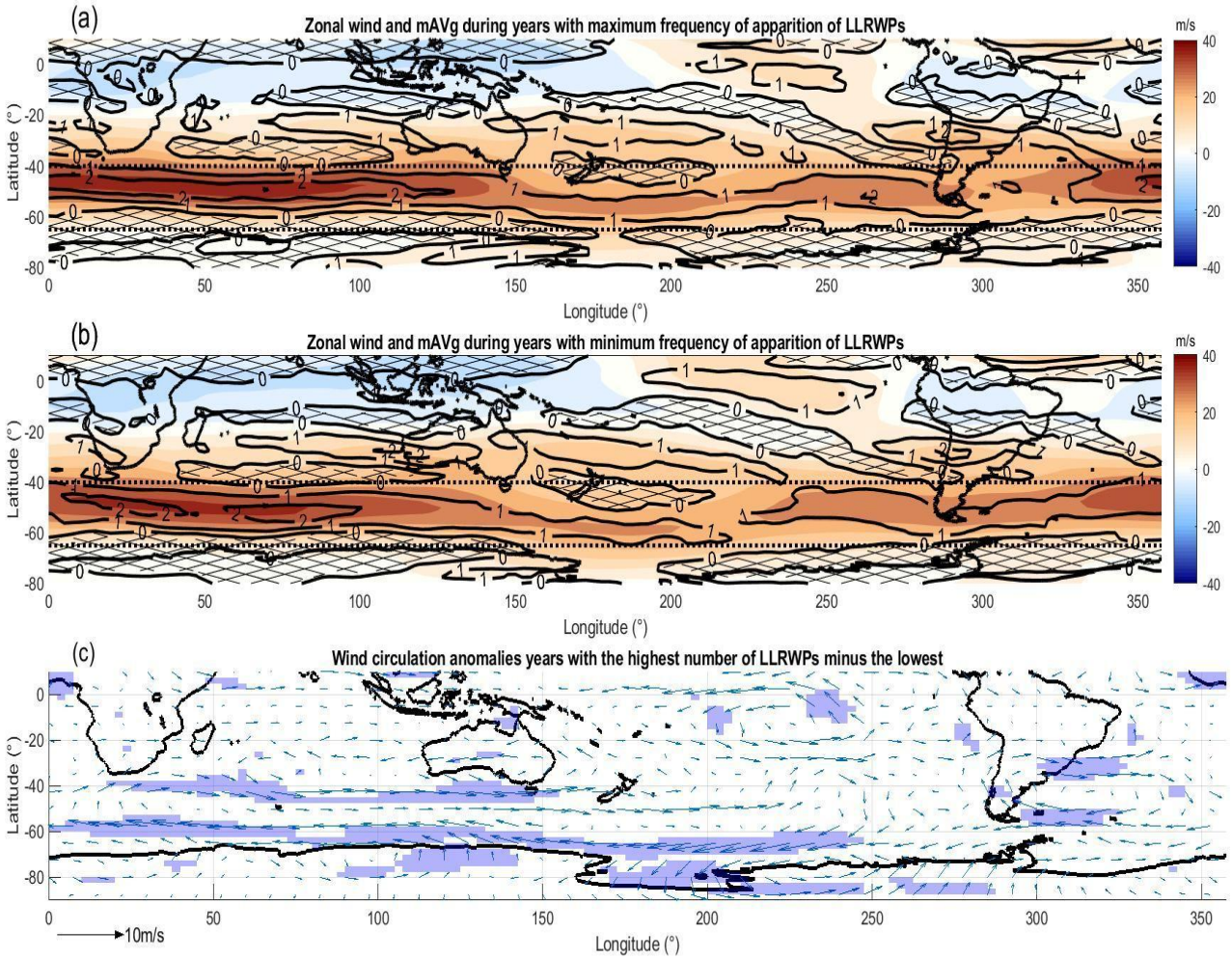

Fig 20. Composite maps of zonal wind speed (coloured areas, expressed in m/s) and mAVg (lines, expressed in 10^{-10} /ms), during years of maximum (a) and minimum (b) frequency of occurrence of LLRWPs in ERA5. Black lines show positive mAVg and areas with negative mAVg are highlighted with a hatching crossed pattern. Black dotted lines show the limits of the area of study. Panel c shows the wind circulation anomalies constructed as the difference between years of maximum and minimum LLRWPs. Blue areas indicate where the anomalies are statistically significant at 10% level.

To complement the above analysis, Fig 21 shows the regression fields of U_{300}, mAVg, anomalies of Z_{300}, and SST anomalies onto the time series of the frequency of occurrence of LLRWPs. Consistent with Fig 20, the increase in LLRWPs is inversely correlated with an increase of zonal mean wind speed (Fig

21a) in the medium-high latitudes (50-65ºS), whereas it is positively correlated with zonal wind speeds at lower latitudes (35–50ºS). In the case of the mAVg (Fig 21b), we observe the same spatial pattern as for U_{300}, although the field is noisier. As during austral summer, the jet stream is approximately zonally symmetric and centred in 50ºS, results of Figs 20 and 21 suggest that northward (southward) displacement of the jet stream favours (disfavors) the propagation of LLRWPs.

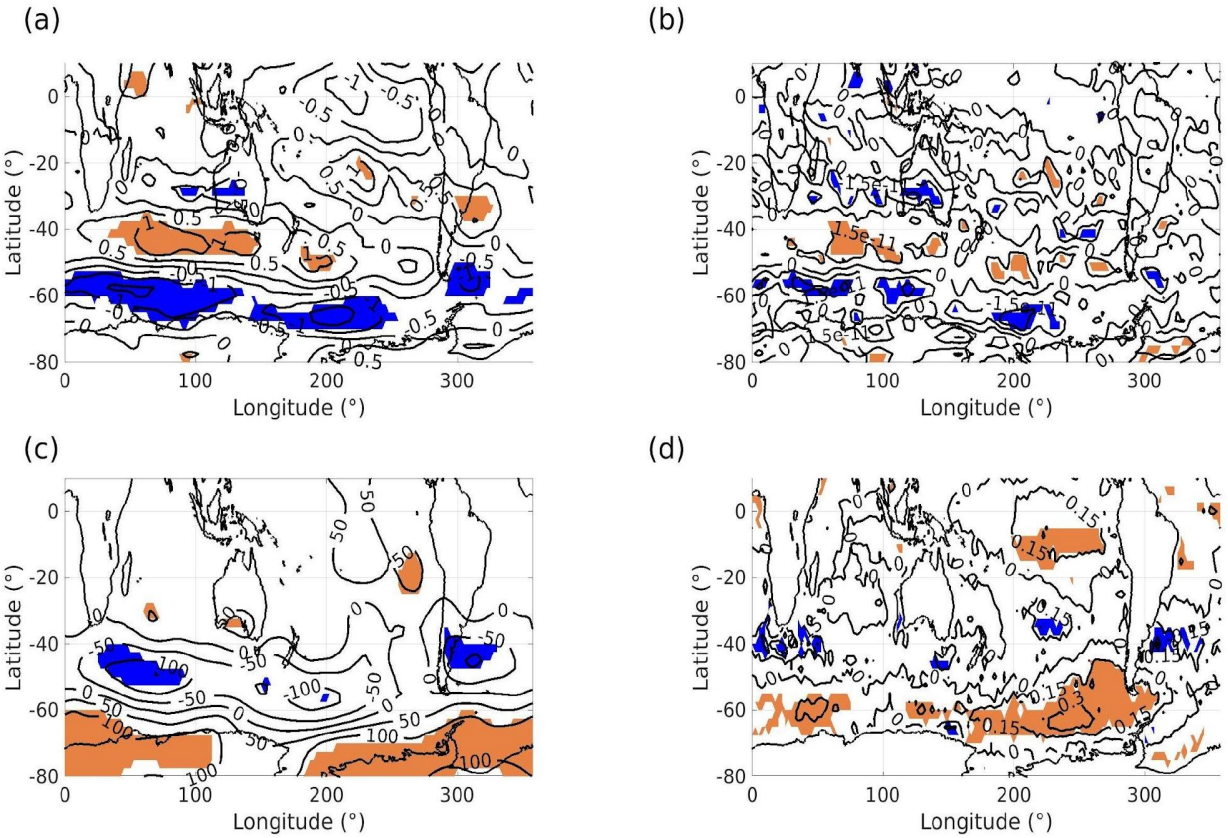

Fig 21. Linear regression-correlation maps of several fields onto the interannual frequency of occurrence of LLRWPs in ERA5: (a) zonal wind speed at 300 hPa (m/s), (b), mAVg (1/ms), (c) geopotential height at 300 hPa (m), and (d) SST anomalies (ºC). The coloured areas indicate where the correlation is significant in the 10% level, with orange (blue) areas corresponding to positive (negative) values. Black lines display values of linear regression coefficient.

Accompanying these changes, there is a decrease in anomalies of Z_{300} in mid latitudes and an increase in high latitudes (Fig 21c), together with cyclonic circulations to the southwest of the continental areas as mentioned before (Fig 20c). Similar results are obtained using NCEP-DOE2 reanalysis (not shown). Thus, taken together these results suggest that years with a high number of LLRWPs are characterised by large-scale circulation anomalies that look very close to the negative phase of SAM. This is consistent with the results of section 5.2 where negative SAM events were found to favour the occurrence and

duration of LLRWPs. Fig 21d further shows that an increase in LLRWPs shows zonal bands of positive (negative) correlation with sea surface temperatures in high (mid) latitudes, consistent with atmospheric forcing. Lastly, a weak correlation with positive sea surface temperature anomalies in the tropical Pacific (Fig 21d) is also seen, again suggesting that El Niño may play a secondary role in setting large-scale conditions that favour LLRWPs propagation.

Why would a stronger, northward-shifted and narrow jet in the Indian-western Pacific basin favour LLRWPs? We hypothesise that this is because the climatological jet in the Atlantic-Indian sector acts as a better waveguide and extends further into the Pacific basin. To address this issue, we calculate the empirical orthogonal functions (EOFs) of the WCI between 30 and 70ºS.

The leading EOF (EOF1) only explains 10% of the total variance, but the corresponding PC1 is highly correlated with the interannual variability of LLRWPs, showing a correlation of 0.51 (in ERA5, medium threshold), statistically significant at 5%. The second EOF is not related to the occurrence of LLRWPs and thus is not considered. Fig 22 shows the spatial pattern of the leading EOF, characterised by a dipolar structure with opposite values to the south and north of 50ºS. The positive correlation indicates that an increase/decrease of the WCI in the mid latitudes is associated with an increase/decrease in the occurrence of LLRWPs. Additionally, the PC1 is negatively correlated with the SAM index (-0.46), and positively correlated with the ONI index (0.45), both results significant at 5%. The strong negative correlation with SAM indicates that during positive SAM, the WCI increases in high latitudes of the Indian-Pacific sector. Conversely, negative SAM phases are associated with an increase in WCI in mid latitudes from the Indian to the Pacific sector, indicating that the northward-shifted jet is acting as a better waveguide compared to the southward-shifted jet during positive SAM phases, favouring the occurrence of LLRWPs.

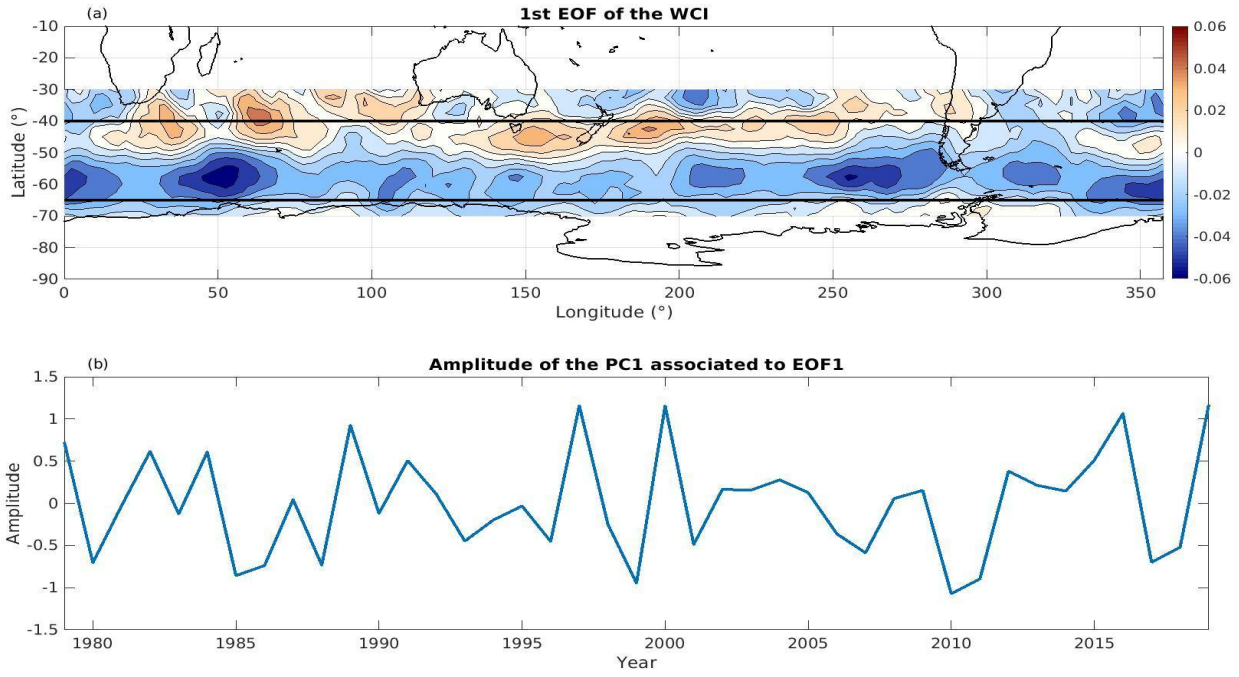

Fig 22. For ERA5, (a) leading EOF of the seasonal variability of the wave coherence index and (b) time series of the PC1.

The changes in the circulation associated with EOF1 are further explored in Fig 23. As expected from the correlation analysis, years with highest (lowest) amplitude of PC1 are characterised by large-scale circulation conditions similar to those during years of maximum (minimum) frequency of occurrence of LLRWPs (compare Figs 20a, 20b and 21a, 21b). Moreover, as in Fig 21c, the difference in wind circulation shows that years with maximum WCI in mid latitudes are characterised by a stronger, narrow and northward shifted jet in the Atlantic-Indian basin that extends into the Pacific sector (Fig 23c). The development of a cyclonic circulation anomaly to the southwest of Australia helps extend the jet into the Pacific. These are the conditions during the negative SAM phases. Conversely, during SAM positive phases, the development of an anticyclonic circulation to the southwest of Australia blocks the jet and creates a region of negative meridional absolute vorticity gradient that prevents the propagation of wave packets.

The signature of El Niño can also be distinguished in Fig 23: weakened upper level equatorial westerlies, subtropical Pacific anticyclonic anomalies, and a strong anticyclonic centre located about 110ºW, 70ºS (e.g., Barreiro 2017). This explains the significant positive correlation of the PC1 with the ONI index. These circulation anomalies are also present, although weaker, in Fig 23c. It is important to note that ENSO teleconnections project onto SAM, such that El Niño tends to favour negative SAM phases (Gong *et al.*, 2010). Thus, given that

in Section 5.3 the ENSO signal is not found to be robust, it is likely that the relationship between ENSO and LLRWPs occurs indirectly through ENSO´s connection with SAM.

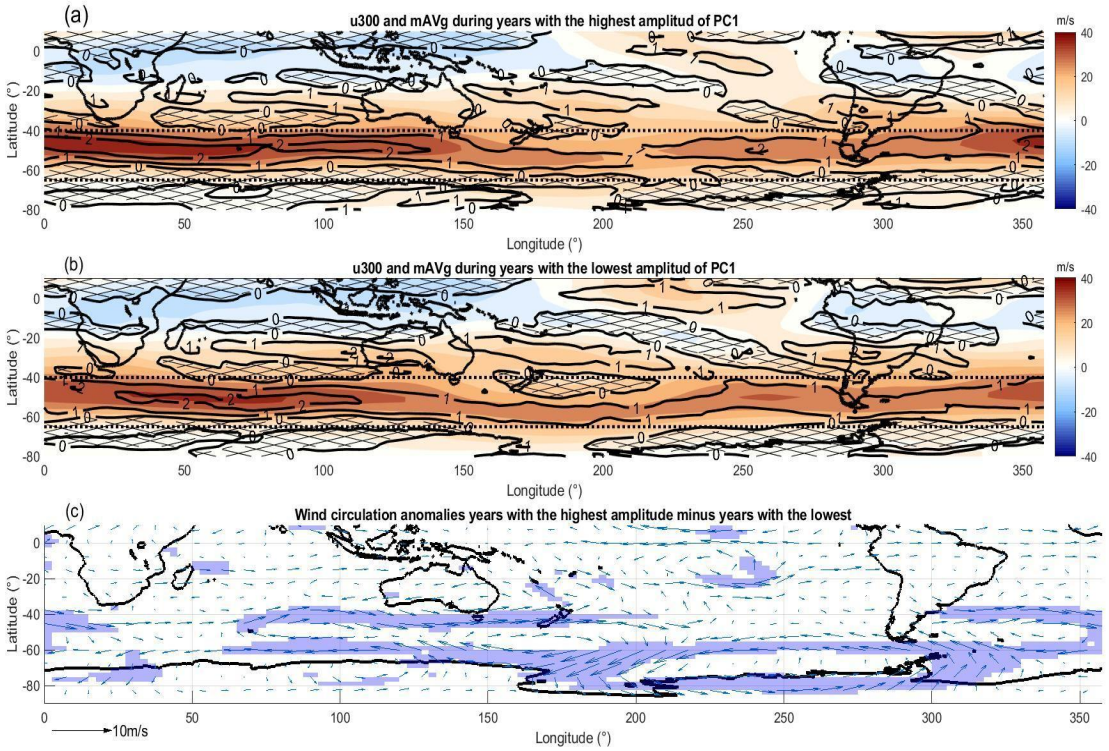

Fig 23. Analogous to Fig 20, but for the extremes of PC1.

Lastly, we computed the mean atmospheric anomalies during years with positive and negative SAM events (Fig 24). We observe that the differences in the mean wind flow are very similar to those found in previous results (Figs 20, and 23) but with a more marked signal, thus providing further evidence that different phases of SAM directly influence LLRWPs propagation.

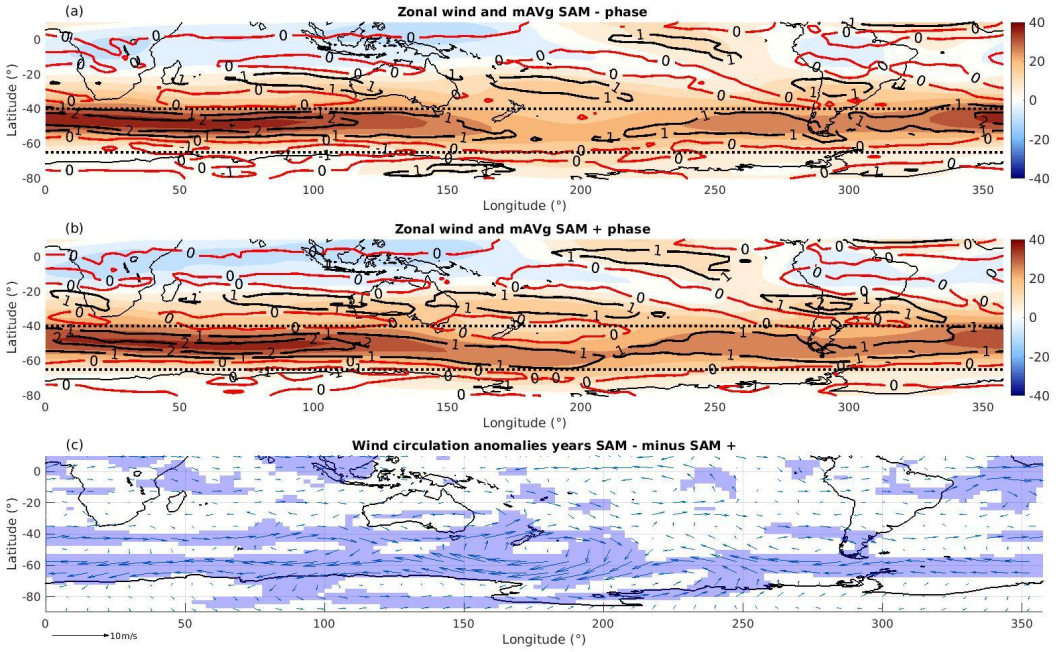

Fig 24. Analogous to Fig 20, but for years with negative and positive SAM events.

5.3 Summary

RWPs are atmospheric perturbations linked to the development of extreme weather events. The development and propagation of these wave packets have been extensively studied in the northern hemisphere, whereas in its southern counterpart most of the studies only focused on the climatological properties of these packets. This chapter addresses the impact of the SAM and ENSO in the variability of RWPs, and which configurations of the atmospheric flow favour or disfavour the development of LLRWPs during austral summer.

A detection algorithm that follows RWPs propagation based on the methodology of Grazzini and Vitart (2015) and Sagarra and Barreiro (2020) was applied to track and register RWPs characteristics. We used ERA5 reanalysis as our main dataset and compared the results obtained against NCEP-DOE 2 reanalysis data to test the robustness of the findings. The interannual variability of RWPs and the characteristics of LLRWPs was assessed, as well as how they are affected by different SAM/ ENSO phases.

We computed composite maps of atmospheric and oceanic variables and searched for circulation anomalies during years with high and low LLRWPs activity. In addition, the mean wind flow during years with high/low LLRWPs activity was investigated. Also, we measured the Wave Coherence Index and applied a principal component analysis to identify spatial patterns that affect the

coherence of the waveguide where RWPs propagate, and link it to SAM/ENSO activity.

Thus, the main results obtained in this study are:

1.- LLRWPs activity is influenced by SAM: LLRWPs appear more frequently and last longer in the atmosphere during years with negative phases of SAM, which was associated with the extension of the waveguide where RWPs propagate into the Pacific during negative SAM. On the contrary, during positive phases of SAM the LLRWPs have the lowest lifespan and frequency of occurrence due to the development of an anticyclonic circulation to the southwest of Australia, blocking RWPs propagation into the Pacific basin. Also, in years with neutral SAM conditions we observe intermediate numbers of LLRWPs.

2.- The impact of ENSO on LLRWPs is not robust. We suggest that the weak relationship found may be due to the effect of ENSO on SAM. Gong *et al.* (2010) suggested that El Niño may set background conditions that favour negative SAM events and La Niña do similarly for positive SAM events. Thus, this may result in an indirect correlation between ENSO and the occurrence of LLRWPs.

3.- Given the link between LLRWPs and extreme weather events, our findings are indicative that extended range forecasting of extreme events may be more feasible during negative SAM years and less accurate when La Niña and positive SAM phases are present.

6| HOW WELL DO FORECAST MODELS REPRESENT OBSERVED LONG-LIVED ROSSBY WAVE PACKETS DURING SOUTHERN HEMISPHERE SUMMER?

The goal of this chapter is to analyse whether the current weather forecast models are able to predict the formation and development of LLRWPs in the southern hemisphere[3].

In previous studies, Gray *et al., (*2014) studied the systematic error of the forecast at predicting the development of Rossby Wave structures, and concluded that Rossby Wave amplitude decreases rapidly with lead time. They hypothesised that this decrease might be associated with the underestimation of the humidity gradient at the tropopause as the simulation advances, which alters the radiative cooling below the tropopause, modifying the PV anomaly field in the process. These results are in agreement with those reported in Chagnon *et al., (*2013), where forecast models underestimate the diabatic enhancement of PV anomalies. Moreover, Giannakaki and Martius (2016) evaluated the representation of the waveguides where RWPs propagate in the forecast models, and found that even though the forecast models were able to predict the location of the waveguide, they often underestimate their strength and extension.

Quinting and Vitart (2019) studied the representation of RWPs in S2S models, and concluded that RWPs are fairly well represented, even though models with coarse grid resolution tend to overestimate the propagation of RWPs. It is also suggested that current weather forecast models do not accurately represent atmospheric blockings in the Atlantic-European sector, which stop RWPs propagation, thus, it could lead to erroneous forecasts of RWPs propagation in this area.

The above mentioned studies only focused on the northern hemisphere and, to our knowledge, there are no studies regarding the model representation of RWPs in the Southern hemisphere. Thus, this chapter's goal is to assess whether S2S models have skill in reproducing the development of LLRWPs. In

[3] Results presented in this chapter have been published in: Pérez-Fernández, I & Barreiro, M. (2023) How well do forecast models represent observed long-lived Rossby Wave packets during southern hemisphere summer? *Atmospheric Science Letters,* Online version of record before inclusion in an issue e1175. Available from: https://doi.org/10.1002/asl.1175.

order to achieve this goal, we use the tracking algorithm of chapter 4.1 to track LLRWPs in a reanalysis, and then apply the same algorithm to two S2S forecast models, starting the forecast the day a LLRWPs was detected. Afterwards, we compare how different are the characteristics and trajectories of the LLRWPs predicted by the forecast models against the LLRWPs observed in the reanalysis.

Additionally, we also assess whether the main southern hemisphere climate variability modes (SAM and ENSO) and the MJO affect the representation of the LLRWPs in the forecast models, and identify under which large scale atmospheric configurations the forecast models are able to accurately predict the development of a LLRWPs for at least 9 days.

This chapter is divided in the following sections:, section 6.1 describes the dataset and methodology used to register predicted LLRWPs in the forecast model, as well as the procedure followed to observe the impact of SAM, ENSO and the MJO in the forecast of LLRWPs; section 6.2 shows the results and their physical interpretation; and 6.3 presents a summary.

6.1 Data and methodology

6.1.1 Tracking of RWPs in reanalysis and S2S models

We consider daily mean meridional winds of ERA 5 reanalysis as done in chapter 5.1, and reforecast data of daily mean meridional winds from the NCEP CFSv2 ensemble model, hereafter NCEP (Saha *et al.*, 2014), and from the CAS FGOALS f2 V1.3, hereafter IAP-CAS (Bao *et al.*, 2019,2020; Li *et al*., 2019, He *et al*., 2019). The NCEP model has a spatial resolution of 1.5º x 1.5º and a forecast length of 45 days, whereas IAP-CAS shows a 1º x 1º of resolution and a forecast length of 65 days. Both S2S models have 4 ensemble simulations and daily reforecast datasets.

The period of study is focused in the southern hemisphere summer, as in section 5, but we limited our period of study between 1999-2010 due to the time constraints of the NCEP and IAP-CAS reforecast dataset. As a result, we have 11 seasons available for the analysis.

In order to characterise RWPs, we follow the same methodology as described in chapter 4.1, that is, computing the wind envelope amplitude that surrounds the wave packet (V_{300env}), latitudinally averaging the data between 40-65ºS.

The methodology to search for LLRWPs in ERA 5 is the same as explained in chapter 4.1, that is, the first step is to filter out low amplitude V_{300env}, and then we apply the RWPs tracking algorithm. For ERA 5 we use the same threshold as in

section 5 (19 m/s, as in Perez *et al.,* 2021) whereas for the NCEP and IAP-CAS we used 18 and 17 m/s, respectively. The chosen thresholds in the forecast models are based on the reforecasted V_{300env} values distribution in the area of study after applying a 7 day running mean values as shown in Fig 25.

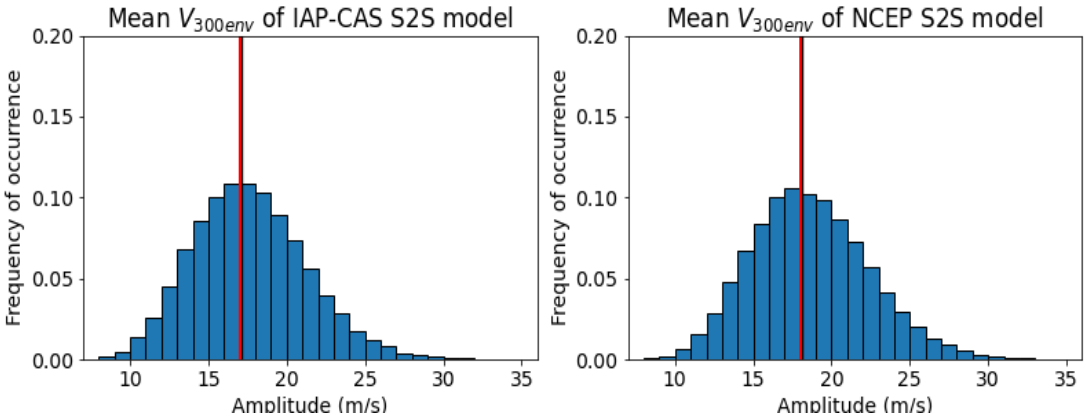

Fig 25. Climatological meridional wind envelope amplitude in the area of study found in the IAP-CAS (left figure) and NCEP (right figure) model. The red line highlights the location of the median of the distribution.

The RWPs tracking algorithm is applied to ERA 5, and only the LLRWPs are retained, registering the dates when LLRWPs are detected (T_d) and the areas where they started propagating (X_d). Next, we apply the RWPs tracking algorithm to the reforecast data. It is worth noting that in the reforecast we are searching for LLRWPs that began their propagation at days T_d near the area X_d. Therefore, we consider the forecasts starting at days T_d. Also, we delete from the data matrix data outside the range of $[X_d - R + V_{min}\ (T_{n-1}),\ X_d+R+V_{max}(T_{n-1})]$ for the first 3 days of simulation. This ensures that the tracking algorithm will not search for RWPs in the reforecast that are not associated with the one observed in the reanalysis. R is the Rossby radius (1000 km), T_n the lead day of the forecast and V_{min} and V_{max} the minimum and maximum speed of propagation of the packets, here considered as 10º and 50º per day in order to allow for small biases in the reforecasted data.

Afterwards, we applied the tracking algorithm for each simulation of the reforecast to search for the forecasted evolution of the LLRWP predicted by the model, and retain only LLRWPs that start their propagation between lead days 1-3 of the forecast. If a LLRWPs matches these conditions, its trajectory is considered as the forecasted evolution of a LLRWPs or FRWPs. On the contrary, if the algorithm does not detect a LLRWPs that fulfil the described condition, we assume that the simulation failed to detect a FRWPs, and

proceed to the next simulation. An example for the NCEP model is displayed in Fig 26, where a LLRWP was detected in ERA 5, and two NCEP simulations, being the FRWPs close to the observed LLRWP.

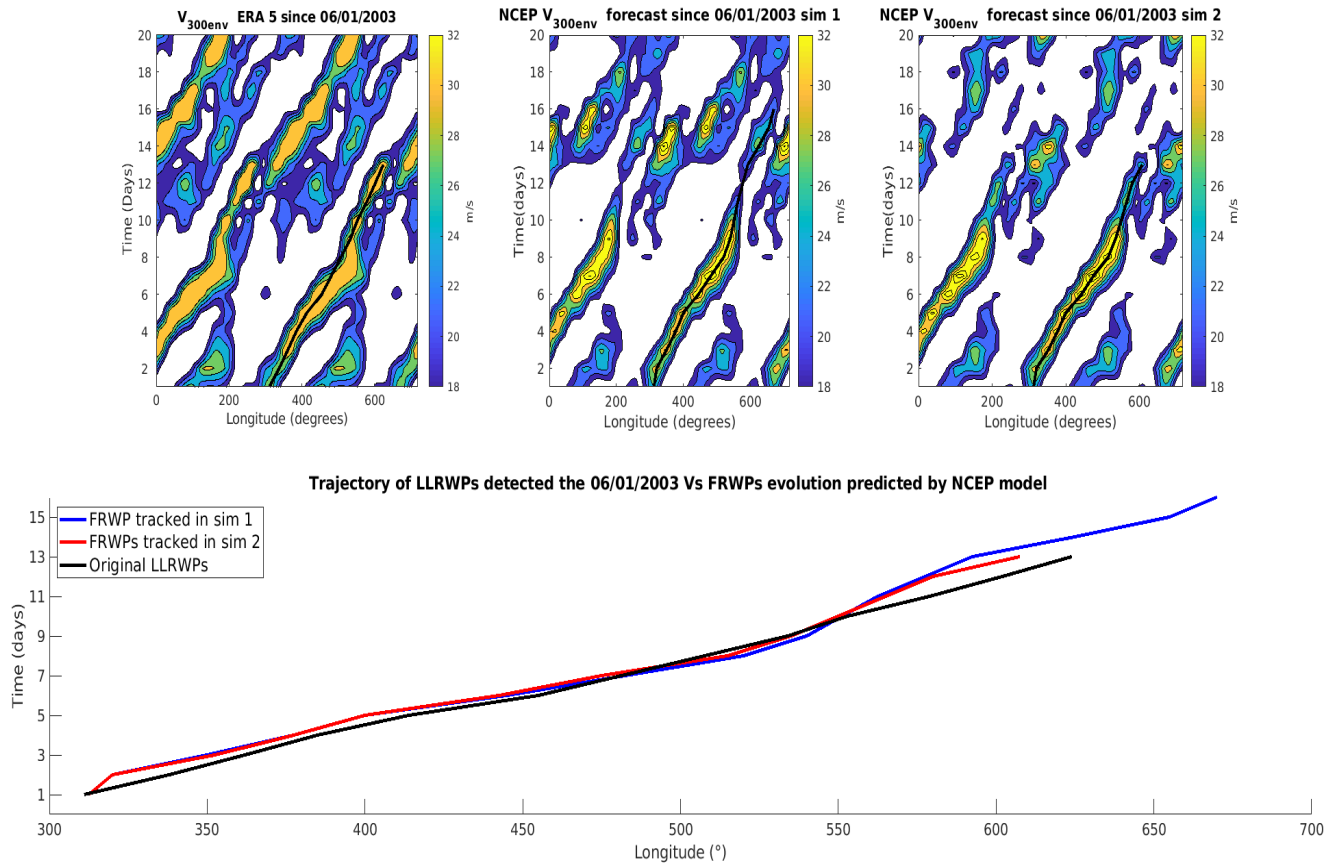

Fig 26. Hovmoller diagram of V_{300env} during the propagation of a LLRWPs observed in ERA 5 at 06/01/2003 (upper left), and NCEP V_{300env} forecast for the first 2 ensemble members (upper mid and upper right), starting the forecast the same day the LLRWPs appear in the ERA 5, dataset plus the graphical representation of the tracked trajectories (down Fig). The black lines in the upper Figs highlight the trajectory of the original LLRWPs (FRWPs) detected in the reanalysis (forecast), and lines in the down Fig the trajectories of the observed LLRWPs (black) and FRWPs (coloured).

6.1.2 Representation of LLRWPs in the forecast models, and the influence of SAM, ENSO and MJO.

We start by analysing if the forecast models are able to predict the development of the LLRWPs, and how similar they are compared to the observed LLRWPs.

To do so, first we measured the proportion of ensemble members able to predict a FRWPs, and the proportion of the FRWPs that lasted more than 8 days during different ENSO/SAM phases. The classification of the SAM and ENSO phases follows the same criteria as in chapter 5.

Next, we measured the displacement in the longitudinal sector between the observed LLRWPs against the FRWPs in each lead day for the first 9 days of simulations. This can help us to assess if the models have a systematic bias at predicting the formation of the LLRWPs, and whether the LLRWPs forecasted by the models propagate with different speeds compared to the observed packets. Furthermore, in order to assess how energetic are the FRWPs compared to the observed LLRWPs, we measure the differences between the V_{300env} values at the centre of the original wave packet minus the V_{300env} values at the centre of the FRWPs, and thus in this way we can study how energetic FRWPs are compared to the observed packets.

In addition, we classified forecasts regarding their capability of detecting and forecasting FRWPs that lasted more than 8 days. Therefore, we classified simulations as best/good/bad/worst forecasts as those that were able to predict the development of a LLRWPs in (100-75)/50/25/0% of the ensemble members, respectively. It is worth pointing out that results of model performance may change by using a larger ensemble. Afterwards, we examined whether LLRWPs forecast is affected by the area where LLRWPs are first detected. To assess this we considered six zonal bands: 0-60ºE, 61-120ºE, 121-180ºE, 181-240ºE, 241-300ºE, 301-359ºE.

Next, we measured the differences in geopotential height anomaly at 300 hPa (anomalies of Z_{300}) using reanalysis and reforecast data during the best/worst LLRWPs forecasts. This is to assess the differences in the mean atmospheric circulation. In order to do so, we constructed the mean anomalies of Z_{300} from days T_d-T_{d+10}, being T_d the starting dates of simulations with the best/worst LLRWPs forecasts. Afterwards, we assess the statistical significance of the results using a Student t-test at 10% level, comparing anomalies of Z_{300} data that belong to dates with best/worst forecasts of LLRWPs against the rest of the dataset, (anomalies of Z_{300} data that do not belong to best/worst forecasts).

Lastly, we studied MJO activity during the periods that showed the best/worst LLRWPs forecasts, so we can assess whether the presence of the MJO during the LLRWPs lifetime affects the models ability to accurately forecast LLRWPs formation and propagation. To do so, we first calculated the climatological frequency of having the MJO in every phase (C), and its standard deviation (STD) during austral summer between 1979-2020. Next, we measured the probability of finding the MJO in a certain phase during the first 10 days since day T_d for the best/worst LLRWPs forecasts. If the relative frequency of

occurrence of a certain MJO phase during good/bad forecasts is outside the range C ± STD, that MJO stage is more frequent/absent than usual.

6.2 Results and discussions.

6.2.1 LLRWPs tracking, ENSO and SAM influence

In this study we found a total of 39 LLRWPs in the austral summer between 1999-2010, (which corresponds to around 3.5 LLRWPs per season). From the 39 packets, 20 were found in neutral SAM years, 14 in negative SAM and 5 in positive SAM. On the other hand, 15 packets were found in La Niña events, 8 in Neutral ENSO and 16 in El Niño years. Results obtained are consistent with the fact that during positive SAM the strengthening of the westerlies diminishes the meandering of the flow, and that positive SAM events disfavour the development of LLRWPs, (Perez *et al.,* 2021).

Both NCEP and IAP-CAS models have 4 simulations available, thus, there are 156 simulations available per model. The NCEP model was able to forecast the development of FRWPs in 86% of the simulations, and 52% of them surpassed the 8 days threshold. FRWPs showed a mean lifespan of 9.1 ± 4.7 days. The IAP-CAS forecasted the development of FRWPs in 84% of the simulations, although barely 40% of them lasted more than 8 days. FRWPs tracked last around 8.2 ± 4.4 days. Oppositely, observed LLRWPs displayed a mean lifespan of 13.0 ± 2.7 days. Therefore, forecast models can predict LLRWPs development but underestimate their lifespan. A distribution of observed LLRWPs and FRWPs lifetime is shown in Fig 27.

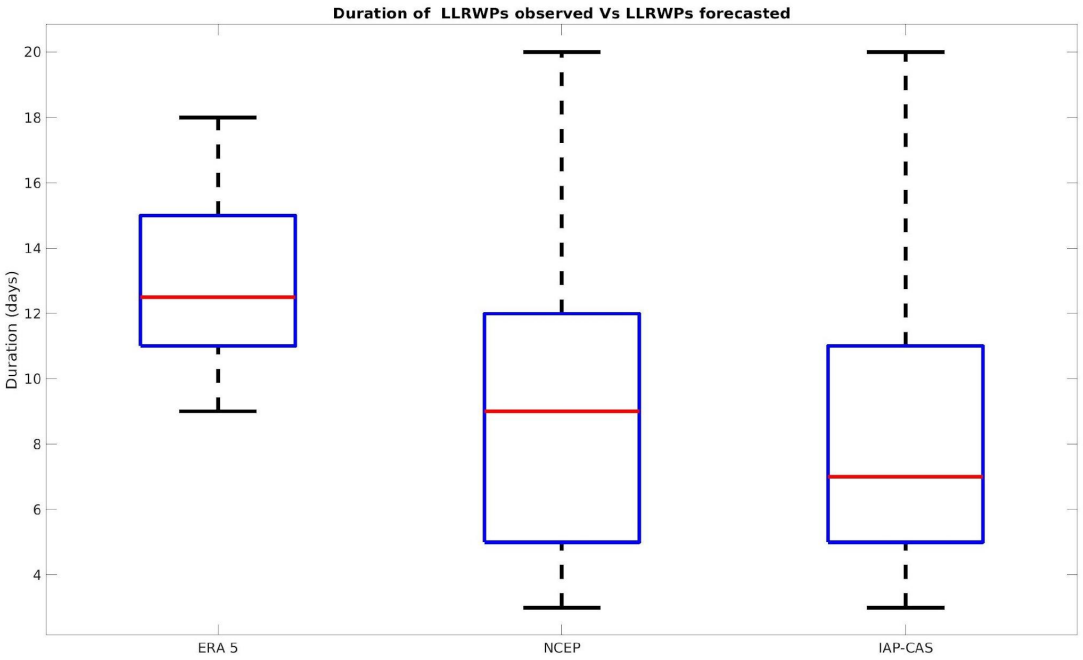

Fig 27. Boxplots distribution of the duration of the LLRWPs observed in ERA 5 (left) against the lifespan of the FRWPs tracked in the NCEP (middle) and IAP-CAS (right) forecast model.

In table 2 we display the percentage of total FRWPs and FRWPs with a lifespan above 8 days regarding the dominant stage of SAM and ENSO phase in the period of study. In the NCEP model, the percentage of total FRWPs found during years with positive SAM is lower compared to other SAM phases, and neutral ENSO shows the largest percentage of detected FRWPs. Overall, in the IAP-CAS model we have similar results to those observed in NCEP. By contrast, in the case of FRWPs that surpassed the 8 day threshold, the highest frequency is found during positive SAM events in the NCEP model, whereas in the IAP-CAS model, we find the lowest proportion for positive SAM events. This large difference might be due to the low number of cases during positive SAM events, which makes the results very sensitive to small differences. Meanwhile, for ENSO events the NCEP model shows the highest (lowest) proportion of FRWPs that surpassed the 8 days threshold in La Niña (neutral) years. On the other hand, in the IAP-CAS the highest proportion of FRWPs with lifespan above 8 days is detected in neutral years, and the lowest during La Niña years.

Total FRWPs detection (%)	El Niño	Neutral	La Niña	SAM +	SAM Neutral	SAM -
NCEP	85	97	78	70	89	85
IAP-CAS	87	84	76	75	87	79
Frequency of FRWPs that lasted more than 8 days in the simulation/ total FRWPs detection (%)						
NCEP	51	38	59	64	38	59
IAP-CAS	41	59	28	20	46	39

Table 2. Proportion of total FRWPs and FRWPs that lasted more than 8 days found in forecasts during different SAM and ENSO stages in NCEP and IAP-CAS models.

From the results in table 2, we generally find that the NCEP model shows higher frequencies of FRWPs that lasted more than 8 days than in the IAP-CAS. This is in accordance with the fact that FRWPs detected in the NCEP model show higher lifespan compared to FRWPs found in the IAP-CAS.

6.2.2 Model representation of LLRWPs and influence of the MJO

Fig 28 displays the zonal displacement between the observed LLRWPs and the location of FRWPs during the first 9 days of the packet's lifespan. FRWPs detected in the NCEP model tend to appear more to the east from the observed packet, whereas those predicted by the IAP-CAS appear more to the west. This pattern remains approximately constant after day one until the 8-9th lead day, when the median of both distributions is near zero. This change could be attributed to the loss of FRWPs as the simulation advances.

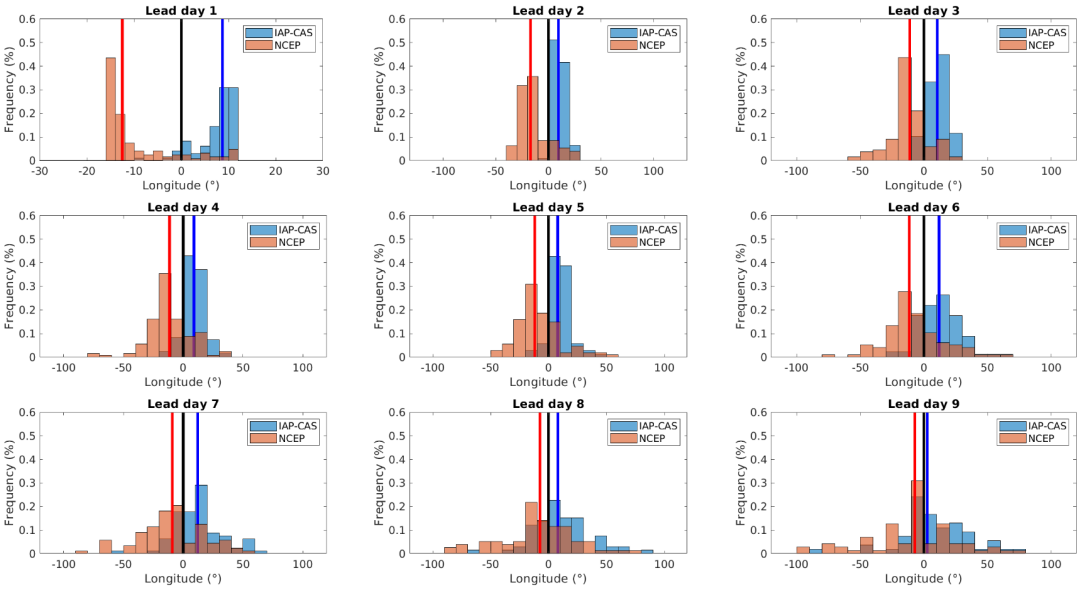

Fig 28. Frequency histogram of the FRWPs displacement from the original LLRWPs found in the reanalysis in each lead day. Positive (negative) bias signals that the FRWPs appear more eastwards (westwards) compared to the observed LLRWPs. Black lines signal the area of 0 bias whereas red (blue) lines show the median location of the FRWPs tracked in the ensemble mean for NCEP (IAP-CAS) forecast.

In Fig 29, we show the difference of V_{300env} at the centre of the packets between the observed LLRWPs minus the tracked FRWPs in each lead day of simulation. Positive (negative) values signal that the forecast model underestimates (overestimates) the energy contained within the packet. At the beginning of the simulation, the NCEP model does not greatly differ from the reanalysis. Nonetheless, starting on the 6^{th} lead day of the simulation, the energy contained in FRWPs decays rapidly, indicating that FRWPs are less energetic compared to the observed LLRWPs. Nevertheless, wave packets tracked in the IAP-CAS always tend to underestimate the energy contained in the observed wave packets. Thus, even though both models detect a similar number of FRWPs, IAP-CAS is much less energetic compared to the reanalysis.

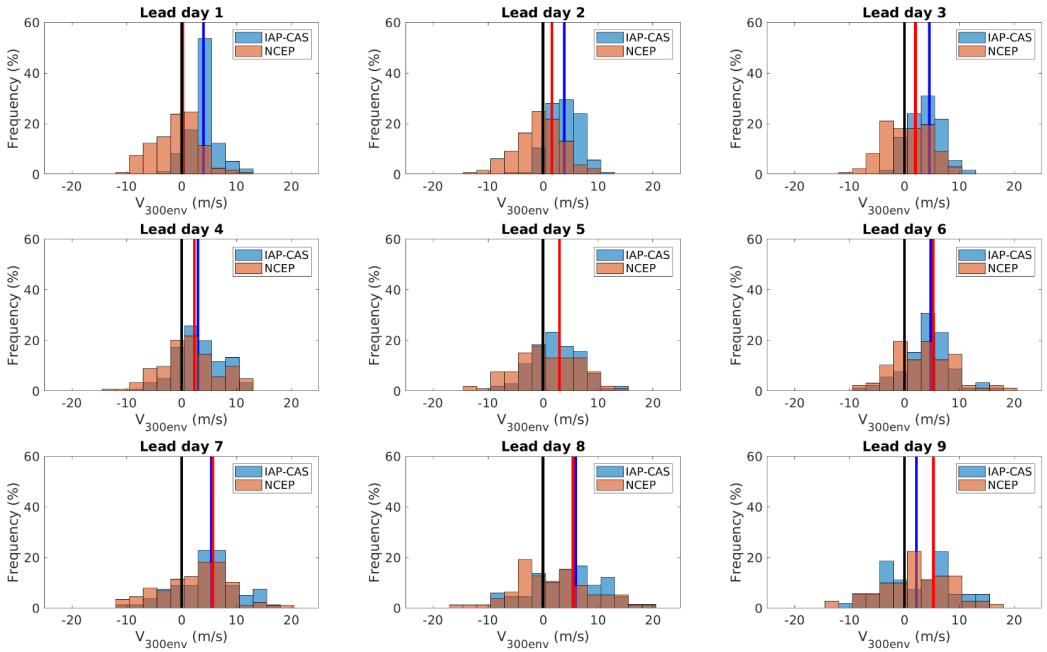

Fig 29. Analogous to Fig 28, but for V_{300env} differences at the centre of the wave packet on the observed LLRWPs against its forecasted trajectory. Positive (negative) values signal that the FRWPs have lower (higher) V_{300env}, thus, RWPs forecasted by the model are less (more) energetic compared to the observed LLRWPs.

Giannakaki and Martius (2016) showed that forecast models in the northern hemisphere tend to underestimate the area and strength of the waveguide. Moreover, Gray *et al.*, (2014) concluded that in the northern hemisphere, the potential vorticity fields where RWPs propagate fall rapidly with lead time in numerical weather prediction models. Therefore, an underestimation of the PV anomaly fields as the forecast advances causes that V_{300env} in the forecast diminishes faster than in the reanalysis. It is plausible to think that a similar process can be at work in the southern hemisphere, therefore, LLRWPs forecasts might be limited to the synoptic scale.

When we focus on the classification of the simulations, nearly 18% of the NCEP simulations belong to the worst forecasts, 23% to bad forecasts, and 59% to good or the best forecasts. Conversely, 36% of the IAP-CAS simulations belong to the worst forecasts, 26% to bad forecasts, whereas only 38% belong to the good/best forecasts. These results further suggest that the NCEP model is better at forecasting LLRWPs compared to the IAP-CAS.

Fig 30 shows the areas where the total proportion of FRWPs/FRWPs that lasted more than 8 days appeared. Both models show that most FRWPs were first detected in the eastern Pacific (241-300ºE), and western South-Atlantic basins (301-359ºE). But when we retain simulations that are part of good and/or best

forecasts, most of FRWPs were first detected at the central-eastern Pacific basin (180-300ºE) in the NCEP model, and in the eastern Pacific (241-300ºE) for the IAP-CAS model. One possibility that might explain these results is that the eastern Pacific basin has a maximum of baroclinicity (Solman *et al.,* 2003), which favours RWPs development. Thus, RWPs that appear in the eastern Pacific basin will propagate toward the Atlantic-Indian sector where the jet stream, which acts as a waveguide where RWPs propagate, reaches its maximum intensity. Consequently, FRWPs gain stability and propagate for longer periods**.**

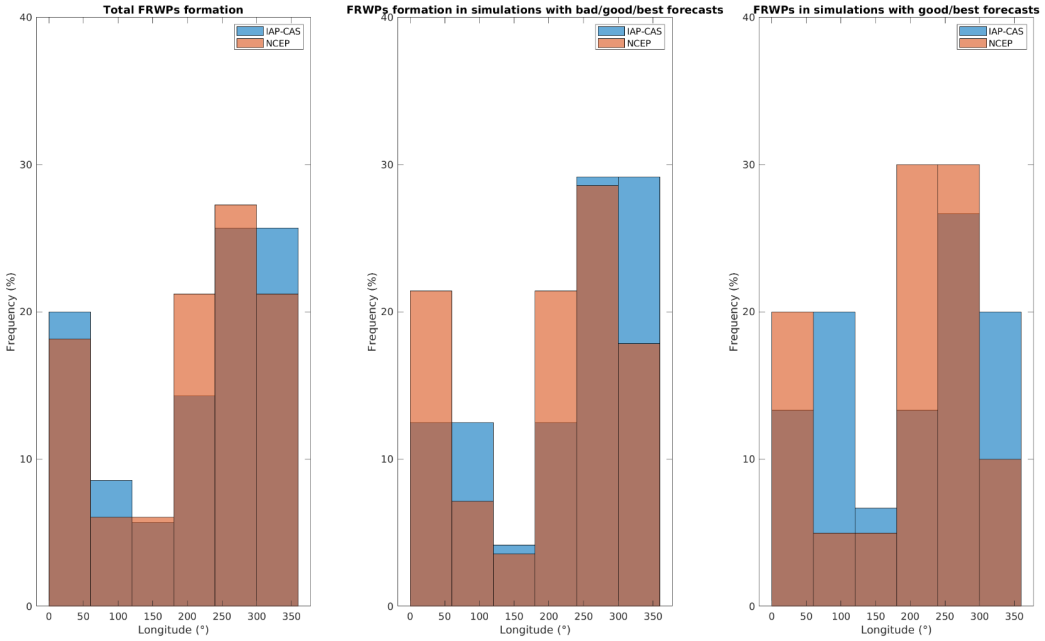

Fig 30. Detection areas of total FRWPs/ proportion FRWPs that lasted more than 8 days in the simulations.

We next examine the mean atmospheric flow in the reanalysis and forecast models during the best/worst forecasts (Fig 31). It is worth mentioning that Perez *et al*., (2021) concluded that the northward displacement of the jet stream (this is, during negative SAM events) causes the development of a cyclonic circulation to the southwest of New Zealand. This enables the extension of the waveguide where RWPs propagate into the Pacific, thus favouring LLRWPs. In agreement with this study, Fig 31 shows in all panels an anomalous cyclonic circulation to the southwest of New Zealand. Moreover, this cyclonic circulation is strongest and is accompanied by generally low geopotential height anomalies

between 40ºS-60ºS during the best forecasts. In addition, anomalies of Z_{300} in high latitudes significantly increase during the best forecasts which, together with the negative anomalies of Z_{300} in midlatitudes, signal the manifestation of negative SAM events. Consequently, results suggest that LLRWPs forecasting might be more feasible during negative SAM years. Alternatively, during the worst forecasts, the circulation anomalies do not show a clear common global pattern. There seems to exist a stationary wave extending from Australia southwards in both models. However, in NCEP forecasts, there are several positive anomalies of Z_{300} anomalies in subtropical latitudes that are not present in IAP-CAS. These findings suggest that some atmospheric processes might lead to the development of a stationary wave near New Zealand which impedes RWPs propagation into the Pacific. Furthermore, the spatial structure suggests that the wave patterns of Fig 31 may be at least partly forced from the tropical region. To further look into that we explore the possibility that the MJO may play a role.

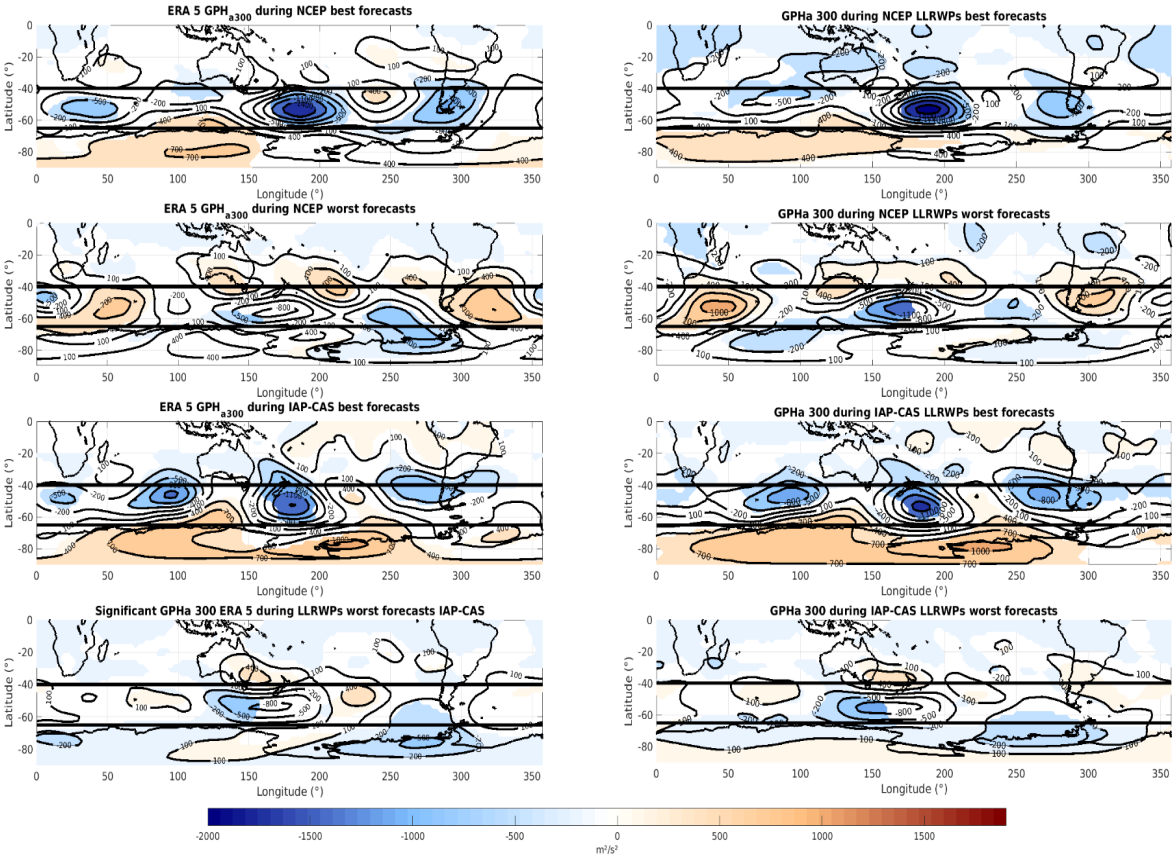

Fig 31. Anomalies of Z_{300} fields from T_d -T_{d+10}, being T_d the dates when we obtained the best/worst forecast in the NCEP and IAP-CAS models. Left (right) Figs show the anomalies of Z300 field obtained using the reanalysis (forecast) data. Orange (blue) areas signal positive (negative) anomalies.

Fig 32 shows the probability of occurrence of a certain MJO phase during the best/worst forecasts against their climatological frequency. We find that during the best forecasts, both models show an anomalously inactive MJO, and phases 4-8 are specially absent, particularly in the IAP-CAS models. Also, the probability of finding phases 1-3 is near climatology. By contrast, during the worst forecasts in the NCEP model, the MJO is more active than usual in phases 3 and 5, oppositely, phases 1-2 are mostly absent, whereas the rest of the phases occur near climatology. In the IAP-CAS model, the worst forecasts are also characterised by an active MJO, particularly in phases 3 and 8, appearing with much higher frequency than the climatology. Thus, in both models the best (worst) forecasts are characterised by an inactive (active) MJO.

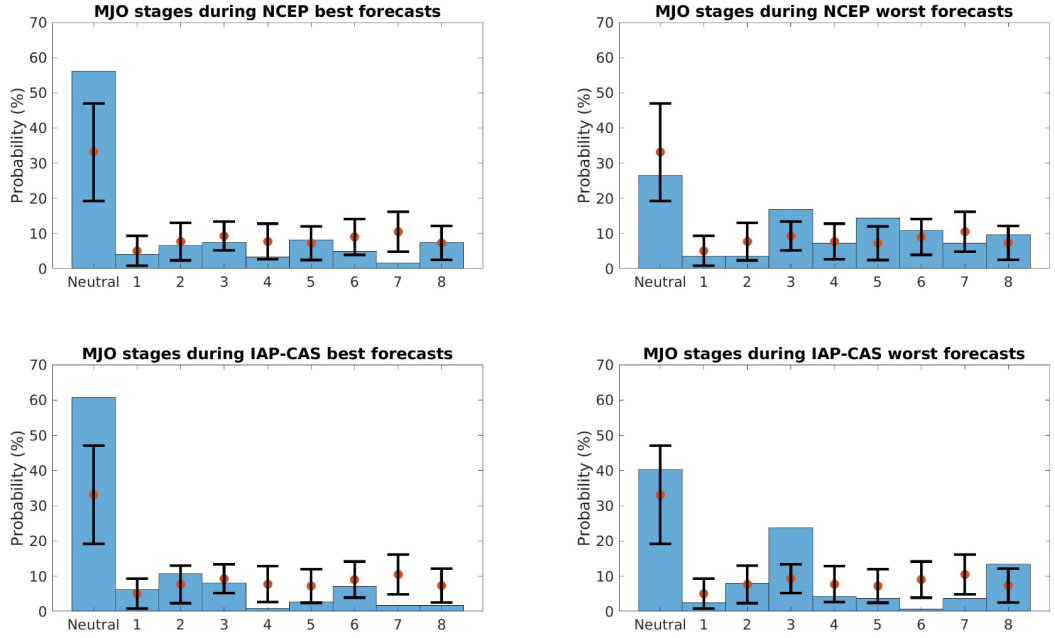

Fig 32. Relative frequency of the MJO phases detected during the propagation of LLRWPs for the best (left Figs) and worst (right Figs) forecasts found in NCEP and IAP-CAS models. Orange dots represent the mean climatological probability of finding the MJO in a specific phase whereas back lines show the range between mean climatological probability ± its standard deviation.

The anomalies of Z_{300} patterns shown in the composite of the worst forecasts of the NCEP and IAP-CAS models (Fig 31), do not match with circulation anomalies associated with their most frequent stages of the MJO (see Fig 1 of Alvarez *et al.,* 2016). One reason that might explain these results is that because the MJO is more active than usual in certain phases, the anomalies observed are a mixture of signals without a defined structure. Therefore, the

maps obtained are not similar between models, and usually show weaker anomalies of Z_{300} values that are less significant than the anomalies associated with the best forecasts.

Results show that an active MJO degrades the LLRWPs forecast, which might be attributed to the interaction between the tropically excited and mid-latitude waves. Nonetheless, we have to take into consideration that even though the MJO forecast is reliable until 25 days in advance (Fu *et al.*, 2013), current biases in the representation of the MJO and its teleconnections (Lim *et al.,* 2018) may degrade LLRWPs predictions.

6.3 Summary

RWPs are atmospheric perturbations that can last for several days to weeks in the atmosphere before disappearing and are considered precursors of extreme weather events. Thus, studying the representation of these long-lived packets in forecast models is a way to understand the model's limitations in predicting extreme weather events in the sub-seasonal time scale. In this study we considered two S2S models (NCEP and IAP-CAS), and observed if they are able to correctly forecast the formation and development of long-lived RWPs. To do so, we compared the observed long-lived RWPs trajectories detected in the ERA 5 reanalysis against the forecasted trajectories predicted by the two forecast models, as well as identified which atmospheric conditions favour the development of good/bad forecast of long-lived RWPs. Results showed that:

-1st Long-lived RWPs predicted by the NCEP are systematically shifted to the east from the original packet, whereas those forecasted by IAP-CAS appear more westward. Nonetheless, forecasted long-lived RWPs by both models propagate with similar speeds.

-2nd Both NCEP and IAP-CAS models struggle at predicting RWPs that last more than 1 week in the atmosphere because packets rapidly lose energy after 6-7 days of simulation, which limits long-lived RWPs forecast to the synoptic scale.

-3rd Good long-lived RWPs forecasts are detected when the wave packets begin their propagation in the eastern Pacific, and during negative SAM events.

-4rd An active Madden Jullian Oscillation degrades LLRWPs representation in the forecast.

7| WAVE BREAKING EVENTS AND THEIR LINK TO ROSSBY WAVE PACKETS AND ATMOSPHERIC BLOCKINGS DURING SOUTHERN HEMISPHERE SUMMER

The aim of this chapter is to study the link between propagating RWPs and RWB events, and also to assess whether RWPs can cause large-scale RWB events with enough stability to be considered an atmospheric blocking. In order to do so, first we search for RWPs, RWB events and atmospheric blockings using specific algorithms for each one of them. Second, we link large-scale RWB events to RWPs that stopped propagating. Third, we study the interannual variability of large-scale RWB events associated with LLRWPs and/or short-lived RWPs (SLRWPs). Four, we assess the link between large-scale RWB (associated with RWPs) with atmospheric blocking development. It is expected that understanding the connection between atmospheric blocking development and RWB events linked to RWPs will improve extreme weather event detection 10-30 days in advance. [4]

The chapter is organised as follows. Section 7.1 describes the datasets, the methodology and parameters used to detect RWPs and RWB events, as well as the procedure followed to link RWB events with RWPs, and RWB events with atmospheric blocking. Section 7.2 shows the verification of the Rossby Wave Breaking algorithm and the characteristics of the large-scale RWB events linked to RWPs. Section 7.3 focuses on the interannual variability of RWB and the potential impact of global modes of variability. Section 7.4 assesses the link between atmospheric blocking and RWB events, and section 7.5 presents a summary of the study.

[4] A scientific article was written with the results obtained in this chapter, and it is under review in the Journal of Geophysical Research- Atmospheres as: Pérez-Fernández, I, Barreiro, M, Ehstand, N, Hernández-García E, López Cristobal. (2022) Wave Breaking Events and their link to Rossby Wave Packets and Atmospheric Blockings during Southern Hemisphere Summer,

7.1 Data and methodology

7.1.1 Data

In this study we transform meridional wind speed at 300 hPa into $V_{300env,}$ following the same methodology from chapter 4.1 in order to characterise the RWPs. This is, subtracting the seasonal and climatological variability, and retaining only transient RWPs (RWPs with a zonal wavenumber between 4-11).

For the detection of RWB events, we computed the potential vorticity field following isentropic coordinates as in (Ndarana and Waugh 2010 a,b, Barnes *et al.*, 2012). In order to calculate the potential vorticity field, we used daily mean temperature and wind speed at 200, 250, 300 and 350 hPa levels interpolated to the isentropic coordinates of 330ºK following Hoskins *et al*., (1985).

In order to locate atmospheric blocks, we used Z_{500}. Finally, the Oceanic Niño Index (ONI) and Antarctic Oscillation index (SAM index) were used in order to characterise the interannual variability of the global climate modes. Both datasets are publicly available on the NOAA website (https://origin.cpc.ncep.noaa.gov/).

7.1.2 Tracking of Rossby Wave Packets and Rossby Wave Breaking events

The detection of the RWPs follows the algorithm described in chapter 4.1, which also measures the characteristics of the RWPs, such as their lifespan and area of detection. After finishing the tracking of RWPs, we classify all RWPs into LLRWPs (lifespan >8 days) and short/medium lived RWPs or SLRWPs (lifetime <=8 days).

In order to detect and track RWB events, we applied the algorithm described in chapter 4.2. Nonetheless, before using the algorithm, we need to decide which isentropic coordinates are the most adequate to track RWB events. Previous studies chose the isentropic coordinates between 310-350ºK (Ndarana and Waugh 2010 a, b, Strong and Magnusdottir 2008) because they represent the levels in which the dynamic tropopause is located in high and subtropical latitudes (Ndaran and Waugh 2010a). For this study, we selected the PV field following the isoline of 330ºK, and search for RWB events that occurred on the line of -2 PVU (1 PVU = 10^{-6} m^2 s^{-1} K kg^{-1}), which is located between the isolines of 310-350ºK where anticyclonic and cyclonic shear dominates.

Given the few studies reported on RWB for the Southern hemisphere it is important to ensure that the detection algorithm works as expected. To do so, we first tracked wave breaking events in the December-March period between 1979-2008 (instead of the complete period 1979-2021), and compared our

results against previous studies (Ndarana and Waugh 2010 a,b, Wang and Magnusdottir 2010).

7.1.3 Linking large-scale Rossby Wave Breaking to propagating Rossby Wave Packets

In this section we explain the methodology used to link RWB activity to the dissipation of RWPs. At the moment of writing this article, the authors were not able to find a study which links RWB events with RWPs in the Southern Hemisphere. In consequence, in this section a methodology to search for RWB events caused by RWPs was proposed. Nonetheless, before describing the methodology, it is important to remark two considerations:

1.-Only large-scale RWB is considered, that is, RWB events with a longitudinal extension of 1000 km (~15º in mid latitudes) or above (Barnes *et al.,* 2012). This is done in order to retain wave breaking events that can strongly affect the large-scale atmospheric circulation and have a spatial scale similar to atmosphere blocking, (11º of extension, Patterson *et al*., 2019).

2.-We search for large-scale RWB events that occur between days T_f - T_{f+4}, being T_f the last day we recorded the trajectory of a propagating RWP. This is done because the RWPs might stay stationary for a few days before disappearing. By examining the evolution and behaviour of potential vorticity fields several days after the dissipation of a RWPs we chose an upper limit of 4 days because after 4 days we barely find large-scale RWB events that could be linked to the disappearing packet.

The methodology used for linking RWPs with large-scale RWB events is as follows:

1.-Apply the RWB tracking algorithm at day T_f, being T_f the day when a RWP finished its propagation.

2.-If the algorithm detects the geographical centre of a large-scale RWB event located between X_f ± 2000 km, being X_f the longitudinal section where the algorithm last observed a RWPs before stopping its propagation, we assume that the wave breaking event registered is linked to the RWP and proceed to step 3. If the described condition is not fulfilled, we continue looking for large-scale RWB events for the following days. If by day T_{f+4} we do not find a large-scale RWB event that matches the described condition, we assume that the RWP did not display a large-scale RWB episode and finish the search. Oppositely, if after applying the wave breaking detection algorithm we detect two or more large-scale RWB events which are in the range X_f ± 2000 km, we select

the large-scale RWB event whose geographical centre is closer to the area of dissipation of the RWP.

3.-We register as T_n the day when a large-scale RWB event linked to a RWP is detected and apply the RWB tracking algorithm on day $T_{n.+1}$. If there is a large-scale RWB event whose geographical centre is within 20º (~1400 km**)** of distance or less from the wave breaking episode found at day $T_{n,}$ we assume that this event is an extension of the RWB event found the previous day. Else, we infer that the RWB episode only lasted for a day.

4.- Step 3 is repeated for the following days until we stop finding wave breaking events that fulfil the condition specified in step 3.

5.- We save the characteristics of the large-scale RWB events, (area and date of detection, longitudinal and latitudinal extension, shear), as well as the days elapsed since the dissipation of the RWPs and the lifespan of the large-scale RWB event.

In step 2, we search for large-scale RWB events in the area located between X_f ± 2000 km because even if X_f signals the centre of the RWP, the packet has a certain longitudinal extension, and thus the large-scale RWB event does not have to necessarily appear near X_f. In Barnes *et al.* (2012) they considered that RWB events that are within 2000 km of the geographical centre of the large-scale RWB belong to the same episode, hence, in this study we look for large-scale RWB events that are up to 2000 km of distance from the area of dissipation of the RWPs.

Additionally, in step 3 we used a distance of 1400 km to search for the continuation of a large-scale RWB episode because using a larger distance can cause the algorithm to select a wrong wave breaking event that is too far away from the original episode that is being tracked.

Fig 33 shows an example of the methodology followed to link RWB events with RWPs that stopped their propagation.

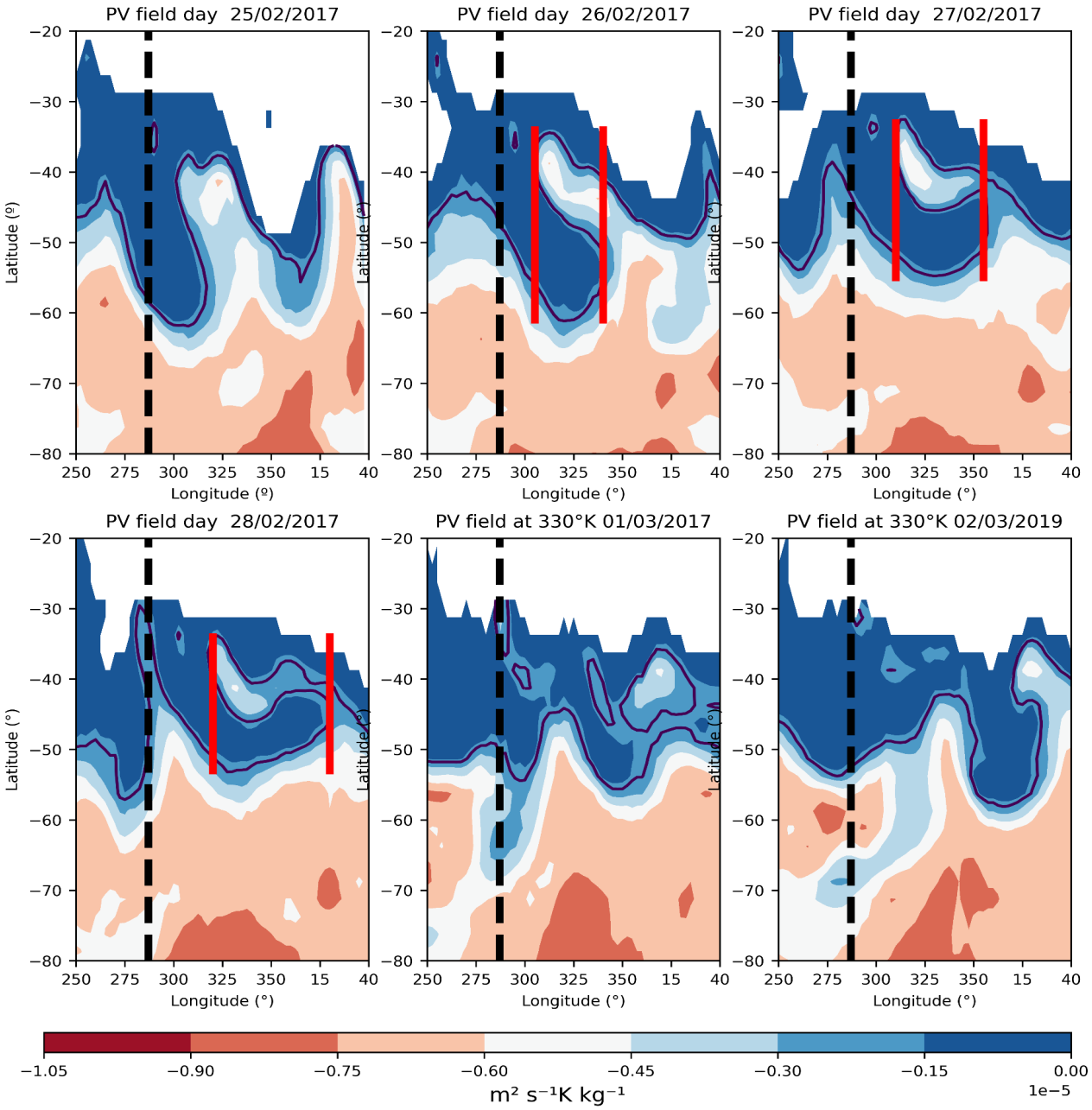

Fig 33. Potential vorticity fields following the 330ºK isosurface between 25/02/2017-01/03/2017. The black discontinuous line shows the longitudinal section where a LLRWPs stopped its propagation at 25/02/2017, whereas the red lines indicate the longitudinal section of RWB detected by the wave breaking algorithm. The bold black line indicates -2 PVU.

7.1.4 Linking large-scale Rossby Wave Breaking events to atmospheric blocking

Lastly, we observed the proportion of large-scale RWB events that are present nearby the development of an atmospheric blocking event. In order to detect atmospheric blocking events, we use the methodology defined in chapter 4.3 to

find areas where instantaneous blocking situations have enough extension and lifespan to be considered atmospheric blockings.

As we described in chapter 4.3, in our study we registered events that have a minimum longitudinal extension of 7.5, 10, 12.5 and 15º and display a minimum lifespan of 4-5 days. This is done in order to assess whether the proportion of atmospheric blocks that might be linked to RWB is sensitive to the blocking conditions. Hence, events that last at least 4 days with a minimum longitudinal extension of 7.5º are the most frequent and represent blocking-like situations, that is, the persistent reversal of the westerly wind flow that are not sufficiently extensive to be considered as a blocking event. On the other hand, those events that last more than 5 days and have a zonal extension of 15º or above are considered the strongest blocks of the dataset.

Before linking RWB events to atmospheric blocking, we verified that our methodology is able to correctly detect the manifestation of atmospheric blocking. This is done by measuring the frequency of occurrence and areas of formation of atmospheric blocking events and comparing the results to those obtained in Mendes *et al.*, (2011). We then study the potential links between large-scale RWB events and blocking events by identifying the atmospheric blocking events that manifest the same day a large-scale RWB event is present in the atmosphere, and such that their respective geographical centres are separated by a maximum of 2000 km. The fulfilment of the latter conditions ensures that the large-scale RWB event is present near the development of the atmospheric block. Lastly, we determine how many of the RWB events that occur near an atmospheric block are associated with propagating RWPs. This analysis assesses the proportion of atmospheric blocks that are associated with large-scale RWB activity, and whether large-scale RWB activity linked to propagating RWPs is directly linked to the development of atmospheric blocking events.

7.2 Results and discussion

7.2.1 Verification of Rossby Wave Breaking algorithm

The analysis of RWB events during the December-March season between 1979-2008 detected a total of 659 RWB events in December, 470 in January, 413 in February and 581 events in March. As for the orientation of the RWB events, 22% of the total wave breaking activity belongs to cyclonic RWB, and the rest to anticyclonic RWB.

Fig 34 shows the longitudinal distribution of RWB frequency of occurrence. The maximum RWB activity occurs in the western-central Pacific (between 120-240º

E), and the lowest activity is located near 0ºE. These results indicate that RWB is weakest at the jet entrance in the Atlantic basin, and largest at the jet exit, consistent with the fact that RWPs activity occurs in the Atlantic-Indian basin where the strong jet acts as waveguide (Pérez *et al.*, 2021).

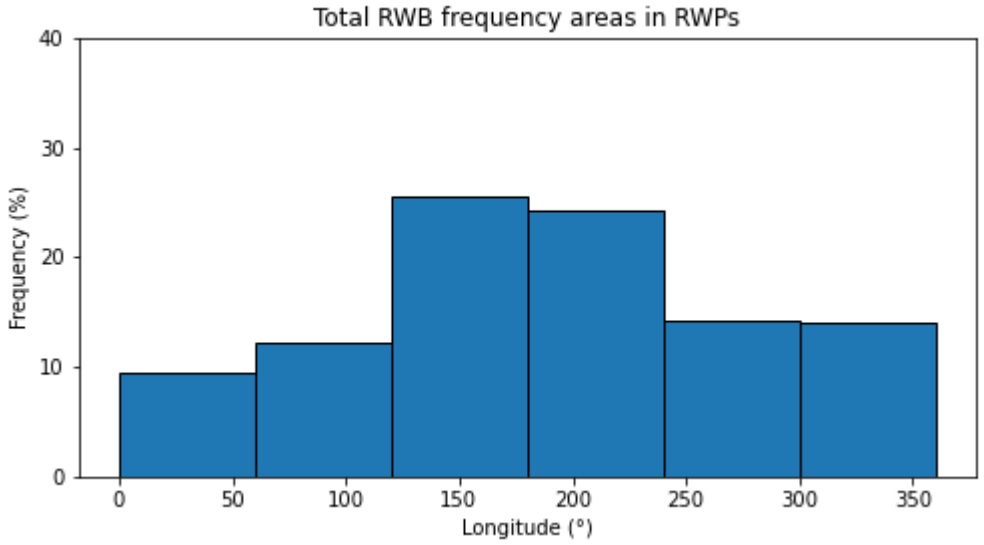

Fig 34. Frequency of occurrence of RWB during summertime in the Southern Hemisphere.

Additionally, Fig 35 shows that the main area of anticyclonic RWB detection is located in the western Pacific, as reported by Ndaran and Waugh (2010b). We also observe two secondary areas of maximum anticyclonic RWB activity, one located in the Indian Ocean and the second in the eastern Pacific-western Atlantic, which is also in agreement with Ndarana and Waugh (2010b). These authors found very little anticyclonic RWB activity in the Indian Ocean during December-February, but found significant RWB activity in that region during March-May, suggesting that the differences with our results are explained because of our consideration of March in the summer season. Thus, overall our results are close to those observed in Ndarana and Waugh (2010b), providing a verification of our RWB algorithm. It is worth pointing out that in our case the areas of RWB frequency have wider meridional extension than those found in Ndarana and Waugh (2010b), because our algorithm registers the whole latitudinal area where the overturning potential vorticity is detected.

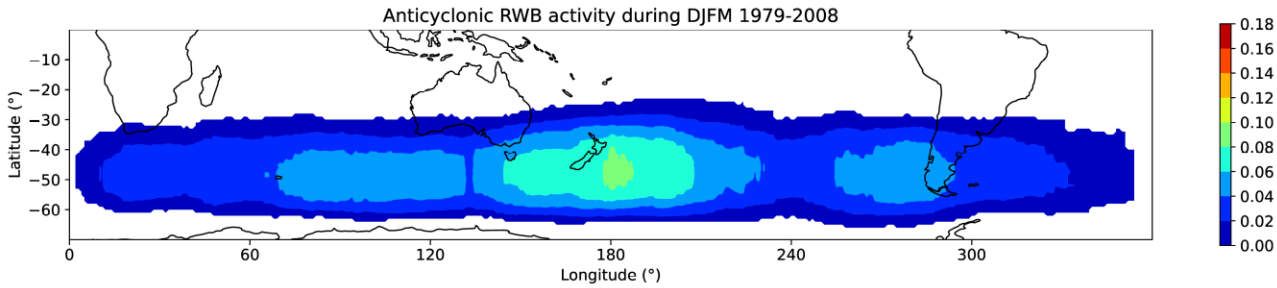

Fig 35. Anticyclonic RWB frequency of occurrence between 1979-2008 (in decimals). Coloured areas show where RWB episodes were detected.

7.2.2 Characteristics of Rossby Wave Breaking after Rossby Wave Packets propagation

For the Southern Hemisphere summertime during 1979-2021, a total of 1256 RWPs were found, which corresponds to around 30 per season. Moreover, 141 were LLRWPs, which is about 11 % of the total RWPs. From the 141 LLRWPs, 45% have associated large-scale RWB, whereas for the SLRWPs (1115 cases) this proportion is close to 39%. In both cases most RWB events show mainly anticyclonic shear: 79% (76%) of the RWB episodes detected after the propagation of a LLRWP (SLRWP) show anticyclonic RWB.

Fig 36 displays the frequency of occurrence of all large-scale RWB events that happened after the end of a LLRWPs or a SLRWPs (Fig 36a and 36b, respectively) as a function of longitude, as well as large-scale RWB linked to all RWPs (Fig 36c). When we focus on large-scale RWB events linked to the end of LLRWPs propagation (Fig 36a), most of these events mainly occur between 240-300 ºE (eastern Pacific basin). On the other hand, large-scale wave breaking events linked to SLRWPs and to all RWPs (Fig 36b and 36c) mainly occur at the region 120-240ºE (western and central Pacific), in agreement with figure 35 and with Ndarana and Waug (2010a), where most RWB activity is detected at the western Pacific basin. Fig 36b and 36c show very similar distributions because SLRWPs represent around 90% of all RWPs, thus the distribution of total large-scale RWB activity linked to RWPs is highly influenced by the SLRWPs. Oppositely, figure 36a shows that large-scale RWB associated with LLRWPs is eastward displaced compared to the rest of the packets. Perez *et al.* (2021) showed that LLRWPs propagation is modulated by SAM, and during negative SAM, when LLRWPs occur more often, the waveguide where RWPs propagate is extended into the Pacific. Thus, one possibility that might explain these results is that when LLRWPs propagate, they propagate further east and break in the eastern Pacific, instead of in the western Pacific sector. Hence, large-scale wave breaking events associated with LLRWPs tend to

occur in the central-eastern Pacific basin, which could imply that long-lived packets might be precursors of weather regime transitions affecting conditions in South America.

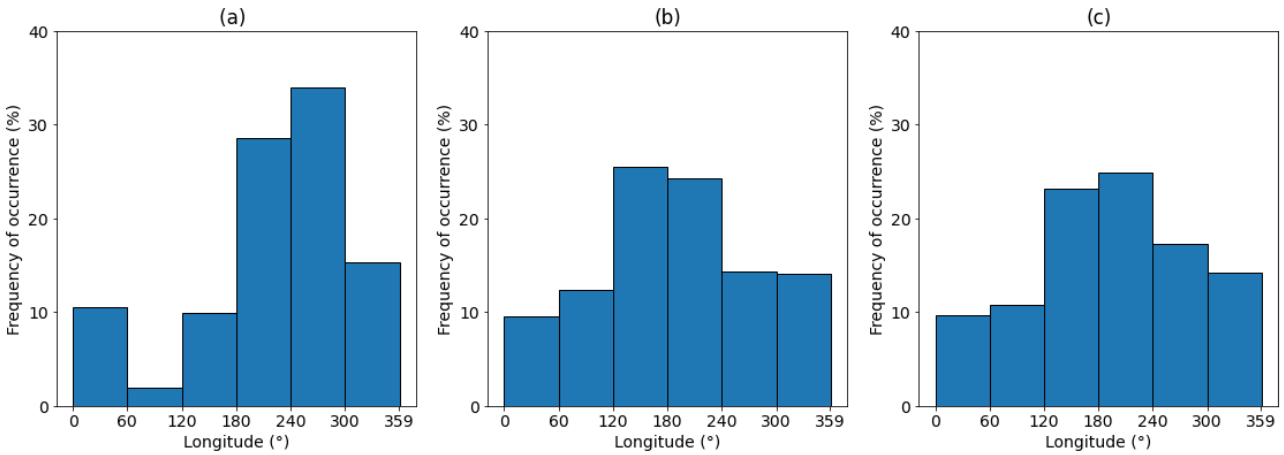

Fig 36. Relative frequency of occurrence of large-scale RWB associated with (a) LLRWPs, (b) SLRWPs and all RWPs (c).

Fig 37 shows temporal and spatial characteristics of large-scale RWB events detected after the dissipation of LLRWPs and SLRWPs. Fig 37a and 37d display the number of days that pass until a RWB event is detected after the dissipation of a LLRWPs or a SLRWPs, respectively. The two distributions are similar, that is, most of the RWB events occur the same or the next day after the RWP stops its trajectory, and 3 days after the RWPs stopped propagating, there is almost no large-scale RWB activity linked to RWPs. Additionally, Fig 37b and 37e show the lifespan of the RWB events linked to SLRWPs/LLRWPs, indicating that most of the large-scale RWB linked to RWPs last between 1-2 days, and that there are no significant differences between distributions. Nonetheless, when we compare the zonal extension of the wave breaking events, (Fig 37c and 37f), RWB events that occur after the propagation of SLRWPs usually cover larger longitudinal extensions compared to those observed after LLRWPs. RWB events linked to LLRWPs show a median longitudinal extension of 22º, and an interquartile range of 12º, whereas RWB associated with SLRWPs have a median of 26.5º and display an interquartile range of 15º. A Kruskall-Wallis test applied to the datasets of figure 37c, indicates that the distributions are significantly different, at 5% level of significance.

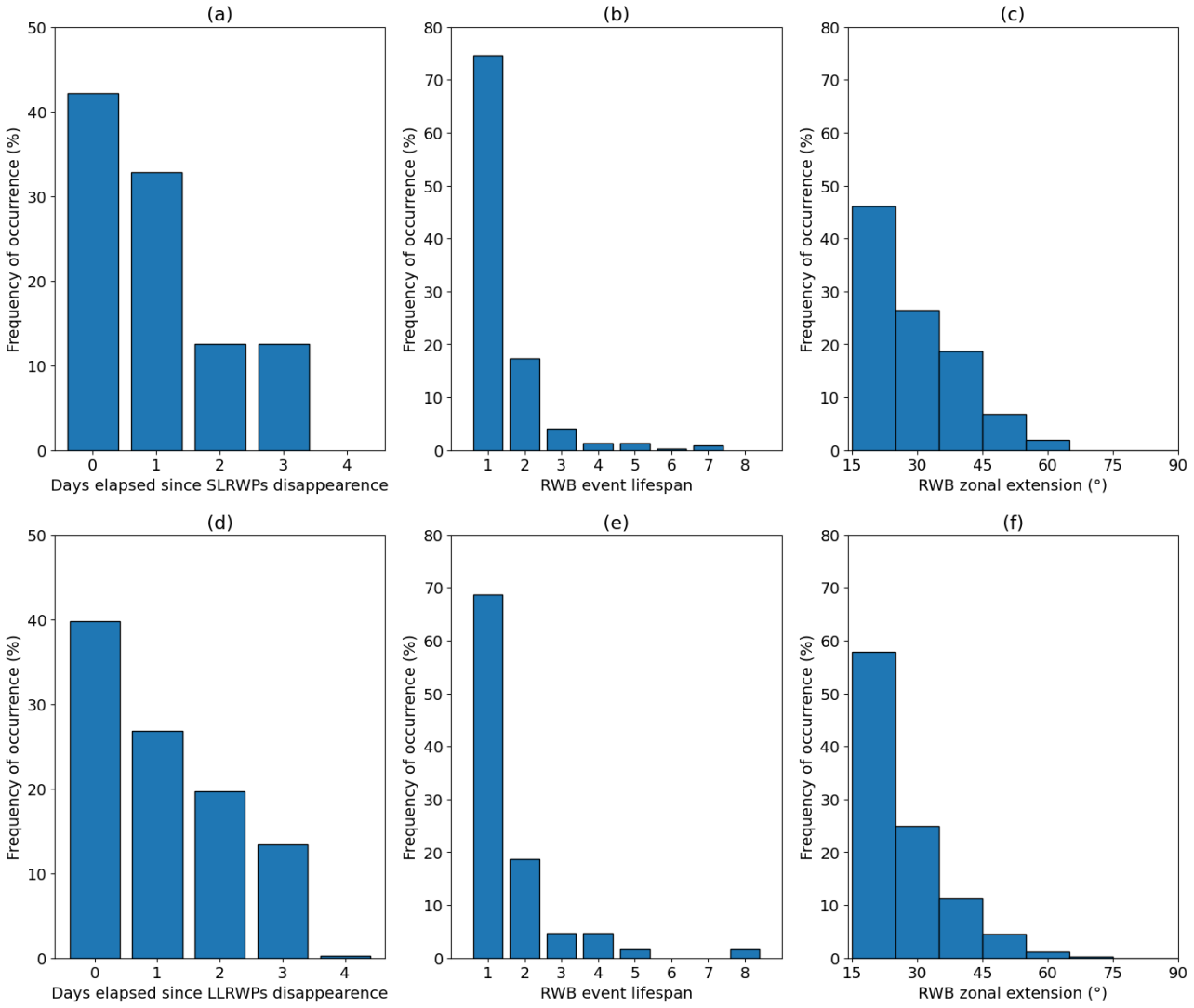

Fig 37. Histogram distribution of several characteristics of RWB associated with SLRWPs (upper figures) and LLRWPs (lower figures). Figures 37a and 37d represent the number of days passed when a large-scale RWB event appears after the end of the SLRWPs and/or LLRWPs propagation respectively, (being day 0 the same day the wave packet stopped propagating). Figures 37b and 37e display the lifespan of the RWB linked to SLRWPs and LLRWPs. Lastly, figures 37c and 37f show the longitudinal extension of the RWB linked to SLRWPs and LLRWPs respectively.

Hence, these results suggest that RWB events caused by SLRWPs cover larger longitudinal extensions of the atmosphere compared to those produced by LLRWPs. Nonetheless, neither LLRWPs nor SLRWPs seem to be directly related to atmospheric blocking development because, even if the associated RWB events have similar spatial scales to a blocking event, they tend to last only about 1-2 days, too short to lead to atmospheric blocking.

7.2.3 Interannual variability of Rossby Wave Breaking events associated to LLRWPs/SLRWPs

In Perez *et al. (*2021) they discovered that there is a negative correlation between SLRWPs and LLRWPs, such as during years with high LLRWPs activity, SLRWPs occur less often. Therefore, in this section we first want to assess if there is a link between large-scale RWB associated with LLRWPs and those associated with SLRWPs. Fig 38a shows the interannual variability in the occurrence of RWB associated with LLRWPs and SLRWPs. Both time series show large year-to-year variability. In the case of LLRWPs, the number of annual RWB events range from 0 to 11, while for SLRWPs it ranges from 6 to 32. During certain periods the frequency of occurrence of RWB associated with the LLRWPs and SLRWPs seem to be out of phase. However, the scatter plot of both time series (Fig 38b), displays no consistent link between large-scale RWB linked to long and short-lived RWPs.

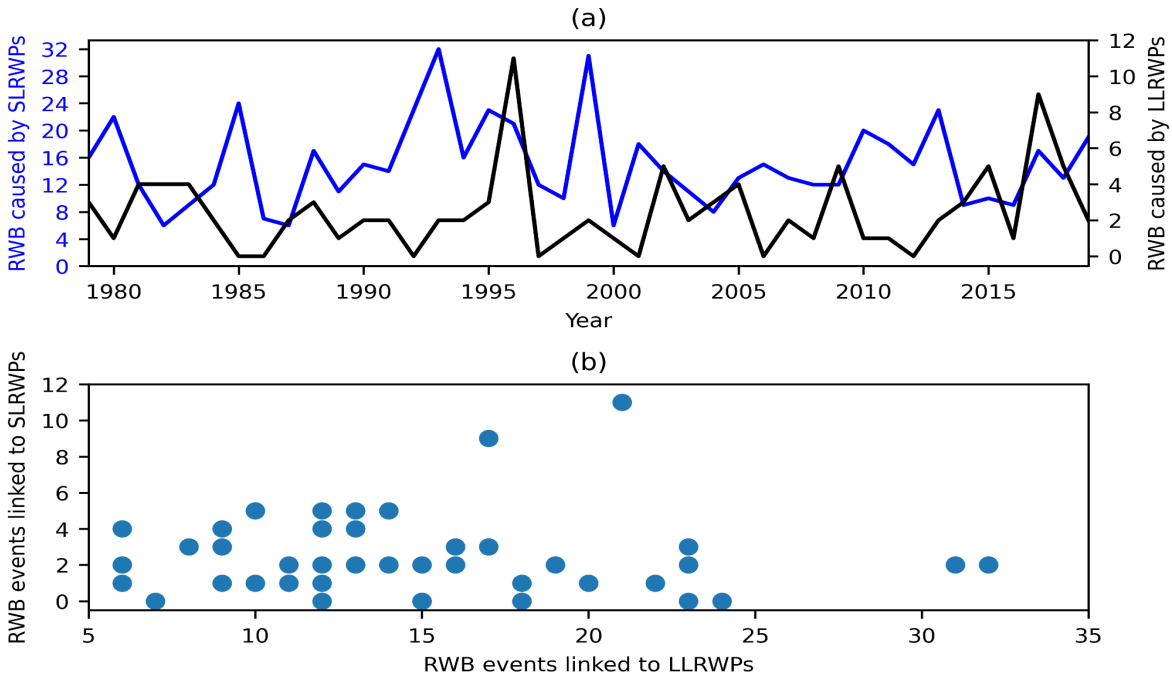

Fig 38. Variability of RWB events linked to RWPs. Upper figure (38a) shows the interannual variability of RWB events associated to LLRWPs (black) and SLRWPs (blue lines) during the period of study, whereas figure (38b) displays the same information of figure a but in a scatter plot.

Fig 39 shows the frequency of occurrence of large-scale RWB events linked to SLRWPs and LLRWPs with the SAM/ENSO indices. When we focus on large-scale RWB linked to LLRWPs (Fig 39a and 39b respectively), the correlation analysis shows a low value of R^2 and high dispersed data distributions. This indicates that there is no linear relationship between the number of RWB events linked to the dissipation of LLRWPs with SAM or ENSO. It is worth noting that one reason that can influence the results is that there are several years without RWB activity linked to LLRWPs, which can increase the difficulty of finding significant correlation between the timeseries of RWB events linked to LLRWPs and SAM or ENSO activity.

Fig 39c and 39d show the interannual variability of RWB events linked to SLRWPs with SAM/ENSO indices (Fig 39c and 39d respectively). Years with La Niña have a higher frequency of occurrence of RWB linked to SLRWPs, and the opposite occurs during El Niño years, with a Spearman correlation coefficient value of -0.36, statistically significant at 5% level. Thus, La Niña years tend to favour the development of RWB events, whereas El Niño years do the opposite. In the case of large-scale RWB linked to SAM, we obtain a Spearman correlation coefficient value of 0.21, but it is not statistically significant (using Student t-test). In agreement, Wang and Magnusdottir (2010) and Gong et *al.,* (2010) concluded that RWB in the tropical/subtropical Pacific is increased during La Niña years, and this was associated with a strong local decrease in the zonal wind in the upper troposphere. At the same time Barreiro (2017) found that El Niño events tend to favour RWPs propagation. Therefore, El Niño seems to induce large scale background conditions that favour the propagation of RWPs and, by extension, diminishes the occurrence of RWB, whereas the upper tropospheric wind flow decrease during La Niña disfavors the propagation of RWPs and propitiate the occurrence of RWB events.

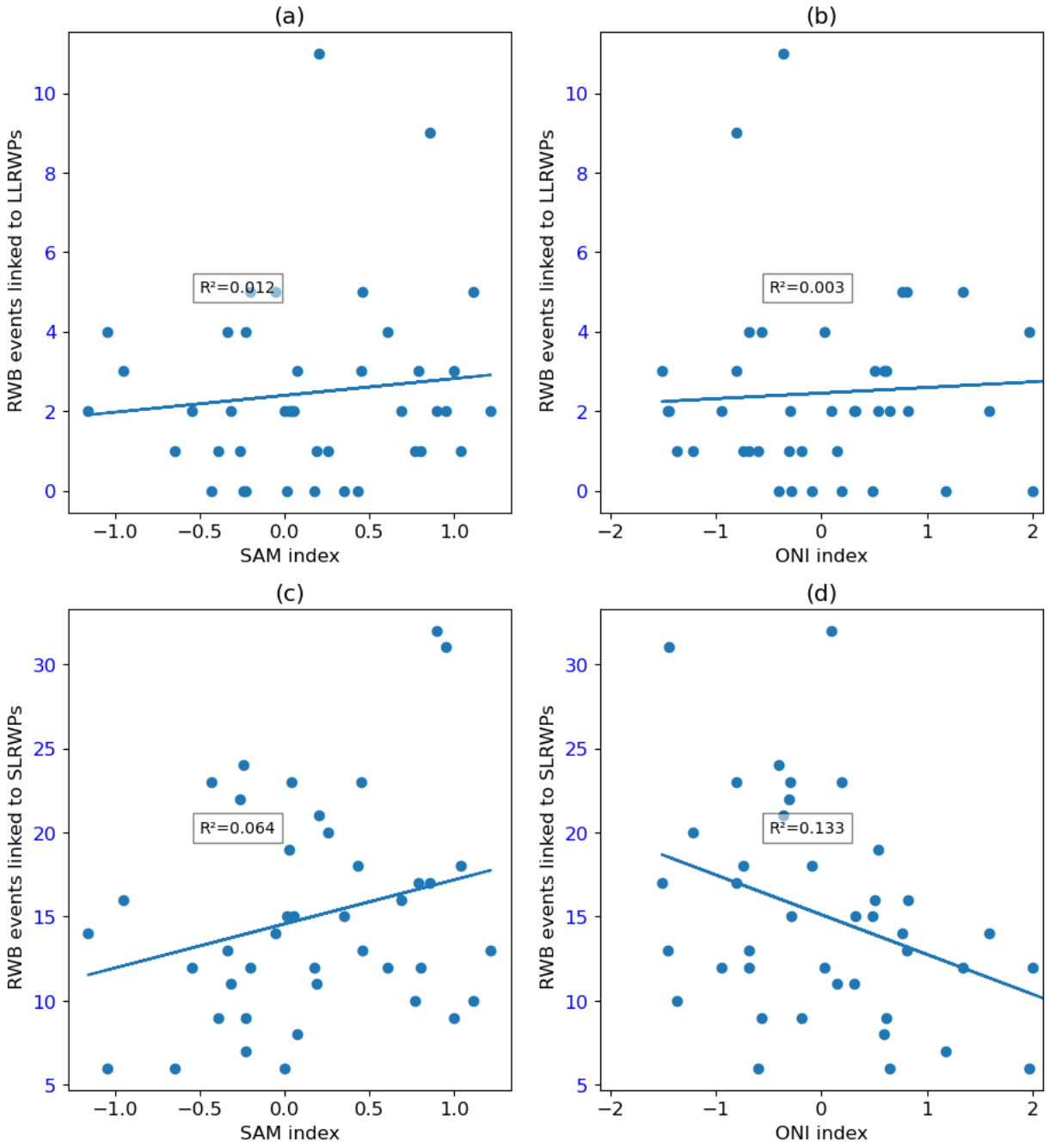

Figure 39. Scatter Plot of RWB events linked to LLRWPs (a,b) and SLRWPs (c,d) against SAM/ENSO indexes.

7.2.4 Link between large-scale Rossby Wave Breaking events and atmospheric blocking

Results of chapter 7.2.2 suggest that the link between RWB associated with RWPs and blocking is not direct because these RWB events tend to last 1 or 2 days. Here we look further into the relationship between RWB and blockings.

Table 3 shows the number of blocking events found as a function of the persistence and longitudinal extension considered. For the less restrictive criteria (blocks that last at least 4 days and with a minimum longitudinal extension of 7.5º) there are 263 events during 1979-2021, which corresponds to around 6 blocking events per summer season. This large number of events reflects the fact that these criteria cause the finding of more blocking-like situations than atmospheric blocks. On the other hand, for the most intense blocks (lifespan of 5 or more days and with a minimum extension of 15º) there are 55 events, this is, a mean of 1.3 events per year. As expected, we observe a decrease in blocking events as the conditions become more restrictive. It is worth mentioning that we find a mean of 3 atmospheric block events per year when we follow the criteria of Mendes *et al.*, (2011), which is similar to the number they found (between 2.9-3.1 events per year).

	7.5º L	10º L	12.5 ºL	15ºL
4d	263	212	168	123
5d	142	107	79	55

Table 3. Number of blocking events found using different criteria, (d) refers to minimum lifespan in days and (L) the minimum longitudinal extension in degrees of the atmospheric blocks detected.

In addition, when we focus on the detection areas of blockings, we find that nearly 50% of the events appear at the central-western Pacific basin (181-240ºE) independently of the zonal extension and persistence of the event. On the other hand, there is a secondary area of blocking development in the western Pacific basin (121-180ºE), where we find around 23-38% of the blocking events, showing the highest (lowest) values during the strongest (weakest) blocking events. Oppositely, we barely detect any blocking in the south-Atlantic (300-359ºE) or the African sector (0-60ºE). These results are summarised in table 4 for the least and most restrictive blocks, and are in agreement with the observations in Hendes *et al*., (2011).

	African sector (0-60ºE)	Indian basin (61-120ºE)	Western Pacific (121-180ºE)	Central Pacific (181-240ºE)	Eastern Pacific (241-300ºE)	South-Atlantic (301-359ºE)
4d 7.5ºL	10	16	63	118	38	18
5d 15ºL	1	2	20	27	4	1

Table 4. Number of summertime blocking events between 1979-2020 in the area of study for two blocking detection criteria: (d) refers to minimum lifespan of the event in days, and (L) to its minimum longitudinal extension in degrees.

The search for large-scale RWB associated with the formation of an atmospheric block reveals that the latter appears close to a RWB event between 15-18% of the time independently of the strength and stability of the block (not shown). Also, in agreement with the results of chapter 7.2.2, we only found RWB linked to propagating RWPs near the development of an atmospheric block around 3-6% of the time, and it does not seem to depend on the intensity and stability of the block.

To summarise, RWB events are present in the austral summer around 1 out of 5 times an atmospheric block is detected, but these RWB events do not seem to be related with the propagating RWPs. Thus, propagating RWPs do not seem to be directly linked to the development of atmospheric blocks. We recall that here we described propagating RWPs as those with speed between 15-45º/day eastward, a zonal number between 4-12 days, and lifespan larger than three days. Therefore, it is possible that planetary RWPs (those with wavenumber between 1-3) and quasi-stationary RWPs (RWPs with zonal wavenumber above 4 and speeds < 15º/day), which were not considered in this study, might play a key role in the development of atmospheric blocking.

In Nakamura and Huang 2018, they stated that periods with high Rossby wave activity can saturate the capacity of the jet to transmit waves, impeding the propagation of oncoming waves and triggering blocking development. They also discussed that transient and stationary wave activity, among other factors, affects the capability of the jet to transport Rossby waves. Therefore, it is possible that stationary or quasi-stationary RWPs might play a key role in atmospheric blocking development by either RWB events or other dynamical processes. Hence, it is possible that the combined interaction between quasi-stationary and propagating RWPs might be linked to atmospheric

blocking development. Thus, further studies should try to address whether there is a link between RWB activity of quasi-stationary and propagating RWPs with atmospheric blocking development.

On the other hand, it is also possible that only quasi-stationary and planetary RWPs are linked to atmospheric blocking. Some studies (Coumo *et al.,* 2014 and Körnhuber *et al*., 2017), found that under certain circumstances, planetary and quasi-stationary synoptic-scale packets resonate together, causing slow-speed synoptic scale Rossby Waves amplification, favouring extreme weather events development on the northern hemisphere during boreal summer. Coumo *et al.*, (2014) also suggested that a similar process might happen in the southern hemisphere. Thus, another possibility for further studies is to address under which circumstances quasi-stationary and planetary waves resonate, creating persistent high-amplitude Rossby waves, and assess if they can be linked to atmospheric blocking development on the southern hemisphere.

Additionally, it is also possible that propagating RWPs influence in atmosphere blocking development by other dynamical processes that are not wave breaking. For example, recurrent RWPs, which are several transient RWPs that propagate in such a manner that the troughs and ridges that build up the wave packets are repeatedly amplified at the same longitudes, may produce unusually persistent surface weather conditions during their lifespan (Davies 2015, Barton *et al*., 2016, Röthlisberger *et al.,* 2019). Regardless, more research is needed in order to link recurrent RWPs with atmospheric blocking events.

Therefore, results obtained in this study suggested that there is no direct link between propagating RWPs and atmospheric blocking development, at least, by wave breaking processes. Nonetheless, we cannot rule out the possibility that propagating RWPs might interact with atmospheric blocking events by other dynamical mechanisms. Hence, further study is needed to assess how these propagating waves interact with atmospheric blocking processes.

7.3 Summary

Rossby wave breaking events are atmospheric perturbations that interfere in the upper troposphere wind and energy flow, and under certain circumstances they can cause an atmospheric block, leading to the development of heatwaves or droughts. In this chapter we studied the relationship between breaking events associated with RWPs and blockings. To do so we first developed a tracking algorithm to identify and follow Rossby wave breaking areas, retaining

only large-scale Rossby wave breaking events. Second we applied an additional tracking algorithm that detects atmospheric blocking. Lastly, we assessed whether Rossby wave breaking events linked to propagating Rossby wave packets are linked to atmospheric blocking development. The results show that:

1.- Both long-lived and short-lived Rossby wave packets cause large-scale wave breaking events after stopping their propagation around 40% of the time, although this number is slightly higher for long-lived packets. Also, wave breaking events linked to long and short lived packets last around 1-2 days, which is not enough time to consider them as a blocking event.

2.- Large-scale Rossby wave breaking events associated with long-lived wave packets tend to manifest at the central-eastern Pacific basin. Therefore, changes in weather regime conditions caused by wave breaking activity linked to long-lived Rossby Wave Packets are more likely to occur at the mid-latitudes of the South America continent.

3.- The frequency of occurrence of wave breaking events linked to long-lived Rossby Wave packets do not seem to be affected by SAM nor ENSO. Oppositely, wave breaking events linked to short-lived Rossby wave packets occur more often during La Niña years.

4.- 1 out of 5 times a blocking event develops, a Rossby wave breaking event is present nearby. However, most of the wave breaking activity is not associated with propagating Rossby wave packets. Thus, propagating Rossby wave packets do not seem to be directly linked to the development of atmospheric blocks, at least, by wave breaking processes.

8| SUMMARY AND OPEN QUESTIONS

Rossby Wave Packets (RWPs) are atmospheric perturbations that manifest as meanders of the jet stream, and are considered precursors of extreme weather events such as cyclones, heat waves or cold spells. Thus, studying what circumstances favour RWPs development, their representation in weather forecast models, and their behaviour at the end of their lifespan, is key to enhance extreme weather events detection and mitigate future damages. Nonetheless, these wave packets have been extensively studied in the northern hemisphere, but in the southern hemisphere there are very few studies and they mostly focus on their climatological properties. In this thesis, we focus on long-lived RWPs, that is, RWPs that last more than 8 days in the atmosphere. The motivation lies in that due the high lifespan of long-lived packets and their link with extreme weather events, understanding which factors affect their occurrence, predictability and life cycle will increase extreme weather event detection beyond 10 days.

Therefore, in this research we aimed to (1) investigate the impact of the main modes of variability of the southern hemisphere on long-lived RWPs activity, (2) assess whether weather forecast models are able to predict the occurrence and propagation of long-lived RWPs and (3) determine whether long-lived RWPs are linked to atmospheric blocking development.

In chapter 5 we studied how the El Niño-Southern Oscillation (ENSO) and the Southern Annular mode (SAM) influence long-lived RWPs activity during austral summer. In order to detect and follow the propagation of the RWPs, we computed a tracking algorithm and registered their characteristics (example in Fig 11). Next, we retained the long-lived RWPs, and studied their frequency of occurrence and lifespan during years with different SAM and ENSO phases, as well as identified the mean atmospheric conditions during years with high/low long-lived RWPs activity. We found that SAM events influence long-lived RWPs activity: during years with positive SAM we barely find any long-lived RWPs, whereas during negative SAM we find the highest frequency of long-lived RWPs and they last significantly longer (See Fig 18 and 19). We also found that during positive SAM years, an anticyclonic circulation manifests at the south of New Zealand (Fig 24), which blocks RWPs propagation into the Pacific and disfavours long-lived RWPs development. On the other hand, during negative SAM events, the waveguide where RWPs propagate is extended into the Pacific and, as a result, long-lived RWPs occur more often and last longer Fig 24). In the case of ENSO events, we found higher long-lived RWPs activity during El Niño years compared to La Niña (Fig 17). but these differences are

not as significant as those observed during SAM events. These results might be associated with the relationship between ENSO and SAM, in the sense that El Niño events favour the development of negative SAM events, whereas La Niña does the same with positive SAM. Thus, the weaker connection between ENSO and long-lived RWPs activity may be the result of an indirect correlation between ENSO and SAM. Overall, results found in this study suggest that the extended forecast of extreme weather events might be more feasible during negative SAM years, whereas in years with positive SAM and La Niña phases it would be more difficult.

The study of chapter 5 assessed long-lived RWPs activity only during austral summer. Therefore, future studies should address how long-lived RWPs interannual variability is affected by SAM and ENSO on the remaining seasons. Regardless, it is important to highlight that in order to answer these questions, another methodology to track RWPs is needed. This is because RWPs propagation outside austral summertime is not zonal due to the split of the jet stream in the Pacific region (or the manifestation of a spiral jet). Consequently, the methodology developed in this study to track RWPs is not reliable during those seasons. Another issue is that we did not consider the variability of LLRWPs on a monthly scale and, knowing that SAM has variability on shorter than seasonal time scales, it would be interesting to study the influence of SAM on long-lived RWPs development on those scales.

In chapter 6, we evaluated the representation of long-lived Rossby Wave Packets in two sub-seasonal weather forecast models (NCEP and IAP-CAS). In order to do so, we first retained the trajectories and characteristics of the long-lived Rossby Wave Packets (e.g. date and area of formation) obtained in chapter 5. Next, we applied the Rossby wave packet tracking algorithm to the ensemble of simulations of NCEP and IAP-CAS reforecast data, considering the forecasts that started the date a long-lived RWP was detected. As a result, we obtained the forecasted trajectory of the long-lived Rossby wave packets predicted by the models, hereafter referred to as forecasted Rossby wave packets. Then, we compared the differences between the observed long-lived Rossby wave packets observed against the forecasted Rossby wave packets. Our results show that both models underestimate the lifespan of the predicted packets (Fig 27), and show a slight bias in the area where the long-lived Rossby wave packets first manifest (the NCEP model predicts the packet more eastwards compared to the observed trajectory, whereas IAP-CAS does it to the west, see Fig 28). Nonetheless, the predicted packets propagate with speeds close to the observed long-lived RWPs. On the other hand, forecasted Rossby wave packets predicted by the models rapidly lose their energy after the first

week of simulation (Fig 29), which limits the forecast of long-lived RWPs to the synoptic time scale.

In addition, we classified the forecasts depending on the proportion of simulations able to predict a forecasted Rossby wave packet that surpassed the 8 days of lifespan. The “best” forecasts are those which predicted the development of a Rossby wave packet that lasted more than 8 days in, at least, 75% of simulations. Oppositely, the “worst” forecasts are those unable to predict a forecasted Rossby wave packet with a lifespan above 8 days in any simulation. Next, we compared the mean atmospheric flow during the best and worst long-lived RWPs forecasts, and the areas of formation of the best long-lived RWPs forecast. Results indicated that the best long-lived RWPs forecasts occur in both models when the packets begin their propagation in the eastern Pacific (Fig 30). In addition, during the best long-lived RWPs forecasts we observe atmospheric circulation patterns which signal the manifestation of negative SAM events (Fig 31), consistent with the results obtained in chapter 5. Oppositely, during the worst forecasts the mean atmospheric flow exhibited atmospheric anomalies that seem to be caused by tropical forcing processes like the Madden-Julian Oscillation (MJO). An analysis of the phases of the MJO during during the best and worst long-lived RWPs forecasts revealed that an active MJO seems to degrade the ability of the models to accurately forecast the development of long-lived RWPs (Fig 32).

This study was limited to just two models due to the limited availability of forecast models with daily reforecast datasets. Therefore, future studies should consider increasing the number of models. Additionally, even though we identified that an active MJO disfavours the accurate forecast of long-lived RWPs, the cause is yet unknown. Therefore, future studies should focus on addressing whether this tendency is caused by the interaction between the teleconnection from the MJO and extratropical dynamics, or by a misrepresentation of the MJO characteristics in the forecast. Also, as for chapter 5, the study of other seasons is necessary.

Lastly, in chapter 7, we assessed the link between Rossby wave breaking activity associated with Rossby wave packets, and also whether Rossby wave breaking events related to propagating Rossby wave packets can produce the development of atmospheric blocking. In order to do so, we start by identifying the areas where the Rossby wave packets stopped propagating from the results obtained in chapter 5. Second, we developed a Rossby wave breaking tracking algorithm and verified that it performs as expected. Third, we applied an atmospheric blocking detection algorithm and searched for atmospheric blocking with different intensities. Fourth, we searched for large-scale Rossby

wave breaking activity linked to Rossby wave packets that stopped propagating, classifying the results according to the lifespan of the wave packet, (short-lived to packets with a lifespan <= 8 days, long-lived to those that lasted above 8 days). Fifth, we studied how large-scale Rossby wave breaking linked to Rossby wave packets are affected by the ENSO and SAM phases. Finally, we studied the link between RWB events and atmospheric blocking development.

Results obtained showed that long-lived and short-lived Rossby wave packets display large-scale Rossby wave breaking events around 4 out of 10 times after they finished propagating. Most large-scale wave breaking activity associated with long-lived packets mainly manifest at the central-eastern Pacific basin, whereas those caused by short-lived packets predominantly occur in the western-central Pacific basin (Fig 37). Therefore, weather regime transitions caused by large-scale wave breaking events linked to long-lived Rossby wave packets are more likely to affect the mid-latitudes of the South America Region. Also, results showed that Rossby wave breaking activity linked to long-lived packets do not seem to be linked to SAM or ENSO phases (Fig 39). On the contrary, large-scale wave breaking events associated with short lived packets are favoured by La Niña events.

Nonetheless, most large-scale Rossby wave breaking events associated with Rossby wave packets last around 1-2 days (Fig 37), which is not enough time to set up an atmospheric blocking. Therefore, large-scale Rossby wave breaking events linked to propagating Rossby wave packets do not seem to be directly linked to atmospheric blocking development. Next, we assessed the frequency of occurrence of large-scale Rossby wave breaking events near the location where an atmospheric blocking event manifested, while also measuring the proportion of large-wave breaking that is associated with Rossby wave packets. We found that, independently of the strength of the atmospheric blocking, nearly 20% of the times a blocking event appears, there is a large-scale Rossby wave breaking event nearby. Nonetheless, most of this Rossby wave breaking activity is not associated with Rossby Wave Packets.

The latter results suggest that propagating Rossby wave packets do not seem to be linked to atmospheric blocking development, at least, by wave breaking processes. However, it is important to remark that in this study we only focused on those Rossby wave packets that are associated with transient structures in the southern hemisphere, that is, waves with wavenumber between 4-11 and that travel between 15-45º/day. Therefore, we cannot assume that planetary (waves with wavenumber between 1-3) or quasi stationary Rossby wave packets are not linked to atmospheric blocking development. Consequently, further research about wave breaking processes that occur associated with

quasi-stationary and planetary Rossby wave packets is needed in order to solve these issues. Also, another possibility is that transient Rossby wave packets might be linked to atmospheric blocking development by dynamical processes not linked to wave breaking events. Finally, as for chapters 5 and 6, these results are only limited to austral summer due to the limitations of the methodology to search for Rossby wave packets, and these issues need to be studied for the rest of the year.

Overall, results obtained in this study deepened our understanding about atmospheric processes that influence the occurrence of long-lived RWPs, the conditions that favour their propagation beyond 8 days, their representation in forecast models and provided insight about their link with atmospheric blocking during austral summer. These findings shed more light about atmospheric phenomena that occur beyond the synoptic scale, and are key to improving the forecast of extreme weather events between 10-30 days.

APPENDIX

A.1 Characteristics of Rossby waves propagation

Rossby Waves manifest in mid-latitudes as meanderings of the jet stream in the upper atmosphere, with the meridional gradient of planetary vorticity as their restoring force. During their lifespan, Rossby waves transport energy, moisture and momentum across large distances. As a result, the propagation of these waves can induce covariability between variables that are located in remote locations, often referred to as teleconnections (Wallace and Gutzler 1981, Branstator 2002, Wirth *et al.,* 2018).

In an idealised representation of a Rossby wave, the meridional wind speed or v is a purely sinusoidal wave with a constant amplitude, forming a latitude circle on an upper tropospheric quasi-horizontal surface of potential temperature, or Θ (Wirth *et al.,* 2018). We can write this description in the following form (equation A1).

$$v(\lambda, t) = A\,cos(k\lambda - wt) \quad \text{(A1)}$$

A is the amplitude of the Rossby Wave (A>0), λ is longitude (in radians), t represents time, *w* the angular frequency and *k* the zonal wavenumber, which symbolises the number of times that the wavelength of a Rossby wave fits in a latitude circle. Planetary Rossby waves are typically characterised by zonal wavenumbers between 1 to 3, whereas synoptic-scale Rossby Waves have wavenumbers >3.

The propagation of Rossby waves has led to the concept of waveguides, and strong zonal jet streams are usually considered efficient waveguides. To show that we follow the theoretical approach presented in Hoskins and Ambrizzi (1993). For a more complete discussion, however, see Wirth *et al.,* (2018) and Wirth (2020).

They start from the dispersion relation of the Rossby waves (James 1994):

$$w = Uk - (\beta - U_{yy}) * k / K^2 \quad \text{(A2)}$$

with U the wind speed, k the zonal wavenumber, l the meridional wavenumber, K the wavenumber of the propagating packet ($K = \sqrt{[l^2+k^2]}$) and β the meridional derivative of the planetary vorticity f $(\partial f/\partial y)$. Assuming a steady response to

forcing, $(w = 0)$ we rearrange equation A2 such that the meridional wavenumber l is expressed as a function of the zonal wavenumber k (eq. A3):

$$l = \pm\{(\beta - U_{yy})/U - k^2\}^{1/2} \text{ (3A)}$$

This equation helps determine whether the propagation of a stationary Rossby wave is possible. If the previous expression has as a solution an imaginary number, the disturbances are evanescent, and thus, the Rossby wave cannot propagate. Due to the fact that ($\beta - U_{yy}$) is always positive, ($\beta>0$, and generally $\beta > U_{yy}$), the key factor that decides whether a Rossby Wave will propagate or not in the atmosphere depends on the total stationary wavenumber or Ks, which is defined in equation A4.

$$Ks = \sqrt{((\beta - U_{yy})/U)} \text{ (A4)}$$

Thus, the condition for a steady Rossby wave to propagate in the atmosphere is that Ks must be a real number. This implies that: (1) the meridional gradient of the absolute vorticity has to be positive, (2) u>0, that is, that the zonal mean flow goes eastward and (3) Ks ≥k.

Nonetheless, the described conditions are true only for steady or quasi-stationary Rossby Waves, and, in this study we focus on transient Rossby waves that propagate zonally. Therefore, we cannot assume that the conditions in the mean flow will remain constant. Nonetheless, assuming that the distance in which the atmospheric conditions change is larger than the dimensions of the Rossby wave, it is possible to predict the evolution of the propagating packet. This technique is called 'ray tracing', and it is usually employed in many physics fields such as optics.

In order to apply the ray tracing technique, we first assume that conditions in the mean flow change as the packet propagates. As a result, eq. (A2) becomes

$$w = w(k,\beta') \text{ (A5)}$$

where $\beta' = (\beta - Uyy)$. Afterwards, we use the identities $-\partial k/\partial y = \partial l/\partial x$, $\partial k/\partial t = -\partial w/\partial x$ and $\partial l/\partial t = -\partial w/\partial y$ (James 1994 Chapter 6), and thus, the rate of change of frequency following the wave packet is:

$$D_p w/Dt = (\partial w/\partial \beta') * \partial \beta'/\partial t' \text{ (A6)}$$

where

$$D_p/Dt = (\partial/\partial t) + c_{gx}\partial/\partial x + c_{gy}\partial/\partial y \text{ (A7)}$$

Eq. A7 denotes the rate of change following the wave packet. Because we assume that β' does not change with time, from eq. A6 we observe that the

packet conserves its frequency as it propagates. For stationary waves this is of course simply zero. A similar relationship describing the variation of wavenumber of the packet can also be derived (eq. A8):

$D_p k/Dt = -(\partial w/\partial \beta')(\partial \beta'/\partial x')$, $D_p l/Dt = -(\partial w/\partial \beta')(\partial \beta'/\partial y')$, (A8)

Since the basic state is purely zonal, β' depends upon y only, and so the zonal wavenumber of a packet is conserved. In contrast, its meridional wavenumber will evolve as the packet moves from one latitude to another.

The meridional wavenumber could in principle be derived by integrating eq A8 with respect to time, although in practice it is much simpler to use the diagnostic relationship based on the dispersion relation with w = 0, (eq A5). Since w, k and l are known and are functions of latitude, we can calculate the group velocity at any location. The trajectory followed by the packet of Rossby waves is therefore described by:

$Dx/Dt = 2\beta' k^2/K^4$ (A10a)

and

$Dy/Dt = 2\beta' k^2/K^4$ (A10b)

where

$l = \pm\sqrt{(K_s^2 - k^2)}$ (A11)

If we now consider the propagation of a wave packet with zonal wavenumber k away from a midlatitude source, it can propagate following two different directions when k < Ks. If in the expression A10 l < 0, the packet will go to the south, whereas if l > 0 it will go to the north. If the Rossby Wave travels north, we expect that Ks will increase as the wave reaches the subtropics. As the critical latitude is approached, (which is the latitude where the Rossby wave cannot keep propagating because u <0), the packet will propagate extremely slowly in a nearly meridional direction. The meridional scale of the Rossby waves will become extremely small (l large). According to this linear theory, the packet would spend an infinite time to reach the critical latitude, which will act as something of a 'black hole' to Rossby wave information approaching it from higher latitudes. Fig A1 gives a schematic illustration of the approach to the critical latitude. If the effects of friction were included, we might anticipate that the Rossby wave dissipated in the vicinity of the critical line. In a truly inviscid world, the linear theory would break down in the vicinity of the critical latitude. A more sophisticated analysis suggests that in these circumstances, the critical line might partially reflect some of the wave activity incident upon it. Nonetheless, because of the breakdown of the zonality and stationarity of the

basic mean flow, it is not clear how the Rossby wave would behave in the area where u=0.

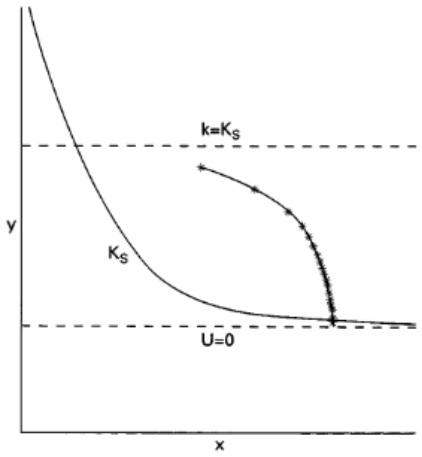

Fig A1. Illustration of an equatorward Rossby ray propagating to a critical latitude where u=0. The variation of Ks is shown, and the crosses indicate the location of the packet after equal intervals of time. (source: James 1994 chapter 6).

On the other hand, when the ray propagates poleward, the packet will move into an environment when Ks is decreasing. As Ks gets smaller, l will decrease as well, consequently, the packet will expand zonally, when Ks=k the ray will be refracted back towards lower latitudes, as can be seen in Fig A2. Eventually, the packet will slow down and approach the critical latitude.

A strong zonal jet will be characterised by a local maximum of the refractive index flanked by turning latitudes to the north and south and thus ray paths oscillate between the two latitudes effectively trapping the waves. Consequently, the jet will act as a waveguide in the zonal direction. Based on this theory, complemented with model simulations, Hoskins and Ambrizzi (1993) show the existence of a waveguide extending from the western south Atlantic up to the western Pacific in the southern hemisphere summer.

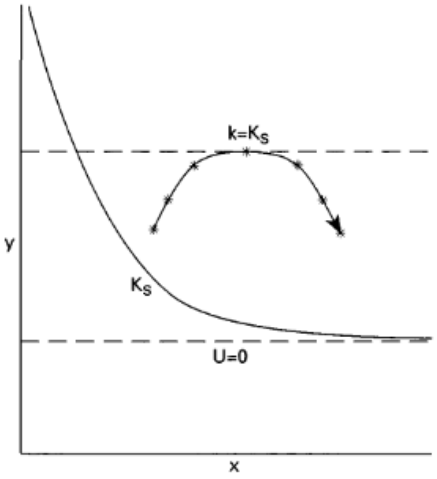

Fig A2. As in Fig A1, but illustrating a poleward propagating ray, reaching the latitude where k=Ks, and bouncing back towards lower latitudes. (source: James 1994 chapter 6).

REFERENCES

Aceituno, P., (1988) On the functioning of the Southern Oscillation in the South American sector. Part I: surface climate. *Mon. Weather Rev.* 116, 505–524.

Aguilar, E., et al. (2005) Changes in precipitation and temperature extremes in Central America and northern South America, 1961–2003, *J. Geophys. Res.*, 110, D23107, doi:10.1029/2005JD006119.

Altenhoff, M, A., Martius, O., Croci-Maspoli, M.,Schwierz, C & Davies,C,H. (2008) Linkage of atmospheric blocking and synoptic-scale Rossby waves: a climatological analysis, Tellus A: Dynamic Meteorology and Oceanography, 60(5), 1053-1063, https://doi.org/10.1111/j.1600-0870.2008.00354.x

Alvarez, M.S., Vera, C.S., Kiladis, G.N. et al. (2016) Influence of the Madden Julian Oscillation on precipitation and surface air temperature in South America. Clim Dyn 46, 245–262.https://doi.org/10.1007/s00382-015-2581-6

Ambrizzi, T., Souza, E. B. d., & Pulwarty, R. S. (2004) The Hadley and Walker regional circulations and associated enso impacts on South American seasonal rainfall. The hadley circulation: Present, past and future,21 (pp. 203–235). The Hadley Circulation: Present, Past and Future. *Advances in Global Change Research* https://doi.org/10.1007/978-1-4020-2944-8_8

Bao, Q., X. F. Wu, J. X. Li, L. Wang, B. He, X. C. Wang, Y. M. Liu, and G. X. Wu. (2019) “Outlook for El Nino and the Indian Ocean Dipole in Autumn-winter 2018–2019.” *Chinese Science Bulletin* (In Chinese) 64 (1): 73–78. https://doi.org/10.1360/N972018-00913

Bao, Q., and J. Li. (2020) Progress in Climate Modeling of Precipitation over the Tibetan Plateau. *National Science Review*. 7(3): 486–487. https://doi.org/10.1093/nsr/nwaa006

Barlow, M., M. Wheeler, B. Lyon, and H. Cullen (2006) Modulation of daily precipitation over southwest Asia by the Madden-Julian Oscillation, *Mon. Weather Rev*., 133, 3579 – 3594. https://doi.org/10.1175/BAMS-D-12-00026.1

Barreiro, M. (2010) Influence of Enso and the South Atlantic Ocean on climate predictability over southeastern South america. *Climate Dynamics*, 35(7–8), 1493–1508. https://hdl.handle.net/20.500.12008/34194

Barnes, A, E and Hartmann, L,D. (2012) Detection of Rossby wave breaking and its response to shifts of the midlatitude jet with climate change. *Journal of Geophysical Research,* 117(D9). https://doi.org/10.1029/2012JD017469

Barreiro, M. (2017) Interannual variability of extratropical transient wave activity and its influence on rainfall over Uruguay. *International Journal of Meteorology*, 37, 4261–4274. https://doi.org/10.1002/joc.5082.

Barton, Y., P. Giannakaki, H. von Waldow, C. Chevalier, S. Pfahl, and O. Martius, (2016) Clustering of regional-scale extreme precipitation events in southern Switzerland. Mon. Wea. Rev., 144, 347–369, https://doi.org/10.1175/MWR-D-15-0205.1

Berrisford, P., Hoskins, J, B and Tyrlis, E. (2007) Blocking and Rossby Wave Breaking on the Dynamical Tropopause in the Southern Hemisphere. *Journal of the Atmospheric Sciences*,64(8), 2881-2898. https://doi.org/10.1175/JAS3984.1.

Bidegain M, Crisci C, del Puerto L, Inda H, Mazzeo N, Taks J and Terra R (2012) Clima de cambios: Nuevos desafíos de adaptación en Uruguay. Projecto FAO-MGAP TCP URU/3302 (web: https://pmb.parlamento.gub.uy/pmb/opac_css/index.php?lvl=notice_display&id=82347, accessed the 09 May of 2023

Branstator, G., (2002) Circumglobal teleconnections, the jet stream waveguide, and the North Atlantic Oscillation. *J. Climate*, 15, 1893–1910, https://doi.org/10.1175/1520-0442(2002)015<1893:CTTJSW>2.0.CO;2

Chagnon, J., S. L. Gray, and J. Methven (2013) Diabatic processes modifying potential vorticity in a North Atlantic cyclone, *Q. J. R Meteorol. Soc*., 139, 1270–1282, https://doi.org/10.1002/qj.2037.

Chang, E. K. M., & Yu, D. B. (1999) Characteristics of wave packets in the upper troposphere. Part I: Northern Hemisphere winter. *Journal of Atmospheric Sciences*, 56(11), 1708–1728. https://doi.org/10.1175/1520-0469(1999)056<1729:COWPIT>2.0.CO;2

Chang, E, K, M. (1999) Characteristics of wave packets in the upper troposphere. Part II: Seasonal and hemispheric variations. *Journal of Atmospheric Sciences*, 56(11), 1729-1747. https://doi.org/10.1175/1520-0469(1999)056<1729:COWPIT>2.0.CO;2

Chang, E, K, M. (2000) Wave Packets and Life Cycles of Troughs in the Upper Troposphere: Examples from the Southern Hemisphere, Summer Season of 1984/1985. *Monthly Weather Review*, 128(1), 25–50. https://doi.org/10.1175/1520-0493(2000)128<0025:WPALCO>2.0.CO;2

Chang E, K, M. (2001) The structure of baroclinic wave packets. *J. Atmos. Sci*. 58: 1694–1713. https://doi.org/10.1175/1520-0469(2001)058<1694:TSOBWP>2.0.CO;2

Chang, E. K. M. (2005) The Impact of Wave Packets Propagating across Asia on Pacific Cyclone Development. *Monthly Weather Review*, 133(7), 1998–2015. https://doi.org/10.1175/MWR2953.1

Codron, F., (2005) Relation between annular modes and the mean state: southern hemisphere summer. *Journal of Climate,* 18, 320–330. https://doi.org/10.1175/JCLI-3255.1

Damião, M .C. M. (2007) Bloqueios Atmosféricos sobre o Hemisfério Sul: Diagnóstico, Impacto Climático e Mecanismos físicos associados, Tese de Doutoramento, Universidade de Lisboa, 250 pp.

Damião, M. C. M, et al. (2008) Blocking Episodes in the Southern Hemisphere: Impact on the Climate of Adjacent Continental Areas, *Pure and Applied Geophysics*, 165: 1-22, 2008, (https://doi.org/10.1007/s00024-008-0409-4).

Damião M,C,M, Cavalcanti, A, F, I., Herdies, L, D (2012) Southern Hemisphere Atmospheric Blocking Diagnostic by ECMWF and NCEP/NCAR data *Revista Brasileira de Meteorologia*, 27(3), 263 - 271. https://doi.org/10.1590/S0102-77862012000300001

Davies, H. C., (2015) Weather chains during the 2013/2014 winter and their significance for seasonal prediction. Nat. Geosci., 8, 833–837, https://doi.org/10.1038/ngeo2561

Davini, P., C. Cagnazzo, S. Gualdi & A. Navarra. (2012) A bidimensional diagnostics, variability, and trends of Northern Hemisphere blocking. *Journal of Climate*. 25: 6496–6509. https://doi.org/10.1175/JCLI-D-12-00032.1

Feldstein, S. B., (2000) The timescale, power spectra, and climate noise properties of teleconnection patterns. *Journal of Climate*, 13, 4430–4440.https://doi.org/10.1175/1520-0442(2000)013<4430:TTPSAC>2.0.CO;2

Feldstein, S.B and S. Lee, (1998) Is the atmospheric zonal index driven by aneddy feedback? *J. Atmos. Sci.*, 55, 3077–3086. https://doi.org/10.1175/1520-0469(1998)055<3077:ITAZID>2.0.CO;2

Garreaud, R,D., Vuille, M., Compagnucci, R., Marengo, J. (2009) Present-day-South American climate. *Palaeogeography, Palaeoclimatology, Palaeoecology* 281 (2009) 180–195. https://doi.org/10.1016/j.palaeo.2007.10.032

Garriott, E.B. (1904) Long-range forecasts. U.S. Weather Bureau. Washington, DC, 32 pp. (report).

Gong D, and Wang S. (1999) Definition of Antarctic oscillation index. *Geophysical Research Letters*, 26: 459–462. https://doi.org/10.1029/1999GL900003

Giannakaki, P., and Martius, O. (2016) An Object-Based Forecast Verification Tool for Synoptic-Scale Rossby Waveguides, *Weather and Forecasting*, 31 (3), 937-946. https://doi.org/10.7892/boris.83861.

Gollan, G. & R.J. Greatbatch. (2017) The relationship between Northern Hemisphere winter blocking and tropical modes of variability. *J. Clim*. 30: 9321–9337.https://doi.org/10.1175/JCLI-D-16-0742.1

Gong, T., Feldestein, B. S., & Luo, D. (2010) The Impact of ENSO on Wave Breaking and Southern Annular Mode Events. *Journal of the atmospheric Sciences*, 67, 2854–2870. https://doi.org/10.1175/2010JAS3311.1

Gong D,Y and Wang S,W. (1999) Definition of Antarctic Oscillation index. *Geophysical Research Letters.* 26,(4): 459–462.https://doi.org/10.1029/1999GL900003

Gray, S.L., Dunning, M, C., Methven, J., Masato, G., Chagnon, M, J., (2014) Systematic model forecast error in Rossby wave structure, Geophys. Res. Lett., 41,2979-2987, https://doi.org/10.1002/2014GL059282

Grazzini, F., & Vitart, F. (2015) Atmospheric predictability and Rossby wave packets. International Journal. of the Royal Meteorological Society, 141(692), 2793–2802. https://doi.org/10.1002/qj.2564

Grimm, A. M. (2011) Interannual climate variability in South America: impacts on seasonal precipitation, extreme events, and possible effects of climate change. *Stochastic Environmental Research and Risk Assessment,* 25(4), 537–554. https://doi.org/10.1007/s00477-010-0420-1

Grimm, A. M., Barros, V. R., & Doyle, M. E. (2000) Climate variability in southern South America associated with El Nino and La Nina events. *Journal of Climate*, 13(1), 35–58. https://doi.org/10.1175/1520-0442(2000)013<0035:CVISSA>2.0.CO;2

Hans, H., Bell, B., Berrisford, P., Hirahara, S., Horány, A., Muñoz-Sabater, J., & Nicolas, J. (2020) The ERA5 global reanalysis. Royal Meteorological Society, 146(730), 1999–2049. https://doi.org/10.1002/qj.3803

Bao He, B., , Q., Wang, X., Zhou, L., Wu, X., Liu, Y., et al. (2019) CAS FGOALS-f3-L model datasets for CMIP6 historical atmospheric model Intercomparison project simulation. *Adv. Atmos. Sci*, 36 (8), 771-778. https://doi.org/10.1007/s00376-019-9027-8.

Bao, Q. & Li, J. (2020) Progress in climate modelling of precipitation over the Tibetan plateau. National Science Review, 7(3), 486– 487. Available from: https://doi.org/10.1093/nsr/nwaa006

Henderson, S.A., E.D. Maloney & E.A. Barnes. (2016) The influence of the Madden–Julian oscillation on Northern Hemisphere winter blocking. *J. Clim*. 29: 4597–4616. https://doi.org/10.1175/JCLI-D-15-0502.1

Hendon, H. H. (2018) Understanding Rossby wave trains forced by the Indian Ocean dipole. *Climate Dynamics*, 50(50), 2783–2798. https://doi.org/10.1007/s00382-017-3771-1

Hitchman, H. M., and Huesmann,S,A. (2007) A seasonal climatology of Rossby wave breaking in the 320–2000-K layer. *J.Atmos. Sci.*, 64(6), 1922–1940. https://doi.org/10.1175/JAS3927.1

Hoskins, B, J., & Ambrizzi, T. (1993) Rossby Wave Propagation on a realistic Longitudinally Varying Flow. *Journal of Atmospheric Science*,50(12), 1661–1671. https://doi.org/10.1175/1520-0469(1993)050<1661:RWPOAR>2.0.CO;2

Hoskins J,B., McIntyre E,M., Robertson W,A. (1985) On the use and significance of isentropic potential vorticity maps. Q. J. R. Meteorol. Soc. 111(470), 877–946. https://doi.org/10.1002/qj.49711147002

Kanamitsu, M., Ebusuzaki, W., Woollen, J., Yang, S.-K., Hnilo, J. J., Fiorino, M., & Potter, L. G. (2002) NCEP-DOE AMIP- II Reanalysis R-2. *American Meteorology Society*, (Vol. 83, pp. 1631–1644). https://doi.org/10.1175/BAMS-83-11-1631

James,N,I (1994) Introduction to circulating atmospheres 2nd Edition Chapter 6. Cambridge University of Reading pág 164-184.

Jing, P and Banerjee, S (2018) Rossby Wave Breaking and Isentropic Stratosphere-Troposphere Exchange During 1981-2015 in the Northern Hemisphere, *Journal of Geophysical Research: Atmospheres*, Vol 123,(17) p 9011-9025. https://doi.org/10.1029/2018JD028997

Kiladis, G. N., J. Dias, K. H. Straub, M. C. Wheeler, S. N. Tulich, K. Kikuchi, K. M. Weickmann, and M. J. Ventrice, (2014) A comparison of OLR and circulation-based indices for tracking the MJO. Mon. Wea. Rev., 142, 1697–1715, https://doi.org/10.1175/MWR-D-13-00301.1

Körnhuber, K., V. Petoukhov, S. Petri, S. Rahmstorf, and D. Coumou, (2017) Evidence for wave resonance as a key mechanism for generating high-amplitude quasi-stationary waves in boreal summer. Climate Dyn., 49, 1961–1979, https://doi.org/10.1007/s00382-016-3399-6

Lackmann, G (2012) Midlatitude Synoptic Meteorology: Dynamics, Analysis and Forecasting and Synoptic-Dynamic Meteorology, Vol 29 (1) by Gary M. Lackmann, Brian E. Mapes and Kevin R. Tyle. *Clean Air J.* [online]. 2019, vol.29, n.1. **http://dx.doi.org/10.17159/2410-972x/2019/v29n1a11**

Lejenas, H. (1984) Characteristics of Southern Hemisphere blocking as determined from a long time series of observational data, *Quarterly Journal of the Royal Meteorological Society*,v.110: 967-979, https://doi.org/10.1002/qj.49711046610

Li, J., Bao, Q., Liu, Y., Wu, G., Wang, L., He, B.,*et al* (2019) Evaluation of FAMIL2 in simulating the climatology and seasonal-to-interannual variability of tropical cyclone characteristics. Journal of Advances in Modeling Earth Systems, 11(4), 1117-1136. https://doi.org/10.1029/2018MS001506

Li J, P, Wang J, X, L. (2003) A modified zonal index and its physical sense. Geophys. Res. Lett. 30: 1632. https://doi.org/10.1029/2003GL017441

Lorenz, D. J., and D. L. Hartmann (2001) Eddy-zonal flow feedback in the Southern Hemisphere. J. Atmos. Sci., 58, 3312–3327. https://doi.org/10.1175/1520-0469(2001)058<3312:EZFFIT>2.0.CO;2

Lupo, A.R. & P.J. Smith. (1995) Climatological features of blocking anticyclones in the Northern Hemisphere. Tellus 47: 439–456. https://doi.org/10.1034/j.1600-0870.1995.t01-3-00004.x

Lupo, A.R., A.D. Jensen, I.I. Mokhov, *et al*. (2019) Changes in global blocking character during the most recent decades. *Atmosphere* 10 (2). https://doi.org/10.3390/atmos10020092

Lupo, A, R (2020) Atmospheric blocking events: a review *Special Issue: The Year in Climate Science Research* 1504 (1), 5-24, https://doi.org/10.1111/nyas.14557

Machado, P, J ., Justino, F., Souza,D,C (2020) Influence of El Niño Southern Oscillation on baroclinic instability and storm tracks in the Southern Hemisphere, *International Journal of Climatology*, 42(S1), E93-E109, https://doi.org/10.1002/joc.6651

Manola, I., Selten, F., H de Vries, H., & Hazeleger, W. (2013) Waveguidability of idealized jets. Journal of Geophysical Research-Atmospheres, 118(18), 10432–10. https://doi.org/10.1002/jgrd.50758

Masato, G., Hoskins, J,B., Woollings,T. (2011) Wave breaking characteristics of mid-latitude blocking. *Quarterly Journal of the Royal Meteorological Society,* 138(666), 1285-1296. https://doi.org/10.1002/qj.990

Masato,G, Hoskins,J,B., Woollings,T. (2013) Wave-Breaking Characteristics of Northern Hemisphere Winter Blocking: A Two-Dimensional Approach. *Journal of Climate*, 26(13), 4535-4549. https://doi.org/10.1175/JCLI-D-12-00240.1

Marengo, A,J., (1992) Interannual variability of surface climate in the Amazon basin. *International Journal of Climatology*. 12, 853–863 http://dx.doi.org/10.1002/joc.3370120808

Marengo, A,J., Jones, R., Alves,M,L., Valverde,C,M (2009) Future change of temperature and precipitation extremes in South America as derived from the PRECIS regional climate modelling system. *International Journal of Climatology*, 29,(15) 2241-2255. http://dx.doi.org/10.1002/joc.1863

Matthews, A. J., B. J. Hoskins, and M. Masutani, (2004) The global response to tropical heating in the Madden–Julian oscillation during the northern winter. Quart. J. Roy. Meteor. Soc., 130, 1991–2011, https://doi.org/10.1256/qj.02.123.

Mayewski, A, P., Maasch,A,K ., White, C, W, J *et al.,* (2017) A 700 year record of Southern Hemisphere extratropical climate variability. *Annals of Glaciology* 39, 127-132 DOI: https://doi.org/10.3189/172756404781814249

McIntyre, E, M., and Palmer,T,N (1983) Breaking planetary waves in the stratosphere. *Nature*, 305, 593–600. https://doi.org/10.1038/305593a0

McIntyre, E, M and Palmer, T.N., Palmer, (1984) The “surf zone” in the stratosphere. *J. Atmos. Terr. Phys*., 46(9), 825–839. https://doi.org/10.1016/0021-9169(84)90063-1

Mendes, M. C. D., Cavalcanti, I. F., & Herdies, D. L. (2011) Southern Hemisphere atmospheric blocking diagnostic by ECMWF and NCEP/NCAR data. *Revista Brasileira de Meteorologia,* 27(3), 263-271. https://doi.org/10.1590/S0102-77862012000300001

Messmer, M., Simmonds, I (2021) Global analysis of cyclone-induced compound precipitation and wind extreme events. *Weather Clim. Extrem.* **32**, https://doi.org/10.1016/j.wace.2021.100324

Michel, C and Riviére, G (2011) The Link between Rossby Wave Breaking and Weather Regime Transitions. *Journal of The Atmospheric Sciences,* 68(8), 1730-1748. https://doi.org/10.1175/2011JAS3635.1

Muza, N, M., Carvalho, V, M, L., Jones, C and Liebmann, B (2009) Intraseasonal and Interannual variability of Extreme Dry and Wet Events over Southeastern South America and the Subtropical Atlantic during Austral Summer. *Journal of Climate,*22(7), 1682–1699. https://doi.org/10.1175/2008JCLI2257.1

Nakamura, N and Huang, Y, S,C (2018) Atmospheric blocking as a traffic jam in the jet stream, *Science,*361(6397),42-47, https://doi.org/10.1126/science.aat0721

Narinesingh, V., J.F. Booth, S.K. Clark & Y. Ming. (2020) Atmospheric blocking: the impact of topography in an idealized general circulation model. *Weather Clim. Dyn*. 39. https://doi.org/10.5194/wcd-2020-2

Ndarana, T and Waugh, D., (2010a) The link between cut-off lows and Rossby wave breaking in the Southern Hemisphere. *Q.J.R Meteorol. Soc*, 136(649), 869-885. https://doi.org/10.1002/qj.627

Ndarana, T and Waugh, W,D (2010b) A climatology of Rossby Wave Breaking on the Southern Hemisphere Tropopause. Journal of the Atmospheric Sciences,Vol 68, 798-811. https://doi.org/10.1175/2010JAS3460.1

O’Brien, L., & Reeder, J. M. (2017) Southern Hemisphere Summertime Rossby Waves and Weather in the Australian Region. Quarterly Journal of the Royal Meteorologica Society, 143(707), 2374–2388. https://doi.org/10.1002/qj.3090

Orlanski and Sheldon (1995) Stages of the energetics of baroclinic systems. Tellus 47A, 5, 1.https://doi.org/10.1034/j.1600-0870.1995.00108.x

Pfahl, S and Wernli, H. (2012) Quantifying the relevance of cyclones for precipitation extremes. *J. Clim.* 25, 6770–6780 https://doi.org/10.1175/JCLI-D-11-00705.1

Patterson, M., Bracegirdle, T., & Woollings, T. (2019) Southern Hemisphere atmospheric blocking CMIP5 and future changes in the Australia-New Zealand sector. *Geophysical Research Letters,*46(15), 9281–9290. https://doi.org/10.1029/2019GL083264

Peters, D., and Waugh, W, D. (2003) Rossby wave breaking in the Southern Hemisphere wintertime upper troposphere. Mon. Wea. Rev., 131(11), 2623–2634. https://doi.org/10.1175/1520-0493(2003)131<2623:RWBITS>2.0.CO;2

Pérez, I., Barreiro, M., & Masoller,C. (2021) ENSO and SAM influence on the generation of long episodes of Rossby Wave Packets during southern hemisphere summer. *Journal of Geophysical Research: Atmospheres*, 126, e2021JD035467.https://doi.org/10.1029/2021JD035467

Pérez-Fernández, I & Barreiro, M. (2023) How well do forecast models represent observed long-lived Rossby Wave packets during southern hemisphere summer? *Atmospheric Science Letters,* Online version of record before inclusion in an issue e1175. Available from: https://doi.org/10.1002/asl.1175.

Quinting, J. F., & Vitart, F. (2019) Representation of synoptic-scale Rossby wave packets and blocking in the S2S prediction project database. *Geophysical Research Letters*, 46, 1070–1078. https://doi.org/10.1029/2018GL081381

Renwick J, A, Revell M, J. (1999) Blocking over the South Pacific and Rossby wave propagation. *Mon Weather Rev*. 127(10): 2233–47.

Reyer, C., Adams, S., Albrecht, T. *et al.* (2017) Climate change impacts in Latin America and the Caribbean and their implications for development. *Reg Environ Change* **17**, 1601–1621 (2017). https://doi.org/10.1007/s10113-015-0854-6

Rex, D. F. (1950) Blocking action in the middle troposphere and its effect upon regional climate. *Tellus*, 2(3), 196–211. https://doi.org/10.3402/tellusa.v2i4.8603

Rosenzweig, C., Iglesius, A., Yang, X. B., Epstein, P, R., and Chivian, E. (2001) Climate change and extreme weather events - Implications for food production, plant diseases, and pests" NASA Publications. 24. https://digitalcommons.unl.edu/nasapub/24

Ryoo, J-M., Kaspi, Y., Waugh, W , D., Kiladis, N, G., Waliser, E, D., Fetzer, J, E and Jinwon, K. (2013) Impact of Rossby Wave Breaking on U.S. West Coast Winter Precipitation during ENSO Events,*Journal of Climate,*26(17), 6360-6382. https://doi.org/10.1175/JCLI-D-12-00297.1

Sagarra, R., & Barreiro, M. (2020) Characterization of extratropical waves during summer of the Southern Hemisphere. *Meteorologica*, 45,63–79. https://hdl.handle.net/20.500.12008/33550

Saha, S., Moorthi, Shrinivas., *et al* (2014) The NCEP Climate Forecast System Version 2, *Journal of climate*, 27 (6), 2185-2208, https://doi.org/10.1175/JCLI-D-12-00823.1

Sazib, N., Mladenova, E, I and Bolten, D, J (2020) Assessing the Impact of ENSO on Agricutlure Over Africa Using Earth Observation Data. *Frontiers in Sustainable Food Systems*, 4 https://doi.org/10.3389/fsufs.2020.509914

Seager, R., Henderson, N., Ting, M., Cane, A. M., Harnik, N., & Kushnir, Y. (2010) Adjustment of the atmospheric circulation to tropical Pacific SST anomalies: Variability of transient eddy propagation in the Pacific- North America sector. *Quarterly Journal of the Royal Meteorological Society*, 136, 277–296. https://doi.org/10.1002/qj.588

Shaw,A,T., Miyawaki,O., Donohoe, A (2022) Stormier Southern Hemisphere induced by topography and ocean circulation. *PNAS*,119(50), https://doi.org/10.1073/pnas.2123512119

Simmons, J. A., and Hoskins,J,B (1978) The life cycles of some nonlinear baroclinic waves. *J.Atmos. Sci.*, 35(3), 414–432. https://doi.org/10.1175/1520-0469(1978)035<0414:TLCOSN>2.0.CO;2

Sinclair, M. R. A. (1996) Climatology of anticyclones and blocking for the Southern Hemisphere, *Monthly Weather Review,*v. 124: 245-263.https://doi.org/10.1175/1520-0493(1996)124<0245:ACOAAB>2.0.CO;2

Skansi, M-M., Brunet,M., Sigró,J., Aguilar,E., Groening, A,J-A, Bentancur, J, O., Geier, C,R,Y Ruth *et al*. (2013) Warming and wetting signals emerging from analysis of changes in climate extreme indices over South America, *Global and Planetary Change,*Vol 100, 295-307, https://doi.org/10.1016/j.gloplacha.2012.11.004.

Solman, S, A.Núñez, M.N.; Rowntree, P.R. (2003) On the evaluation of the representation of mid-latitude transients in the Southern Hemisphere by HadAM2B GCM and the impact of horizontal resolution, *Atmósfera*, 16 (4). : https://www.redalyc.org/articulo.oa?id=56516404

Souders, B. M., Colle, A. B., & Chang, M. K. D. (2014a) The climatology and characteristics of Rossby Wave Packets using a feature-based tracking technique. *Monthly Weather Review*, 142(10), 3528–3548. https://doi.org/10.1175/MWR-D-13-00371.1

Souders, B. M., Colle, A. B., & Chang, M. K. D. (2014b) A Description and Evaluation of an Automated Approach for Feature-Based Tracking of Rossby Wave Packets. *Monthly Weather Review*, 142(10), 3505–3527. https://doi.org/10.1175/MWR-D-13-00317.1

Strong, C and Magnusdottir, G. (2008) Trophospheric Rossby Wave Breaking and the NAO/NAM, *Journal of the Atmospheric Sciences*,65(9), 2861-2876 https://doi.org/10.1175/2008JAS2632.1

Thompson, D. W. J., and J. M. Wallace, (2000) Annular modes in the extratropical circulation. Part I: Month-to-month variability. *J. Climate*, 13, 1000–1016. https://doi.org/10.1175/1520-0442(2000)013<1000:AMITEC>2.0.CO;2

Thompson, D.W.J., Solomon, S., (2002) Interpretation of recent southern hemisphere climate change. Science 296, 895–899. https://doi.org/10.1126/science.1069270

Thorncroft, D. C., Hoskins, J, B, and McIntyre,E,M (1993) Two paradigms of baroclinic-wave life- cycle behaviour. Quart. J. Roy. Meteor. Soc., 119(509), 1755. https://doi.org/10.1002/qj.49711950903

Tibaldi, S. and Molteni, F (1990) On the operational predictability of blocking. Tellus A, 42, 343-365. https://doi.org/10.1034/j.1600-0870.1990.t01-2-00003.x

Trenberth, E. K. (1981) Observed Southern Hemisphere Eddy Statistics at 500 mb: Frequency and Spatial Dependence. Journal of Atmospheric Science, 38(12), 2585–2605. https://ui.adsabs.harvard.edu/link_gateway/1981JAtS...38.2585T/doi:10.1175/1520-0469(1981)038%3C2585:OSHESA%3E2.0.CO;2

Ungerovich, M., Barreiro, M., Masoller, C (2020) Influence of Madden-Julian Oscillation on extreme rainfall events in Spring in southern Uruguay. *International Journal of Climatology,* 41(5), 3339-3351 http://dx.doi.org/10.1002/joc.7022

Wallace, J. M., and D. S. Gutzler, (1981) Teleconnections in the geopotential height field during the Northern Hemisphere winter. Mon. Wea. Rev., 109, 784–812, https://doi.org/10.1175/1520-0493(1981)109<0784:TITGHF>2.0.CO;2

Wang, Y and Magnusdottir, G (2010) Tropospheric Rossby Wave Breaking and the SAM, *Journal of Climate,* 24(8), 2134-2146, https://doi.org/10.1175/2010JCLI4009.1

Wiedenmann, M,J., Lupo,R,A., Mokhov, I, I and Tikhonova, A, E. (2002) The Climatology of Blocking Anticyclones for the Northern and Southern Hemispheres: Block Intensity as a Diagnostic. *Journal of Climate*, 15(23), 3459-3473. https://doi.org/10.1175/1520-0442(2002)015<3459:TCOBAF>2.0.CO;2

Wheeler, M. C., & Hendon, H. H. (2004) An all-season real-time multivariate MJO index: Development of an index for monitoring and prediction. *Monthly weather review*, *132*(8), 1917-1932. http://dx.doi.org/10.1175/1520-0493(2004)132%3C1917:AARMMI%3E2.0.CO;2

White, W.B. & N.E. Clark. (1975) On the development of blocking ridge activity over the central North Pacific. *J. Atmos. Sci*. 32: 489–502. https://doi.org/10.1175/1520-0469(1975)032<0489:OTDOBR>2.0.CO;2

Wiedenmann, M,J., Lupo,R,A., Mokhov, I, I and Tikhonova, A, E. (2002) Journal of Climate, 15(23), 3459-3473. https://doi.org/10.1175/1520-0442(2002)015<3459:TCOBAF>2.0.CO;2

Wirth, V., Riemer, M., Chang, E, K, M., & Martius, O. (2018) Rossby Wave Packets on the Midlatitude waveguide- a review. *Monthly Weather Review*, *146*(7), 1965-2001. https://doi.org/10.1175/MWR-D-16-0483.1

Wirth, V. (2020) Waveguidability of idealized midlatitude jets and the limitations of ray tracing theory. *Weather Climate Dynamics*, 1, 111–125. https://doi.org/10.5194/wcd-1-111-2020

WMO: Atlas of Mortality and Economic Losses from Weather, Climate and Water Extremes (1970- 2019) (WMO-No. 1267).

Weijenborg, c ., Vries, H., Haarsma, J, R (2012) On the direction of Rossby wave breaking in blocking, *Climate Dynamics*, 39, 2823–2831. https://doi.org/10.1007/s00382-012-1332-1

Woollings, T., Barriopedro, D., Methven, J., Son, S.-W., Martius, O., Harvey, B., *et al.* (2018) Blocking and its response to climate change. *Current Climate Change Reports,* 4, 287–300. https://doi.org/10.1007/s40641-018-0108-z

Yeh, T, C (1949) On energy dispersion in the atmosphere. *Journal of Meteorology*, 6(1), 1–16. https://ui.adsabs.harvard.edu/link_gateway/1949JAtS....6....1Y/doi:10.1175/1520-0469(1949)006%3C0001:OEDITA%3E2.0.CO;2

Zhang, C (2005) Madden-Julian Oscillation. Rev. Geophys. Reviews of Geophysics 43.(2) (2005). DOI:https://doi.org/10.1029/2004RG000158

Zhang, X., Ximing C (2011) Climate change impacts on global agricultural land availability. *Environmental Research Letters*, 6 (1), https://doi.org/10.1088/1748-9326/6/1/014014

Zheng, M., Chang, E. K., & Colle, B. A. (2013) Ensemble sensitivity tools for assessing extratropical cyclone intensity and track predictability, *Weather and forecasting*, 28(5), 1133-1156, https://doi.org/10.1175/WAF-D-12-00132.1

Zheng, F, Li., Li, J., Ding, R., Feng, J (2017) Cross-Seasonal Influence of the SAM on Southern Hemisphere Extratropical SST and its Relationship with Meridional Circulation in CMIP5 models. *International Journal of Climatology*,38(3), 1499-1519. https://doi.org/10.1002/joc.5262

Zimin, A. V., Szunyogh, I., Hunt, R. B., & Ott, E. (2006) Extracting envelopes of Nonzonally Propagating Rossby Wave Packets. Monthly Weath-er Review, 134(4), 1329–1333. https://doi.org/10.1175/MWR3122.1

Zimin, V. A., Szunyogh, I., Patil, J. D., Hunt, R. B., & Ott, E. (2003) Extracting envelopes of Rossby Wave Packets. Monthly Weather Review,131(5), 1011–1017. https://doi.org/10.1175/1520-0493(2003)131<1011:EEORWP>2.0.CO;2